

# Systems analysis of oscillator models in the space of phase response curves

Pierre Sacré

Supervised by Professor Rodolphe Sepulchre

Systems and Modeling Research Unit  
Department of Electrical Engineering and Computer Science  
Faculty of Applied Sciences  
University of Liège, Belgium

A thesis submitted for the degree of  
*Doctor of Philosophy in Engineering Sciences*

August 2, 2013



## Abstract

Oscillators—whose steady-state behavior is periodic rather than constant—are observed in every field of science. While they have been studied for a long time as closed systems, they are increasingly regarded as open systems, that is, systems that interact with their environment. Because their functions involve interconnection, the relevance of input–output systems theory to model, analyze, and control oscillators is obvious.

Yet, due to the nonlinear nature of oscillators, methodological tools to study their systems properties remain scarce. In particular, few studies focus on the interface between two fundamental descriptions of oscillators, namely the (internal) state-space representation and the (external) circle representation. Starting with the pioneering work of Arthur Winfree, the phase response curve of an oscillator has emerged as the fundamental input–output characteristic linking both descriptions.

The present dissertation aims at studying the systems properties of oscillators through the properties of their phase response curve. The main contributions of this dissertation are the following.

We distinguish between *two fundamental classes of oscillators*. These classes differ in the local destabilizing mechanism that transforms the stable equilibrium of a globally dissipative system into a periodic orbit.

To address input–output systems questions in the space of response curves, we equip this space with the right *metrics* and develop a (*local*) *sensitivity analysis* of infinitesimal phase response curves. This main contribution of the thesis is completed by the *numerical tools* required to turn the abstract developments into concrete algorithms.

We illustrate how these analysis tools allow to address pertinent systems questions about models of *circadian rhythms* (robustness analysis and system identification) and of *neural oscillators* (model classification). These two biological rhythms are exemplary of both main classes of oscillators. We also design elementary *control strategies to assign the phase of an oscillator*.

Motivated by an inherent limitation of infinitesimal methods for relaxation type of oscillators, we develop the novel geometric concept of “*singularly perturbed phase response curve*” which exploits the time-scale separation to predict the phase response to finite perturbations.

In conclusion, the present dissertation investigates input–output systems analysis of oscillators through their phase response curve at the interface between their external and internal descriptions, developing theoretical and numerical tools to study models arising in the biology of cellular rhythms.



## Résumé

Les oscillateurs—dont le comportement à l'équilibre est périodique plutôt que constant—sont présents dans tous les domaines de la science. Alors qu'ils ont été étudiés pendant longtemps comme des systèmes fermés, ils sont de plus en plus considérés comme des systèmes ouverts, c'est-à-dire, des systèmes qui interagissent avec leur environnement. Comme leurs fonctions se basent sur une interconnexion, la pertinence de la théorie entrée–sortie des systèmes pour modéliser, analyser et contrôler les oscillateurs est dès lors évidente.

Cependant, à cause de la nature non-linéaire des oscillateurs, il existe peu d'outils méthodologiques pour étudier leurs propriétés systémiques. En particulier, peu d'études se focalisent sur l'interface entre deux représentations fondamentales des oscillateurs, à savoir la représentation (interne) d'état et la représentation (externe) sur le cercle. Depuis les travaux pionniers d'Arthur Winfree, la courbe de réponse de phase d'un oscillateur a émergé comme la caractéristique entrée–sortie fondamentale liant ces deux représentations.

Cette thèse a pour but d'étudier les propriétés systémiques des oscillateurs à travers les propriétés de leur courbe de réponse de phase. Les contributions principales de cette thèse sont les suivantes.

Nous distinguons *deux classes fondamentales d'oscillateurs*. Ces classes diffèrent par le mécanisme local qui déstabilise le point d'équilibre stable d'un système globalement dissipatif pour le transformer en orbite périodique.

Afin d'aborder des questions systémiques entrée–sortie dans l'espace des courbes de réponse de phase, nous équipons cet espace des *métriques* appropriées et nous développons une *analyse locale de sensibilité* des courbes infinitésimales de réponse de phase. Cette contribution principale de la thèse est complétée par les *outils numériques* nécessaires afin de convertir les développements abstraits en algorithmes concrets.

Nous illustrons la manière dont ces outils d'analyse permettent de aborder des questions pertinentes sur des modèles de *rythmes circadiens* (analyse de robustesse et identification de système) et d'*oscillateurs neuronaux* (classification de modèles). Ces deux modèles sont représentatifs de chacune des deux classes. Nous développons aussi des *stratégies élémentaires pour contrôler la phase d'un oscillateur*.

Motivé par les limitations inhérentes des méthodes infinitésimales pour les oscillateurs de relaxation, nous développons le nouveau concept géométrique de "*courbe de réponse de phase singulièrement perturbée*" qui exploite la séparation d'échelles de temps pour prédire la réponse de phase à des perturbations finies.

En résumé, cette thèse propose une analyse systémique entrée–sortie des oscillateurs au moyen de leur courbe de réponse de phase, à l'interface entre leur représentations externe et interne, développant ainsi des outils théoriques et numériques pour étudier des modèles de la biologie des rythmes cellulaires.



## Acknowledgements

Completing the present thesis has been a great example of oscillatory process, in which my research pace (abruptly) oscillated between high and low values, corresponding to moments of scientific enthusiasm and doubt, respectively.

First and foremost, I heartily thank my advisor, Rodolphe Sepulchre, who provided two fundamental ingredients necessary for the existence of this thesis. His scientific enthusiasm and invaluable expertise created the local excitation required to destabilize conventional viewpoints and lead to novel research paths. His personal patience and genuine humanity initiated the global dissipation essential to clear scientific and personal doubts, giving me self-confidence and optimism, especially when I needed them the most.

I secondly thank Guillaume Drion with whom I started this long adventure since the very beginning. Sharing this experience with him developed scientific but also and primarily personal (and sports) bonds between us that will last.

Many thanks are also due to my friends and colleagues (former and present) at the University of Liège, from Belgium and from many places over the world. They triggered a rich working environment and a multicultural atmosphere. Special thanks go to Bamdev Mishra for bringing a spicy touch to the everyday research life in our office and to the coffee-break group for entertaining breaks, lunches, and debates. Closer collaboration with postdoctoral researchers Denis Efimov, Alexandre Mauroy, and Alessio Franci was of great help.

I sincerely acknowledge Prof. G. Kerschen (my Master thesis supervisor), Prof. J. Martial, and Prof. M. Georges who got my foot on the research ladder.

The members of the Jury are acknowledged for their interest and time devoted to the reading and evaluation of this manuscript.

Last, but not least, my enormous gratitude goes to my family and friends for constantly supporting me and for helping me to disconnect from research.



# Contents

<b>1</b>	<b>Introduction</b>	<b>1</b>
1.1	Research context and need . . . . .	2
1.2	Contributions of the dissertation . . . . .	4
1.3	Outline of the presentation . . . . .	5
1.4	Publications . . . . .	7
<b>2</b>	<b>Oscillators as open systems</b>	<b>9</b>
2.1	Endogenous mechanisms of oscillators . . . . .	10
2.1.1	Generic design principles for oscillators . . . . .	11
2.1.2	Two motif interpretations for oscillators in biology . . . . .	13
2.2	Exogenous functions of oscillators . . . . .	17
2.3	Systems questions for oscillators . . . . .	19
2.3.1	How to compare oscillators? . . . . .	19
2.3.2	How to identify sensitive parameters in oscillators? . . . . .	20
2.3.3	How to exploit the geometry underlying oscillators? . . . . .	20
2.4	Methods from the state space to the circle . . . . .	21
2.5	Summary . . . . .	22
<b>3</b>	<b>Phase response curves</b>	<b>23</b>
3.1	Phase response curves from experiments . . . . .	24
3.2	Phase response curves from state-space models . . . . .	26
3.2.1	State-space models . . . . .	27
3.2.2	Phase maps and isochrons . . . . .	28
3.2.3	Response to phase resetting inputs . . . . .	31
3.3	Phase response curves in phase models . . . . .	33
3.3.1	Phase models for single oscillators . . . . .	33
3.3.2	Phase models for coupled oscillators . . . . .	35
3.4	Phase response curves and asymptotic methods . . . . .	38
3.4.1	Averaging theory . . . . .	38
3.4.2	Singular perturbation theory . . . . .	40
3.4.3	Numerical validations . . . . .	41

3.5	Computations of phase response curves . . . . .	42
3.5.1	Periodic orbits . . . . .	42
3.5.2	Infinitesimal phase response curves . . . . .	42
3.5.3	Phase response curves . . . . .	43
3.6	Summary . . . . .	45
<b>4</b>	<b>Metrics in the space of phase response curves</b>	<b>47</b>
4.1	Basics of differential geometry on manifolds . . . . .	48
4.2	Natural equivalence properties . . . . .	49
4.3	Metrics . . . . .	51
4.3.1	Metric on Hilbert space $\mathcal{H}^1$ . . . . .	51
4.3.2	Metric on the quotient space $\mathcal{H}^1/\mathbb{R}_{>0}$ . . . . .	52
4.3.3	Metric on the quotient space $\mathcal{H}^1/\text{Shift}(\mathbb{S}^1)$ . . . . .	53
4.3.4	Metric on the quotient space $\mathcal{H}^1/(\mathbb{R}_{>0} \times \text{Shift}(\mathbb{S}^1))$ . . . . .	54
4.4	Summary . . . . .	55
<b>5</b>	<b>Sensitivity analysis in the space of phase response curves</b>	<b>57</b>
5.1	Basics of local sensitivity analysis . . . . .	59
5.2	Sensitivity analysis for oscillators . . . . .	60
5.2.1	Sensitivity analysis of a periodic orbit . . . . .	60
5.2.2	Sensitivity analysis of a phase response curve . . . . .	61
5.2.3	Sensitivity analysis of entrainment . . . . .	62
5.3	Numerics of sensitivity analysis . . . . .	62
5.4	Summary . . . . .	63
<b>6</b>	<b>Singularly perturbed phase response curves</b>	<b>65</b>
6.1	Basics of singular perturbation theory . . . . .	66
6.1.1	Classical results of singular perturbation theory . . . . .	66
6.1.2	Geometry of relaxation oscillators . . . . .	67
6.2	Limitations of infinitesimal phase response curves . . . . .	69
6.3	Singularly perturbed phase response curves . . . . .	70
6.3.1	Singularly perturbed phase maps and isochrons . . . . .	71
6.3.2	Singularly perturbed phase response curves . . . . .	74
6.4	Summary . . . . .	78
<b>7</b>	<b>Systems analysis of circadian rhythm models in the space of phase response curves</b>	<b>81</b>
7.1	Parametric robustness analysis . . . . .	82
7.2	Parametric system identification . . . . .	93
7.3	Summary . . . . .	95

<b>8</b>	<b>Systems analysis of neural oscillator models in the space of phase response curves</b>	<b>99</b>
8.1	Model classification . . . . .	100
8.2	Geometric prediction . . . . .	105
8.3	Summary . . . . .	109
<b>9</b>	<b>Phase oscillator control in the space of phase response curves</b>	<b>111</b>
9.1	Design and control of phase oscillator . . . . .	112
9.2	Phase oscillator control strategies . . . . .	113
9.2.1	A motivating example . . . . .	113
9.2.2	Design of control strategies . . . . .	114
9.2.3	Application to motivating example . . . . .	118
9.3	Summary . . . . .	119
<b>10</b>	<b>Conclusion</b>	<b>123</b>
10.1	Summary . . . . .	123
10.2	Perspectives . . . . .	125
<b>A</b>	<b>Numerical tools</b>	<b>127</b>
A.1	Numerical computation of periodic orbits . . . . .	127
A.2	Numerical computation of infinitesimal phase response curves .	130
A.3	Numerical computation of sensitivities . . . . .	131
<b>B</b>	<b>Omitted derivations</b>	<b>133</b>
B.1	Sensitivity of the periodic orbit . . . . .	133
B.2	Sensitivity of the phase response curve . . . . .	135



# Chapter 1

## Introduction

*“This is a story about dynamics: about change, flow, and rhythm, mostly in things that are alive. (...)*

*This is a story about dynamics, but not about all kinds of dynamics. It is mostly about processes that repeat themselves regularly. In living systems, as in much of mankind’s energy-handling machinery, rhythmic return through a cycle of change is a ubiquitous principle of organization. So this book of temporal morphology is mostly about circles, in one guise after another. The word phase is used (...) to signify position on a circle, on a cycle of states. Phase provides us with a banner around which to rally a welter of diverse rhythmic (temporal) or periodic (spatial) patterns that lie close at hand all around us in the natural world.”*

*Arthur Winfree (1942–2002)*

The first lines of the seminal book “The Geometry of Biological Time” [195] emphasize the importance of rhythm as a universal design principle in nature and engineering as well as its fundamental abstraction as a dynamical phenomenon evolving on the circle.

Following those pioneering steps, the present dissertation studies rhythms as open systems whose dynamics evolve on the circle. We term such systems “oscillators”.

## 1.1 Research context and need

Oscillators are observed in every field of science and engineering. Currently, they are perhaps the most widely studied dynamical systems across systems biology [25, 60, 65, 195], neuroscience [85, 89], chemistry [40, 101], physics [86, 139], astronomy [17], and engineering [131, 133, 169, 170].

For a long time, oscillators have been studied as closed systems evolving isolated from their environment (e.g. the revolution and the rotation of celestial bodies, the swinging movement of the pendulum of a clock, the motion of the wheel of a moving car, etc.).

More recently, and especially with recent advances in biology, oscillators are increasingly regarded as open systems in interaction with their environment. As clocks, rhythm generators, or rhythmic relays, they play a role in many biological functions (e.g. circadian rhythms, neural oscillators, mitotic cycles, glycolytic oscillators, and many others, see [60, 65, 195]). Because those functions involve interconnection at their core, the relevance of input–output systems theory to model, analyze, and control oscillators is obvious. It was recognized early (see e.g. Wiener [190]).

Historically, the theory of open systems was primarily developed for linear time-invariant systems evolving around a stable equilibrium. It led to the development of (frequency-domain) Laplace representation in the 1950s and then (time-domain) state-space representation in the 1960s. Laplace representations are compact representations most helpful to analyze or synthesize the system behavior. State-space representations are critical to model the internal mechanisms of a system and understand the link between its internal circuitry and its resulting external behavior.

Starting in the late 1960s, extensions of systems theory to nonlinear time-invariant systems allowed to consider differential equations with periodic orbits (i.e. oscillators), leading to the emergence of (time-domain) circle representation and (time-domain) state-space representation. Likewise, circle representations are compact representations most helpful to study entrainment and synchronization phenomena (see e.g. Winfree [193, 195], Kuramoto [100, 101], Glass [60, 61], Strogatz [170, 171], for exemplative milestones). There also, state-space representations are essential to model and study the internal circuitry of the system: in particular, sufficient conditions for the existence and stability of periodic orbits (see e.g. Andronov [6], Varigonda and Georgiou [179, 180], Stan and Sepulchre [156, 165, 166]) and synchronization in networks of oscillators (see e.g. Angeli [7], Pavlov [136, 137], Slotine [159, 189], Stan and Sepulchre [165, 167], Sontag [147, 162, 163]).

There is a conceptual analogy between Laplace representation of linear time-invariant systems and circle representations of oscillators (see Figure 1.1):

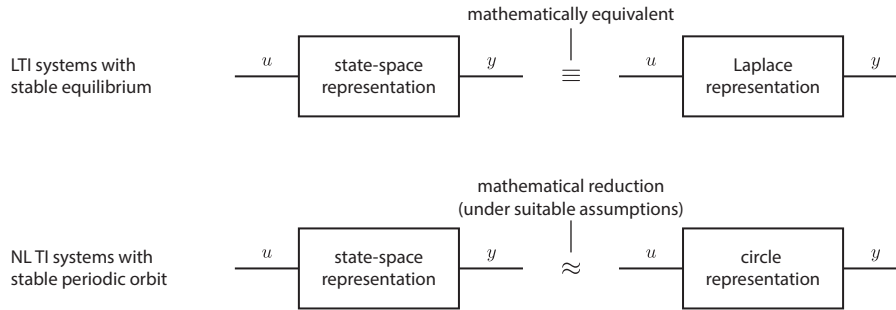


Figure 1.1 – Conceptual analogy between Laplace and circle representations. The circle representation for nonlinear time-invariant (NL TI) systems with a stable periodic orbit is analogous to the Laplace representation for linear time-invariant (LTI) systems with a stable equilibrium.

- they are independent of the complexity of the state-space representation and they may be computed from the state-space representation;
- they provide information suitable to be compared to experimental data (harmonic excitation experiments and phase resetting experiments) and are thus greatly appreciated by experimentalists.

This analogy is not complete. While the Laplace representation is mathematically equivalent to the state-space representation, the circle representation is a mathematical reduction of the state-space representation, valid under suitable assumptions.

If the interface between state-space and Laplace representations has been at the core of linear systems theory, few studies focus on the interface between circle and state-space representations of oscillators. Studies on the circle focus on canonical circle representations disconnected from any state-space representation or valid only in a narrow neighborhood of the bifurcation giving birth to the oscillator. Most studies in the state space focus on properties of trajectories and disregard the peculiar circular function of oscillators owing to the periodic nature of their behavior.

Under two distinct assumptions (weak input or impulse train), a state-space representation can be reduced to a circle representation. In both cases, the key player in the reduction is the so-called phase response curve which is a fundamental input–output information of oscillators at the interface between state-space and circle representations. The present dissertation aims at studying the systems properties of oscillators through the properties of their phase response curve.

## 1.2 Contributions of the dissertation

In the above context, the present dissertation contributes at bridging the gap between input–output systems theory in (internal) state-space and (external) circle representations. We address systems questions for oscillators in the space of phase response curves, at the interface between both descriptions.

In particular, this dissertation includes the following specific contributions.

As a conceptual contribution, we discriminate between *two fundamental classes of oscillators* throughout this dissertation. Oscillators are viewed as globally dissipative systems whose stable equilibrium is locally destabilized by a local excitation. Both classes differ in the local destabilizing mechanism: a delay in the feedback loop or a dynamical hysteresis induced by autocatalysis.

The main contribution of this dissertation is to equip the space of phase response curves with the right *metrics* and to develop a *(local) sensitivity analysis* of infinitesimal phase response curves, offering a novel framework to input–output systems analysis for oscillators.

The *metrics* allow to compare oscillators in the space of phase response curves accounting for natural equivalence properties.

The *(local) sensitivity analysis* of infinitesimal phase response curves provides a systematic and computationally tractable approach to identify important parameters of an oscillator model in the parameter space, around a nominal set of parameter values. It is complementary to more global—but less tractable—tools such as bifurcation analysis or parameter space exploration.

In addition to the abstract developments, we provide the *numerical tools* required to turn those developments into concrete algorithms.

A methodological contribution is to illustrate how these analysis tools allow to address pertinent questions about models of *circadian rhythms* (robustness analysis and system identification) and *neural oscillators* (model classification). Circadian rhythm models are exemplary of delayed negative-feedback oscillators; neural oscillators are exemplary of hysteresis-and-adaptation oscillators.

As a side contribution, we design elementary *control strategies to assign the phase of an oscillator*.

Finally, motivated by the limitation of infinitesimal phase response curves for relaxation oscillators, we develop the novel geometric concept of “*singularly perturbed phase response curve*” which exploits the time-scale separation to predict the phase response of the oscillator to finite perturbations.

Our contributions are highlighted more specifically at the end of each chapter introduction.

## 1.3 Outline of the presentation

The dissertation is organized as illustrated in Figure 1.2.

Chapter 2 gives a general overview on oscillators as open systems. In particular, it focuses on the endogenous mechanisms of oscillators, but also and primarily, on their exogenous functions. Then, it reformulates input–output systems questions for oscillators and stresses the importance of studying the interface between state-space and circle representations.

Chapter 3 provides a comprehensive review on the concept of phase response curve: from experiments, from state-space models, and in phase models of single and coupled oscillators. It also shows how standard asymptotic methods can be used to reduce the dynamics on the circle and how exact and approximate phase response curves can be computed from a state-space representation.

Chapter 4 proposes metrics in the space of phase response curves to study input–output systems questions. It identifies two natural equivalence properties (scaling and phase shifting) in this space and defines metrics in the four spaces resulting from various combinations of these equivalence properties

Chapter 5 introduces a local sensitivity analysis in the space of phase response curves. In particular, it recalls the sensitivity analysis of periodic orbits and derives the sensitivity analysis of infinitesimal phase response curves and entrainment behavior.

Chapter 6 focuses on a geometric approach to study singularly perturbed relaxation oscillators, for which the infinitesimal approach used in Chapter 5 fails to capture the input–output oscillator behavior. In particular, it defines two novel concepts: singularly perturbed phase maps and singularly perturbed phase response curves.

Chapter 7 reports the systems analysis of circadian rhythms in the space of phase response curves. It develops scalar measures for parametric robustness analysis and a gradient-descent algorithm for parametric identification.

Chapter 8 presents the systems analysis of neural oscillators in the space of phase response curves. It proposes a new classification method directly based on the shape of the phase response curves. Then it predicts the shape of *finite* phase response curves for a popular neural oscillator model.

Chapter 9 motivates the interest of oscillator design and control on the circle. Then it develops control strategies to assign the phase of an oscillator.

Chapter 10 concludes the dissertation, summarizing its outcomes, their implications, and what the future holds, beyond this work.

Appendix A provides the numerical tools required to turn the abstract developments into concrete algorithms to compute periodic orbits, infinitesimal phase response curves, and their sensitivity. Appendix B collects derivations omitted in the main text for presentation purpose.

The reader only interested in a particular illustration (Chapter 7, 8, or 9) may follow the partial flow materialized by the incoming arrows in Figure 1.2.

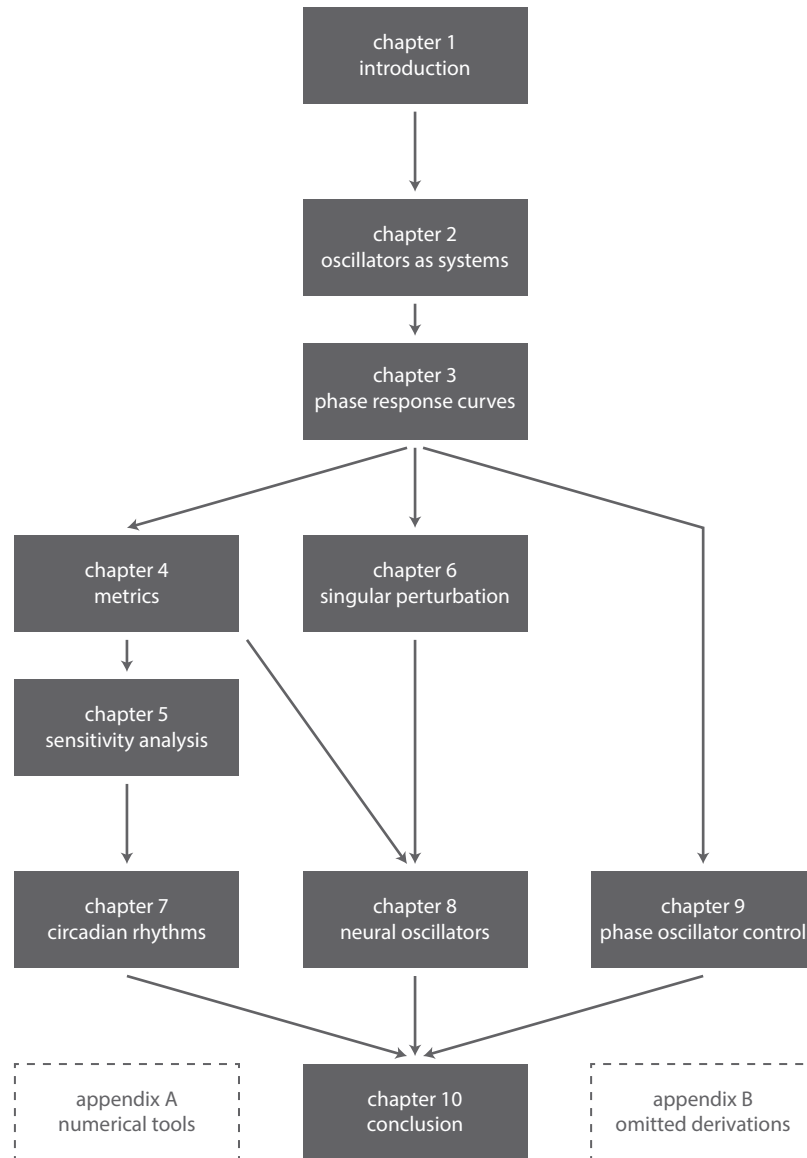


Figure 1.2 – Dissertation road map. The dissertation is organized as illustrated on this figure. The reader only interested in a particular illustration (Chapter 7, 8, or 9) may follow the partial flow materialized by the incoming arrows.

## 1.4 Publications

The main results of this dissertation are presented in the following publications:

- P. Sacré, A. Franci, and R. Sepulchre. On the phase response curve for relaxation and bursting oscillators. In preparation
- P. Sacré and R. Sepulchre. Sensitivity analysis of oscillator models in the space of phase response curves: oscillators as open systems. Submitted to *IEEE Control Syst. Mag.* (preprint <http://arxiv.org/abs/1206.4144>)
- P. Sacré and R. Sepulchre. Sensitivity analysis of circadian entrainment in the space of phase response curves. In V. Kulkarni, G.-B. Stan, and K. Raman, editors, *Systems and Synthetic Biology: A Systematic Approach*. Springer. To appear (preprint <http://arxiv.org/abs/1211.7317>)
- A. Mauroy, P. Sacré, and R. Sepulchre. Kick synchronization versus diffusive synchronization. In *Proc. 51st IEEE Conf. Decision and Control*, pages 7171–7183, Maui, HI, Dec. 2013
- P. Sacré and R. Sepulchre. Matching an oscillator model to a phase response curve. In *Proc. 50th IEEE Conf. Decision and Control and 2011 European Control Conf.*, pages 3909–3914, Orlando, FL, Dec. 2011
- D. V. Efimov, P. Sacré, and R. Sepulchre. Controlling the phase of an oscillator: a phase response curve approach. In *Proc. 48th IEEE Conf. Decision and Control and 28th Chinese Control Conf.*, pages 7692–7697, Shanghai, China, Dec. 2009

In addition, a collaboration with Marc Hafner (EPFL, Switzerland) lead to the following publication (not included in this dissertation):

- M. Hafner, P. Sacré, L. Symul, R. Sepulchre, and H. Koepl. Multiple feedback loops in circadian cycles: robustness and entrainment as selection criteria. In *Proc. 7th Int. Workshop Computational Systems Biology*, pages 51–54, Luxembourg, June 2010



## Chapter 2

# Oscillators as open systems

Many oscillators are, by nature, *open systems*, that is, systems that interact with their environment. As clocks, rhythm generators, or rhythmic relays, their function often lies in their robust ability to respond to particular inputs, to behave collectively when they are interconnected within a network, or both.

Because these functions involve interconnection at their core, the relevance of input–output systems theory to model, analyze, and control oscillators is obvious and was recognized early (see Wiener [190]). Yet, due to their nonlinear nature, the input–output systems analysis of oscillators remains scarce.

Motivated by this gap in the literature, we review the endogenous mechanisms giving birth to oscillatory systems, but also and primarily, focus on their exogenous functions. We also reformulate input–output systems questions for oscillatory systems. Although classical in their formulation, most of these questions have been addressed only for equilibrium systems, that is, systems whose isolated steady-state behavior is a stable equilibrium.

This chapter is organized as follows. Section 2.1 introduces the endogenous ingredients necessary to all oscillatory systems. It also distinguishes two fundamental classes of oscillators based on two distinct paradigms to create the necessary local excitation destabilizing the steady state. Section 2.2 describes the exogenous functions of oscillators, in response to particular inputs or in networks of coupled oscillators. Section 2.3 addresses input–output systems questions for oscillators. Section 2.4 stresses the importance of studying these questions at the interface between circle and state-space representations.

*Contributions.* The main conceptual contributions of this chapter are (i) to identify two fundamental classes of oscillators rooted in two distinct paradigms to create oscillations, (ii) to consider oscillators as open dynamical systems, and (iii) to reformulate input–output systems questions for oscillators.

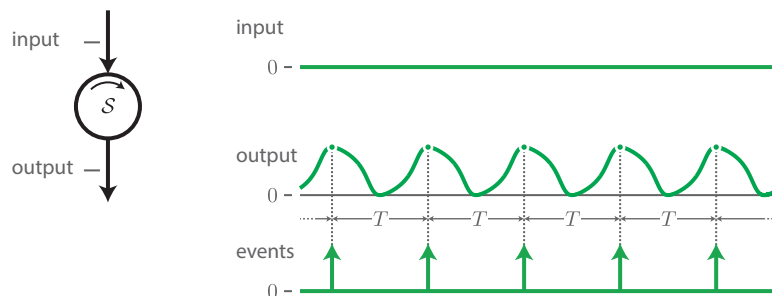


Figure 2.1 – Endogenous periodic steady-state behavior of oscillators. In isolation condition, oscillators exhibit a periodic steady-state behavior. For illustration purpose, it is convenient to represent this periodic oscillation by a periodic train of events.

## 2.1 Endogenous mechanisms of oscillators

In isolation condition, oscillators are characterized by a periodic—rather than constant—steady-state behavior (see Figure 2.1). This periodic steady-state behavior is represented by an output signal that returns to its starting point after some fixed time and continues to do so in the whole future.

In many situations, an experimentalist does not observe continuously the output of an oscillatory system. Quite the opposite, he observes the regular occurrence of a particular event. Few examples of such observed events are the onset of daily locomotor activity of rodents [30], the eclosion of insects [142], the initiation of an action potential in neural or cardiac cells [19, 36, 125], or the onset of mitosis in yeast [82]. The scarcity of this experimental information (one event every period) may come from the spiking nature of the oscillations, from a lack of high time-resolution measurements provided by measurement reporter devices (like green fluorescent proteins), or even from the experimental choice of recording specific events. (For illustration convenience, we will often conceptualize a periodic behavior as a train of events. Unless otherwise specified, it does not imply that the illustrated concepts are not valid for smooth oscillators.)

In this section, we identify the necessary key ingredients responsible for stable oscillations, namely a global dissipation to create a globally attractive equilibrium and a local excitation to locally destabilize this steady-state equilibrium. We illustrate those fundamental ingredients in the van der Pol oscillator in two limits (i.e. quasi-harmonic and relaxation limits). Then, we give a motif interpretation of those mechanisms as they often appear in biology.

### 2.1.1 Generic design principles for oscillators

Over the years, a large number of qualitative and quantitative models have been proposed to describe oscillators. Among all those models, two fundamental design principles have emerged as critical elements of oscillations [134, 156, 167].

1. The first key ingredient is a global dissipation (or inhibition) that creates a globally attractive equilibrium.
2. The second key ingredient is a local excitation that locally destabilizes the steady-state equilibrium.

The oscillation emerges as the bounded attractor that separates the global dissipation from the local excitation.

In the following, we illustrate those concepts on the van der Pol oscillator.

#### The van der Pol oscillator: an illustrative model

The van der Pol oscillator is an oscillator with nonlinear damping governed by the second-order differential equation

$$\ddot{y} - \mu(1 - y^2)\dot{y} + y = u_1 + \mu\dot{u}_2, \quad u_1 \in \mathbb{R}, \quad u_2 \in \mathbb{R}, \quad y \in \mathbb{R}. \quad (2.1)$$

where  $u_1$  and  $u_2$  are inputs,  $y$  is an output, and  $\mu > 0$  is a parameter.

Historically, this equation was proposed by Balthazar van der Pol in 1920 to study oscillations in vacuum tube circuits [178]. To be more precise, it models a simple electrical circuit with nonlinear resistance (see Figure 2.2). The inductor and capacitor are assumed to be linear, time-invariant and passive, that is,  $L > 0$  and  $C > 0$ . The resistive element is an active circuit characterized by the  $v$ - $i$  characteristic  $i = \phi_{\text{NL}}(v) = v^3/3 - v$ . The output  $y \in \mathbb{R}$  is the voltage across the capacitor  $C$ . The input  $u_1 \in \mathbb{R}$  is the tension generated by a voltage source in series with the inductor  $L$ . The input  $u_2 \in \mathbb{R}$  is the current generated by a current source and injected in the circuit. The parameter  $\mu$  is equal to the ratio  $\sqrt{L/C}$ .

The van der Pol oscillator played a seminal role in the development of nonlinear oscillation theory. One reason of this success is probably its ability (with only one single parameter  $\mu$ ) to exhibit two very different regimes of oscillations. For weak nonlinearities ( $\mu \ll 1$ ), the oscillator displays quasi-harmonic oscillations. For strong nonlinearities ( $\mu \gg 1$ ), it displays relaxation oscillations.

In the following, we identify two distinct viewpoints on the mechanisms giving birth to oscillations, which depend on how we dissect the circuit interconnection (see Figure 2.3). Each viewpoint is convenient to explain the behavior in one regime of oscillations.

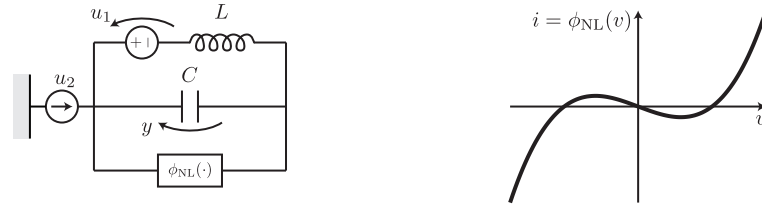


Figure 2.2 – Electrical circuit of the van der Pol oscillator. The inductor and capacitor are assumed to be linear, time-invariant and passive, that is,  $L > 0$  and  $C > 0$ . The resistive element is an active circuit characterized by the  $v$ - $i$  characteristic  $i = \phi_{NL}(v)$ .

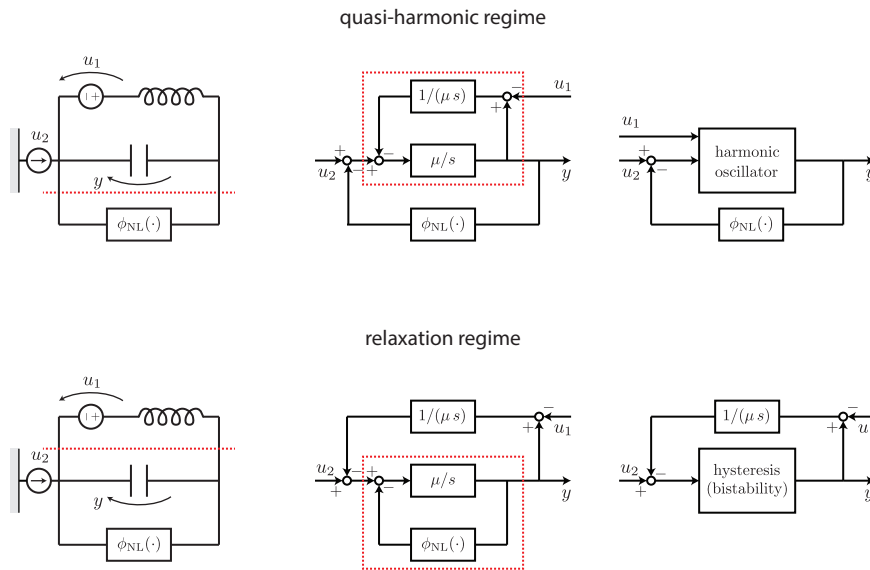


Figure 2.3 – Two viewpoints on the mechanisms underlying the van der Pol oscillators. (Top) In the quasi-harmonic regime, we view the oscillator as a harmonic oscillator ( $LC$  circuit) with a static nonlinear feedback (resistive element). (Bottom) In the relaxation regime, we view the oscillator as a dynamical hysteresis (fast  $RC$  circuit) with slow adaptation (inductor  $L$ ).

**Quasi-harmonic regime** ( $\mu \ll 1$ ). In this limit, we view the van der Pol oscillator as a  $LC$  circuit in parallel with a nonlinear resistive element  $i = \phi_{\text{NL}}(v)$  (see Figure 2.3, top). A systems analogy is a harmonic oscillator ( $H_1(s) = 1/(s^2 + 1)$  and  $H_2(s) = \mu s/(s^2 + 1)$ ) with a static nonlinear feedback.

The global dissipation is provided by the (globally negative) static nonlinearity and the local excitation is generated by the negative slope at the origin (see Figure 2.2) which destabilizes the negative feedback loop, violating the small gain theorem.

The energy interpretation is that the sustained exchange of energy between a capacitor and an inductor is regulated by a static element (a tunnel-diode circuit) that dissipates energy when the current is high and restores energy when the current is low.

**Relaxation regime** ( $\mu \gg 1$ ). In this limit, we view the van der Pol oscillator as a  $RC$  circuit (with the resistance) in parallel with an inductor  $L$  (see Figure 2.3, bottom). A systems analogy is a dynamical hysteresis, characterized by an integrator ( $H(s) = 1/s$ ) with a static nonlinear negative feedback. This hysteresis is turned into a relaxation oscillation when the input slowly adapts to follow the hysteresis loop, resulting in the closed-loop dynamics.

The global dissipation is provided by the (slow) negative feedback which provides an adaptation mechanism and the local excitation is generated by the (fast) autocatalysis that creates a dynamical hysteresis.

The energy interpretation is that the  $RC$  circuit exhibits a fast bistable behavior. The energy in the capacitor is stored for a high positive or high negative potential difference across it depending on the initial conditions. The inductor slowly integrates and induces periodic switches between two quasi-stable steady states.

### 2.1.2 Two motif interpretations for oscillators in biology

In the following, we provide a motif interpretation of the underlying mechanisms responsible for oscillations. A motif is a conceptual picture of the model architecture. Each node of the motif is assumed to exhibit a monotonic input–output behavior (in the sense of Angeli and Sontag [8, 9]) and may be either excitatory ( $E$ ) or inhibitory ( $I$ ). Excitatory nodes have an increasing monotonic behavior while inhibitory nodes have a decreasing monotonic behavior.

Breaking motifs and plotting the input–output “characteristic” for each “submotif” reveal the mechanism underlying the oscillator. The input–output “characteristic” may be thought of as a step-input steady-state response or a (nonlinear) static gain (see [8, 9] for details).

In biology, two main motifs have emerged as fundamental building blocks of oscillators (see Figure 2.4). They differ in the local excitation mechanism that destabilizes the steady-state equilibrium.

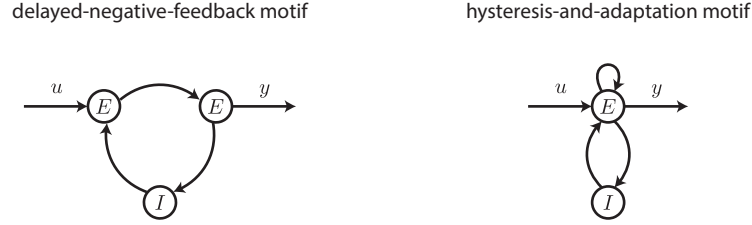


Figure 2.4 – Two motif interpretations for oscillatory systems in biology. (Left) The delayed-negative-feedback motif is a negative feedback loop with (at least) three components in the loop and with an odd number of inhibitory components. (Right) The hysteresis-and-adaptation motif is a negative feedback loop between an excitatory and an inhibitory component. In addition, there is an autocatalytic (positive) feedback on the excitatory component.

### Delayed-negative-feedback motif

The first motif is a negative feedback loop with (at least) three components in the loop and with an odd number of inhibitory components. The global dissipation is provided by the inhibitory (negative) feedback loop. The local excitation is created by the time delay introduced in the feedback loop by the chain of (at least) two excitatory intermediates.

We break the motif as illustrated in Figure 2.5. Each submotif has a monotone characteristic. From a mechanistic point of view, the oscillations are induced by the slow modulation of a monostable equilibrium. This motif exhibits smooth oscillations.

An exemplary model of the delayed-negative-feedback motif was first developed by Goodwin [68,69] in the 1960s to model the periodic enzyme synthesis in bacteria

$$\tau_m \dot{m} = -m + K_m \frac{1}{1 + [(p + u)/\kappa]^\nu} \quad (2.2a)$$

$$\tau_e \dot{e} = -e + K_e m \quad (2.2b)$$

$$\tau_p \dot{p} = -p + K_p e \quad (2.2c)$$

$$y = e \quad (2.2d)$$

where the state variables  $m$ ,  $e$ , and  $p$  indicate the concentrations of mRNA, enzyme, and end-product protein. This model can be seen as a cascade of three linear systems and a static nonlinearity with a feedback. Parameters  $K_i$  and  $\tau_i$  (with  $i = m, e, \text{ or } p$ ) denote the static gains and the time constants of the linear blocks, respectively. Parameters  $\kappa$  and  $\nu$  shape the static nonlinearity. For simplicity, the input  $u$  enters directly in the static feedback and the output  $y$  is the concentration of enzyme.

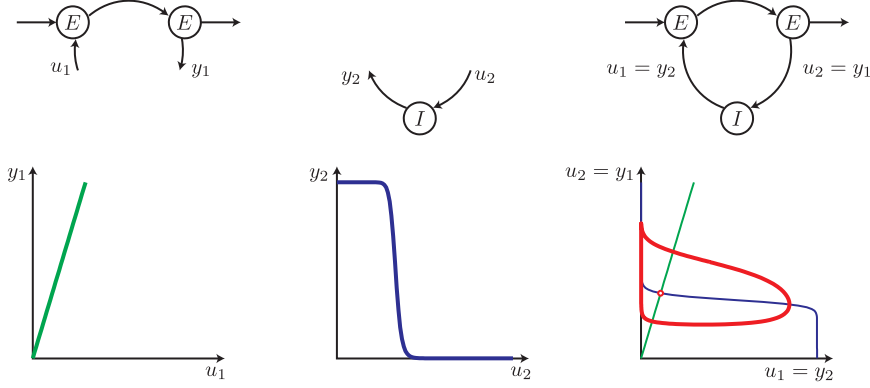


Figure 2.5 – Dissection of delayed-negative-feedback motif. (Left) This submotif exhibits a monotone increasing characteristic. In addition to this static behavior, a delay is introduced by the chain of excitatory component. (Center) This submotif exhibits a monotone decreasing characteristic. (Right) Combining those submotifs produces smooth oscillations. They result from the global dissipation produced by the negative-feedback loop and the local excitation created by the delay in the loop.

The submotif system corresponding to the chain of excitatory nodes (Figure 2.5, left) is given by

$$\tau_m \dot{m} = -m + K_m u_1, \quad (2.3a)$$

$$\tau_e \dot{e} = -e + K_e m, \quad (2.3b)$$

$$y_1 = e. \quad (2.3c)$$

The submotif system corresponding to the inhibitory node (Figure 2.5, center) is given by

$$\tau_p \dot{p} = -p + K_p u_2, \quad (2.4a)$$

$$y_2 = \frac{1}{1 + [p/\kappa]^\nu}. \quad (2.4b)$$

The mechanism of this motif is conceptually similar to the mechanism identified in the quasi-harmonic regime of the van der Pol oscillator. Indeed, the local excitation comes in the negative feedback loop: one creates a negative slope at the origin (van der Pol) and the other induces a delay (delayed-negative-feedback).

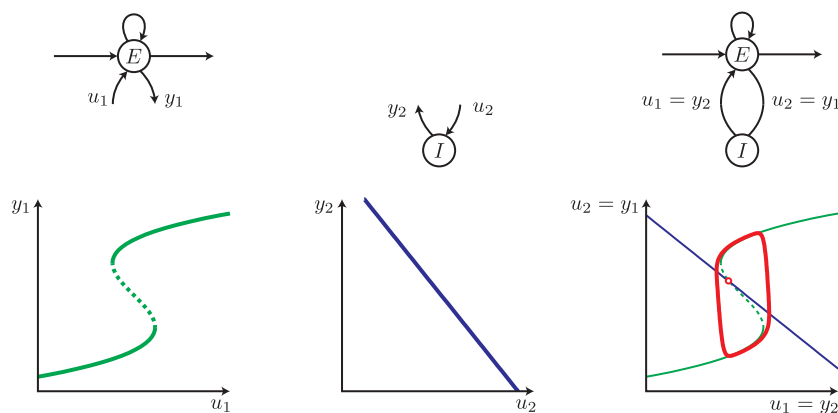


Figure 2.6 – Dissection of hysteresis-and-adaptation motif. (Left) This submotif exhibits a bistable characteristic (hysteresis) induced by the autocatalysis on the excitatory component. (Center) This submotif exhibits a monotone decreasing characteristic. (Right) Combining those submotifs produces relaxation oscillations. They result from the global dissipation produced by the negative-feedback loop and the local excitation created by the dynamical hysteresis.

### Hysteresis-and-adaptation motif

The second motif is a negative feedback between an excitatory and an inhibitory component. In addition, there is an autocatalytic (positive) feedback on the excitatory component. The global dissipation is again provided by the inhibitory (negative) feedback loop. The local excitation is created by the dynamical hysteresis induced by the autocatalytic (positive) feedback loop (this autocatalytic feedback may result from a fast  $E-E$  interaction).

Once again, we break the motif as illustrated in Figure 2.6. The submotif of the excitatory node with the positive feedback leads to a characteristic which exhibits bistability for some region of constant input values. From a mechanistic point of view, the oscillations are created by the dynamical hysteresis and a slow adaptation. This motif exhibits relaxation oscillations.

An exemplative model of the hysteresis-and-adaptation motif was developed by FitzHugh and Nagumo [48, 130] to model an excitable system as a neuron

$$\dot{v} = v - v^3/3 - w + u \quad (2.5a)$$

$$\tau \dot{w} = a - bw + v \quad (2.5b)$$

$$y = v \quad (2.5c)$$

where  $v$  is a voltage-like variable and  $w$  is a recovery variable. The input  $u$  is the magnitude of applied current and the output is the voltage-like variable  $v$ .

The submotif systems are given by

$$\dot{v} = v - v^3/3 + u_1, \quad (2.6a)$$

$$y_1 = v, \quad (2.6b)$$

and

$$\tau \dot{w} = a - bw + u_2, \quad (2.7a)$$

$$y_2 = -w. \quad (2.7b)$$

The mechanism of this motif is identical to the mechanism identified in the relaxation regime of the van der Pol oscillator.

## 2.2 Exogenous functions of oscillators

In this section, we describe exogenous functions of oscillators summarized in Figure 2.7. Those exogenous functions fall into two classes: functions in response to particular inputs (top) or functions as part of the collective behavior in a network (bottom). This description is not intended to be exhaustive.

### Response of an oscillator to particular inputs

In a deterministic framework, the response of an oscillator to periodic inputs leads to the concept of entrainment [74, 146] (see Figure 2.7, top left). A system is entrainable if its steady-state response to a periodic input is a periodic output with the same period (or frequency) as the input.

The concept of entrainment is for example central to the study of circadian rhythms. Circadian entrainment is a biological process at the core of most living organisms which need to adapt their physiological activity to the 24 hours environmental cycle associated with earth's rotation (e.g. variations in light or temperature condition) [140].

In a stochastic framework, the response of an oscillatory system to fluctuating inputs leads to the concept of reliability [20, 111, 116]. A stochastic system is reliable if the same (fluctuating) input elicits essentially identical responses following a transient time interval independently on the initial condition of the system, that is, the response to a given signal is reproducible.

The concept of reliability plays for example a central role in the context of sensory systems. A driving spiking input containing sensory information (e.g. from the retina) is transmitted or not depending on the intrinsic properties of the relay and on the modulating input which alters the specifics of transmission [4, 5].

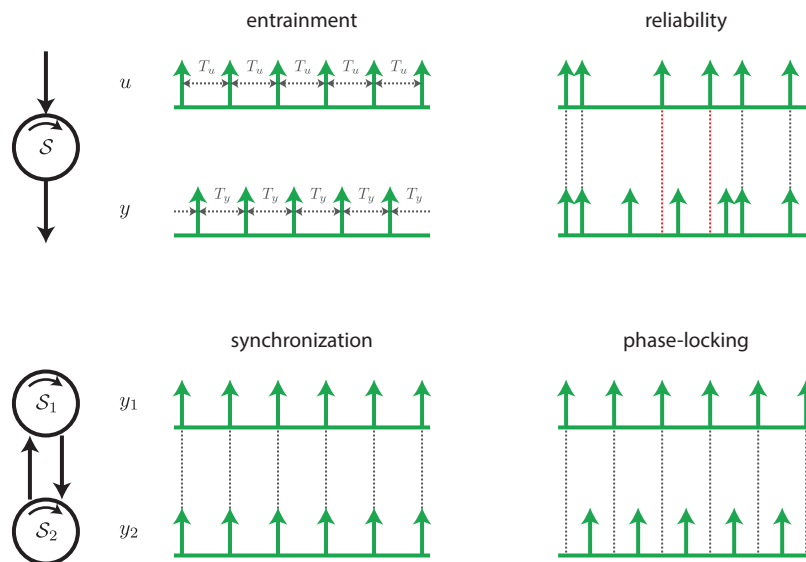


Figure 2.7 – Exogenous functions of oscillators. The function of oscillatory systems often lies in their robust ability to respond to particular inputs (top) and to behave collectively when coupled to each other (bottom).

### Collective behavior of coupled oscillators

The behavior of an oscillatory system coupled to other oscillatory systems leads to the concept of collective behavior: synchronization or phase-locking [100, 126]. Systems have a collective behavior if each oscillatory system may influence some or all the others in such a way that each oscillator maintains a constant phase difference with respect to the others.

The scientific interest in collective behaviors (and in particular in synchronization) of coupled oscillators goes back to the work by Huygens (1673) on coupled pendulum clocks [86] and, nowadays, is perhaps the most widely studied dynamical concept (see for example the inspiring books of Winfree [195] or Strogatz [170] and recent reviews on the subject [33, 34, 123]).

### Response and collective behavior in a network of oscillators

A network of oscillatory systems in which each oscillator influences some of the others to achieve a collective behavior may also be subject to external inputs. In this case, the collective behavior of the network impacts how the network is entrained by periodic inputs or relays fluctuating inputs (see Figure 2.8).

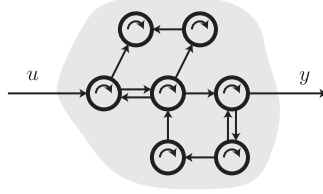


Figure 2.8 – Oscillators in a network. In many situations, an oscillatory system belongs to a larger network of coupled oscillators. The network has its own input and its own output.

## 2.3 Systems questions for oscillators

In this section, our objective is to address input–output systems questions for oscillators. Although classical in their formulation, most of those questions have been addressed only for equilibrium systems, that is, systems whose isolated steady-state behavior is a stable equilibrium.

### 2.3.1 How to compare oscillators?

Given experimental observations, mathematical modelers have conjectured different internal mechanisms leading to different mathematical models of the same phenomenon. For example, in the 1990s, two different models of the mitosis (the mechanism responsible for the cell division cycle) were published in the same issue of the same journal. Albert Goldbeter proposed a model based on the delayed negative-feedback motif [63], while John Tyson suggested a model based on the hysteresis-and-adaptation [177].

In this context, a first natural question is thus “How to compare oscillatory systems?”. How to compare two mathematical models? How to compare a mathematical model to experimental data?

Comparing systems with a proper metric has been central to systems theory (see e.g. Zames [39, 197], Vinnicombe [183], Georgiou [57] for exemplary milestones), offering novel frameworks for system identification and robustness analysis.

Following those steps and motivated by the prevalence of input–output characteristics in experiments, we aim at developing the right metrics (accounting for natural invariance properties) for oscillatory systems.

### 2.3.2 How to identify sensitive parameters in oscillators?

With recent experimental advances in biology, the molecular bases of biological processes have been increasingly unfolded in various organisms. However, even though the architecture of those biological processes is better known, the specific design and robustness mechanisms implemented in those architectures remain unknown [134, 168]. In addition, the values of the model parameters are often chosen empirically using trial-and-error techniques due to few quantitative experimental data (see the quantitative model for circadian rhythms [108, 109]).

In this context, a second natural question is thus “How to identify sensitive parameters in oscillatory systems?”. How can a system characteristic change in response to changes in the parameter values or to changes in the system structure?

Sensitivity analysis is classical in systems theory (see e.g. [53, 153, 175, 181]). Sensitivity analysis for oscillators has been widely studied in terms of the sensitivity of the trajectories [22, 95, 144] and of the zero-input steady-state behavior (period and periodic orbit locus) [87, 168, 191, 192]. More recently, empirical phase-based performance measures have been proposed [14, 77, 78]. However, those sensitivity analysis tools miss the input–output nature of experiments.

We aim at developing a sensitivity analysis for oscillatory systems that can be linked to the available input–output experimental data in the context of biological oscillators.

### 2.3.3 How to exploit the geometry underlying oscillators?

Experimental data reveal that, for some oscillatory systems, the mechanism leading to oscillations relies on the underlying geometric structure. In neurodynamics, the time-scale separation plays a central role. Studying the system at the different time scales may help to better understand the mechanisms.

In this context, a third natural question is thus “How to exploit the geometry underlying oscillators?”

Singular perturbation methods are natural tools for systems with a strong time-scale separation [45, 46]. The essence of this theory is that the discontinuity of solutions caused by singular perturbation is avoided if the system is analyzed in separated time scales. The concept of fast-threshold modulation exploits the geometric structure underlying oscillatory systems to predict synchronization properties [160]. However, this concept does not have a clear generalization for high dimensional models and for large networks.

We aim at exploiting the geometry underlying the system in order to predict input–output properties of the systems that can be validated experimentally, such as entrainment or synchronization.

## 2.4 Methods from the state space to the circle

In this section, we emphasize the parallel developments of state-space methods and circle methods for oscillators.

### Methods in the state space

State-space representations are essential to model and study the internal circuitry of the system.

Sufficient conditions for the existence and stability of periodic orbits have been proposed for different classes of systems: relay relaxation oscillators [179, 180] or passive oscillators [167].

Synchronization between trajectories of state-space models is analyzed as an incremental stability property [112] (i.e. the trajectories converge to one another rather than being attracted toward some equilibrium position). The leading concepts of Lyapunov analysis [7], dissipativity analysis [10, 80, 154, 163, 167], and—to a growing extent—contraction analysis [136, 137, 147, 159, 162, 189], provide natural system theoretic tools to study synchronization.

### Methods on the circle

Circle representations focus on the analysis of entrainment and synchronization phenomena (see e.g. Winfree [193, 195], Kuramoto [100, 101], Glass [60, 61], Strogatz [170, 171], for exemplative milestones).

### At the interface between state-space and circle methods

The key ingredient connecting state-space and circle representations is the concept of phase map. A phase map  $\Theta$  is a mapping that associates with every point  $x$  in the basin of attraction of the oscillator  $\mathcal{B}(\gamma)$  (included in the state space  $\mathcal{X}$ ) a phase  $\theta$  on the unit circle  $\mathbb{S}^1$ , that is,

$$\Theta : \mathcal{B}(\gamma) \subseteq \mathcal{X} \rightarrow \mathbb{S}^1 : x \mapsto \theta. \quad (2.8)$$

Away from a finite number of isolated points, the phase map  $\Theta$  is a continuous map. In general (for nonzero input), the phase dynamics are often hard to derive.

Due to the nonlinear nature of the system, the phase map is often not known explicitly. However, in many situations, the global knowledge of the phase map is not required to study oscillator dynamics. Instead, a local asymptotic phase model may be computed from the information obtained through phase resetting experiments.

Starting with the pioneering work of Arthur Winfree [195], the phase response curve (PRC) of an oscillator has emerged as a fundamental input–output

characteristic of oscillators. Analogously to the static gain of a transfer function, the phase response curve measures a steady-state (asymptotic) property of the system output in response to an impulsive input. For the static gain, the measured quantity is the integral of the response; for the phase response curve, the measured quantity is the phase shift between the perturbed and unperturbed responses. Because of the periodic nature of the steady-state behavior, this phase shift depends in magnitude and in sign (advance or delay) on the phase of the impulsive input. The phase response curve is therefore a curve rather than a scalar. In many situations, the phase response curve can be determined experimentally and provides unique data for the model identification of the oscillator. Likewise, numerical methods exist to compute the phase response curve from a state-space model of the oscillator. Finally, the phase response curve is the fundamental mathematical information required to reduce a  $n$ -dimensional state-space model to a one-dimensional (phase) center manifold of a hyperbolic periodic orbit.

## 2.5 Summary

In this chapter, we gave an overview of oscillators as open systems, starting from the endogenous mechanisms creating the oscillation, enlightening the exogenous character of their functions, and addressing input–output systems questions. We briefly reviewed oscillator models in the state space and on the circle.

## Chapter 3

# Phase response curves

As a preliminary to the results developed in the sequel, we aim at giving an overview of phase response curves, as the fundamental bridge between systems methods in the state space (for the detailed modeling) and systems methods on the circle (for the analysis).

This chapter is organized as follows. Section 3.1 introduces intuitively the concept of phase response curves from the viewpoint of an experimentalist performing phase resetting experiments. Section 3.2 provides the appropriate mathematical framework to define the notion of phase response curves in the context of input–output time-invariant state-space models. It emphasizes the role of the phase map and its isochrons to study oscillators on the unit circle. Section 3.3 reviews the use of phase response curves in phase models for single oscillators and coupled oscillators. Section 3.4 shows how standard asymptotic methods (averaging theory and singular perturbation theory) may be used to derive approximate phase models. Section 3.5 discusses numerical methods that compute (exact or approximate) phase response curves from a state-space model.

*Contributions.* The main contribution of this chapter is to provide a comprehensive review on the concept of phase response curve: from experiments, from state-space models, and in phase models. Two technical contributions of this chapter are (i) to derive phase maps and dynamics on the circle for oscillators by exploiting classical asymptotic methods and (ii) to introduce a novel first-order approximate method for computing phase response curves.

The material of Section 3.4 is the result of a collaboration with Alexandre Mauroy (postdoctoral researcher at the University of California, Santa Barbara).

### 3.1 Phase response curves from experiments

An experimentalist often observes an oscillatory system comes through the regular repetition of a particular event (e.g. the onset of daily locomotor activity of rodents [30] in the original work plotting a phase response curve). One of the simplest modeling experiments is to perturb the oscillatory behavior for a short period of time (short with respect to the oscillation period) and to record the altered timing of the subsequent occurrences of the observable event once the system has recovered its prior rhythmicity. The phase of the oscillator is said to have “reset”. In general, the phase reset does not only depend on the perturbation itself (magnitude and shape) but also on its timing (or phase) during the cycle. In this section, we formalize the basic experimental paradigm of phase resetting experiments for rhythms and introduce intuitively the concept of phase response curves following the terminology in [60, 195].

In isolation condition (closed system), an oscillatory system exhibits a precise rhythm, that is, a periodic behavior, and the period  $T$  of the rhythm is assumed constant (Figure 3.1, top). To facilitate the comparison of rhythms with different periods (for example due to the variability in experimental preparation), it is convenient to introduce the notion of phase. In the absence of perturbation, the phase is a “normalized cyclic time” evolving on the unit circle. Associating the onset of the observable event with phase 0 (or  $2\pi$ ), the phase variable  $\theta(t)$  at time  $t$  corresponds to the fraction of a period elapsed since the last occurrence of the observable event. It grows linearly with time, that is,  $\theta(t) := \omega(t - \hat{t}_i) \pmod{2\pi}$  where  $\omega := 2\pi/T$  is the angular frequency of the oscillator and  $\hat{t}_i$  is the time of the last observable event.

Under the effect of a stimulus (phase resetting input) at time  $(t_s - \hat{t}_0)$  after one observable event, the next event times  $\hat{t}_i$  (for  $i = 1, 2, \dots$ ) are altered. For simplicity, we temporarily assume that the original rhythm is restored immediately after the first post-stimulus event, meaning that observable events occur at the original period  $T$ . We denote by  $\hat{T} := \hat{t}_1 - \hat{t}_0$  the time interval between two successive events that occur immediately before and after the stimulus. It is convenient to normalize each quantity in order to facilitate comparison between different experimental setups. Multiplying by  $\omega = 2\pi/T$ , we have  $\theta := \omega(t_s - \hat{t}_0)$  and  $\hat{\tau} := \omega\hat{T} = \omega(\hat{t}_1 - \hat{t}_0)$ .

The effect of a stimulation is to produce a phase shift  $\Delta\theta$  between the perturbed and unperturbed oscillators. The phase shift  $\Delta\theta$  is given by

$$\Delta\theta := 2\pi - \hat{\tau} \quad (\text{wrapped in } [-\pi, \pi]). \quad (3.1)$$

Given a phase resetting input  $u(\cdot)$ , the dependence of the phase shift  $\Delta\theta$  on the phase  $\theta$  at which the stimulus was delivered is commonly called the phase response curve (PRC). We denote it by  $Q(\theta; u(\cdot))$ , in order to stress that it is a function of the phase which also depends on the input  $u(\cdot)$ .

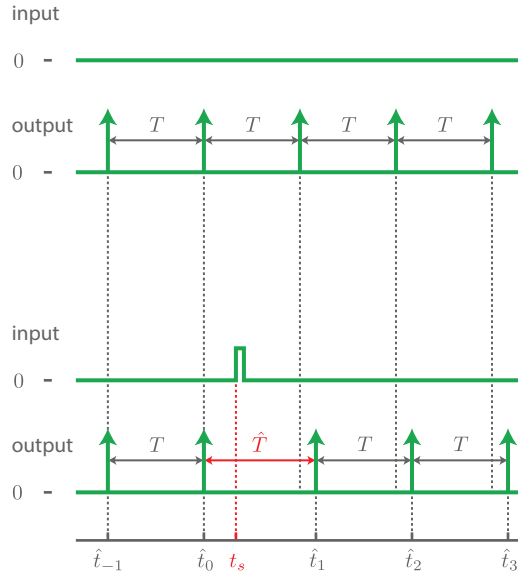


Figure 3.1 – Schematic representation of a phase resetting experiment for oscillators. (Top) In isolation condition (closed system), the observable event (vertical arrow) occurs every  $T$  units of time. (Bottom) Under the effect of a stimulus (phase resetting input) at time  $(t_s - \hat{t}_0)$  after an event, the successive observable event times  $\hat{t}_i$  (for  $i = 1, 2, \dots$ ) are altered.  $\hat{T} := \hat{t}_1 - \hat{t}_0$  denotes the time interval between the pre- and post-stimulus events. Under the simplifying assumption that the prior rhythm is restored immediately after the first post-stimulus event and, using normalized time, the perturbation in timing is modeled by the phase shift  $\Delta\theta := 2\pi - \hat{\tau}$  (wrapped in  $[-\pi, \pi)$ ) or the new phase  $\theta^+ := 2\pi - (\hat{\tau} - \theta) \pmod{2\pi}$ . The phase shift  $\Delta\theta$  measures the phase difference between the perturbed and unperturbed oscillators. The new phase  $\theta^+$  is the phase (at time  $t_s$ ) from which the oscillator appears to resume.

An alternative representation emphasizes the new phase  $\theta^+$  instead of the phase difference. Just before the stimulus the oscillator had reached phase  $\theta$ ; just after, it appears to resume from the new phase  $\theta^+$ . The new phase  $\theta^+$  is given by

$$\theta^+ := 2\pi - (\hat{\tau} - \theta) \pmod{2\pi}. \quad (3.2)$$

Given a phase resetting input  $u(\cdot)$ , the dependence of the new phase  $\theta^+$  on the phase  $\theta$  at which the stimulus was delivered is called the phase transition curve (PTC). We denote it by  $R(\theta; u(\cdot))$ , mimicking the notation for the phase response curve.

Under our approximation that the initial rhythm is recovered immediately after the perturbation, the phase shift computed from the first post-stimulus event is identical to the asymptotic phase shift computed long after the perturbation. This assumption neglects the transient change in the rhythm until a new steady-state is reached. To model the transient, we call  $\hat{\tau}_i := \omega(\hat{t}_i - \hat{t}_0)$  the normalized time from the event before the stimulus to the  $i$ th event, which leads to the phase shift  $\Delta\hat{\theta}_i := 2\pi - \hat{\tau}_i$  (wrapped in  $[-\pi, \pi)$ ) and the new phase  $\hat{\theta}_i^+ := 2\pi - (\hat{\tau}_i - \theta) \pmod{2\pi}$ . If the oscillating phenomenon is time-invariant, we expect an asymptotic new steady-state behavior such that  $\lim_{i \rightarrow \infty} (\hat{\tau}_{i+1} - \hat{\tau}_i) = 2\pi$ ,  $\lim_{i \rightarrow \infty} \Delta\hat{\theta}_i =: \Delta\theta$ , and  $\lim_{i \rightarrow \infty} \hat{\theta}_i^+ =: \theta^+$ .

*Remark.* The operator  $\text{wrap} : \mathbb{R} \rightarrow [-\pi, \pi) : \Delta\theta \mapsto [\Delta\theta + \pi \pmod{2\pi}] - \pi$  wraps any phase difference  $\Delta\theta \in \mathbb{R}$  into the principal interval  $[-\pi, \pi)$ . It plays a similar role to the modulo  $2\pi$  operator that maps any real number on the principal interval  $[0, 2\pi)$ .

## 3.2 Phase response curves from state-space models

In this section, we review the mathematical characterization of phase response curves for oscillators described by time-invariant state-space models. We first recall basic definitions about periodic orbits in state-space models of open dynamical systems. Then, we introduce the concept of phase maps and isochrons that are key players in the study of oscillators on the unit circle and we illustrate them with simple examples. Finally we define phase response curves as steady-state input-output characteristics of oscillators.

### 3.2.1 State-space models

We consider open dynamical systems described by *nonlinear time-invariant state-space models* (see [44, 72, 92, 161] for details)

$$\dot{x} = f(x, u) \quad (3.3a)$$

$$y = h(x) \quad (3.3b)$$

where *state variables*  $x(t)$  evolve on some subset  $\mathcal{X} \subseteq \mathbb{R}^n$ , and *input* values  $u(t)$  and *output* values  $y(t)$  belong to some subsets  $\mathcal{U} \subseteq \mathbb{R}$  and  $\mathcal{Y} \subseteq \mathbb{R}$ , respectively. The states  $(x_1, \dots, x_n)$  typically represent internal variables involved in the system dynamics. They may be concentrations of chemical species (e.g. mRNA or proteins), or the membrane potential and the gating variables of a neuron. The input variable  $u$  can be seen as an external signal that acts as a stimulus. It may represent the action of the light or the action of the applied current. The output variable  $y$  can be thought of as a describing response that allows a partial read-out of the system state vector  $(x_1, \dots, x_n)$ . For example, it may be a measurement provided by a green fluorescent protein or by an electrode.

The *vector field*  $f : \mathcal{X} \times \mathcal{U} \rightarrow \mathbb{R}^n$  and the *measurement map*  $h : \mathcal{X} \rightarrow \mathcal{Y}$  support all the usual smoothness conditions that are necessary for existence and uniqueness of solutions. The *input signal*  $u : [0, \infty) \rightarrow \mathcal{U}$  is locally essentially compact (i.e. images of restrictions to finite intervals are compact). We write  $\phi(t, x_0, u(\cdot))$  for the *solution* at time  $t$  to the initial value problem  $\dot{x} = f(x, u)$  with the initial condition  $x_0 \in \mathcal{X}$  at time 0, that is,  $\phi(0, x_0, u(\cdot)) = x_0$ . (For presentation convenience, we consider single-input and single-output systems. All developments can be easily generalized to multiple-input and multiple-output systems.)

An *oscillator* is an open dynamical system whose zero-input steady-state behavior is periodic rather than constant. Formally, we assume that the zero-input system  $\dot{x} = f(x, 0)$  admits a locally hyperbolic stable *periodic orbit*  $\gamma \subseteq \mathcal{X}$ . Picking an initial condition  $x_0^\gamma$  on the periodic orbit  $\gamma$ , we describe the entire invariant set by the locus of the (nonconstant)  $T$ -periodic solution  $\phi(\cdot, x_0^\gamma, \mathbf{0})$ , that is,

$$\gamma := \{x \in \mathcal{X} : x = \phi(t, x_0^\gamma, \mathbf{0}), t \in [0, T)\}, \quad (3.4)$$

where the *period*  $T > 0$  is the smallest positive constant such that  $\phi(t, x_0^\gamma, \mathbf{0}) = \phi(t + T, x_0^\gamma, \mathbf{0})$  for all  $t \geq 0$  (and where  $\mathbf{0}$  is the input identically equal to 0). The corresponding *angular frequency*  $\omega$  is given by  $\omega = 2\pi/T$ .

The *basin of attraction* of  $\gamma$  (or oscillator stable set) is the maximal open set from which the periodic orbit  $\gamma$  attracts, that is,

$$\mathcal{B}(\gamma) := \left\{ x_0 \in \mathcal{X} : \lim_{t \rightarrow +\infty} \text{dist}(\phi(t, x_0, \mathbf{0}), \gamma) = 0 \right\} \quad (3.5)$$

where  $\text{dist}(x, \gamma) := \inf_{y \in \gamma} \|x - y\|_2$  is the distance from the point  $x \in \mathcal{X}$  to the set  $\gamma \subseteq \mathcal{X}$  based on the Euclidean norm  $\|\cdot\|_2$  in  $\mathbb{R}^n$ .

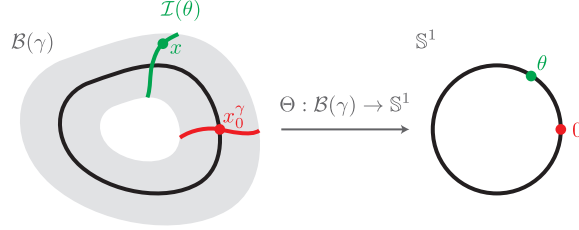


Figure 3.2 – Phase maps and isochrons. The asymptotic phase map  $\Theta : \mathcal{B}(\gamma) \rightarrow \mathbb{S}^1$  associates with each point  $x$  in the basin  $\mathcal{B}(\gamma)$  a scalar phase  $\Theta(x) = \theta$  on the unit circle  $\mathbb{S}^1$  such that  $\lim_{t \rightarrow +\infty} \|\phi(t, x, \mathbf{0}) - \phi(t + \theta/\omega, x_0^\gamma, \mathbf{0})\|_2 = 0$ . The image of  $x_0^\gamma$  through the phase map  $\Theta$  is equal to 0. The set of points associated with the same phase  $\theta$  (i.e. a level set of the phase map) is called an isochron and is denoted by  $\mathcal{I}(\theta)$ .

### 3.2.2 Phase maps and isochrons

The concept of phase maps, as well as the notion of isochrons, are important ingredients to study oscillator models. The brief exposition of phase maps given below follows the terminology and definitions of [60, 195]. Some notations are illustrated in Figure 3.2.

Since the periodic orbit  $\gamma$  is a one-dimensional manifold in  $\mathbb{R}^n$ , it is homeomorphic to the unit circle  $\mathbb{S}^1$ . It is thus naturally parametrized in terms of a single scalar phase. The smooth bijective *phase map*  $\Theta : \gamma \rightarrow \mathbb{S}^1$  associates with each point  $x$  on the periodic orbit  $\gamma$  its phase  $\Theta(x) =: \vartheta$  on the unit circle  $\mathbb{S}^1$ , such that,

$$x - \phi(\vartheta/\omega, x_0^\gamma, \mathbf{0}) = 0. \quad (3.6)$$

This mapping is constructed such that the image of the reference point  $x_0^\gamma$  is equal to 0 (i.e.  $\Theta(x_0^\gamma) := 0$ ) and the progression along the periodic orbit (in absence of perturbation) produces a constant increase in  $\vartheta$ . The *phase variable*  $\vartheta : \mathbb{R}_{\geq 0} \rightarrow \mathbb{S}^1$  is defined along each zero-input trajectory  $\phi(\cdot, x_0, \mathbf{0})$  starting from a point  $x_0$  on the periodic orbit  $\gamma$ , as  $\vartheta(t) := \Theta(\phi(t, x_0, \mathbf{0})) = \omega t + \Theta(x_0)$  for all times  $t \geq 0$ . The phase dynamics are thus given by  $\dot{\vartheta} = \omega$ .

For a hyperbolic stable periodic orbit, the notion of phase can be extended to any point  $x$  in the basin  $\mathcal{B}(\gamma)$  by defining the concept of asymptotic phase. The *asymptotic phase map*  $\Theta : \mathcal{B}(\gamma) \rightarrow \mathbb{S}^1$  associates with each point  $x$  in the basin  $\mathcal{B}(\gamma)$  its asymptotic phase  $\Theta(x) =: \theta$  on the unit circle  $\mathbb{S}^1$ , such that,

$$\lim_{t \rightarrow +\infty} \|\phi(t, x, \mathbf{0}) - \phi(t, \phi(\theta/\omega, x_0^\gamma, \mathbf{0}), \mathbf{0})\|_2 = 0. \quad (3.7)$$

Again, this mapping is constructed such that the image of  $x_0^\gamma$  is equal to  $\mathbf{0}$  and such that the progression along any orbit in  $\mathcal{B}(\gamma)$  (in absence of perturbation) produces a constant increase in  $\theta$ . The *asymptotic phase variable*  $\theta : \mathbb{R}_{\geq 0} \rightarrow \mathbb{S}^1$  is defined along each zero-input trajectory  $\phi(\cdot, x_0, \mathbf{0})$  starting from a point  $x_0$  in the basin of attraction of  $\gamma$ , as  $\theta(t) := \Theta(\phi(t, x_0, \mathbf{0})) = \omega t + \Theta(x_0)$  for all times  $t \geq 0$ . The asymptotic phase dynamics are thus given by  $\dot{\theta} = \omega$ .

The notion of asymptotic phase variable can be extended to any nonzero-input trajectory  $\phi(\cdot, x_0, u(\cdot))$  in the basin  $\mathcal{B}(\gamma)$ . In this case, the asymptotic phase variable is defined as  $\theta(t) := \Theta(\phi(t, x_0, u(\cdot)))$  for all times  $t \geq 0$ . The asymptotic phase dynamics in the case of a nonzero input is hard to derive in general.

*Remark.* For notational convenience, we also introduce the map  $x^\gamma : \mathbb{S}^1 \rightarrow \gamma$  which associates with each phase  $\theta$  on the unit circle a point  $\phi(\theta/\omega, x_0^\gamma, \mathbf{0}) =: x^\gamma(\theta)$  on the periodic orbit. By construction, this map is a re-parametrization of the periodic trajectory starting from the initial condition  $x_0^\gamma$ . It is equal to the inverse of the phase map, that is,  $x^\gamma(\cdot) = \Theta^{-1}(\cdot)$ .

Level sets of the asymptotic phase map  $\Theta$ , that is, sets of all points in the basin of  $\gamma$  with the same asymptotic phase, are termed *isochrons*. Formally, the *isochron*  $\mathcal{I}(\theta)$  associated with the asymptotic phase  $\theta$  is the set

$$\mathcal{I}(\theta) := \{x \in \mathcal{B}(\gamma) : \Theta(x) = \theta\}. \quad (3.8)$$

Considering hyperbolic periodic orbits, isochrons are codimension-1 submanifolds (diffeomorphic to  $\mathbb{R}^{n-1}$ ) crossing the periodic orbit transversally and foliating the entire basin of attraction [71].

In general, the structure of the (asymptotic) phase maps and their isochrons are very complex. This often makes their analytical computation impossible and even their numerical computation intractable (or at least very expensive, in particular for high-dimensional oscillator models). Most numerical techniques relies on backward integration [75, 135, 158]. Recently, Mauroy and Mezić developed an elegant forward integration method [121] and extended this notion to stable fixed points [122].

In the following, we illustrate the notion of phase maps on simple examples.

**Example 1** (Integrate-and-fire oscillators). The integrate-and-fire dynamics are expressed as one-dimensional state dynamics between two threshold values (see [1, 93]): a scalar state variable  $x$  monotonically increases between two thresholds  $\underline{x}$  and  $\bar{x}$ , according to the dynamics

$$\dot{x} = f(x), \quad \text{with } f(x) > 0, \quad (3.9)$$

for all  $x \in [\underline{x}, \bar{x}]$ . Upon reaching the upper threshold  $\bar{x}$ , the state is instantaneously reset to the lower threshold  $\underline{x}$ . Roughly speaking, the oscillator integrates between the two thresholds and fires when reaching the upper threshold.

The asymptotic phase map  $\Theta$  that corresponds to the integrate-and-fire dynamics is the bijective change of variable given by

$$\Theta(x) : x \mapsto \omega \int_{\underline{x}}^x \frac{1}{f(\xi)} d\xi, \quad (3.10)$$

with the lower threshold  $\underline{x}$  (resp. the upper threshold  $\bar{x}$ ) being mapped to  $\theta = 0$  (resp.  $\theta = 2\pi$ ).

**Example 2** (Oscillators in polar coordinates). The simplest form of two-dimensional oscillators is expressed in polar coordinates

$$\dot{\psi} = f_{\psi}(\psi, r) \quad (3.11a)$$

$$\dot{r} = f_r(\psi, r) \quad (3.11b)$$

where  $\psi \in \mathbb{S}^1$  is a geometric phase on the circle and  $r > 0$  is a positive radius. Assuming the existence of  $\bar{r}$  such that  $f_r(\psi, \bar{r}) = 0$  and  $(\partial f_r / \partial r)(\psi, \bar{r}) < 0$  guarantees the existence of a periodic orbit with  $r = \bar{r}$ . Additional symmetry assumptions on the vector fields yield isochrons preserving this symmetry.

*Radial symmetry.* We assume the radial symmetry of the geometric phase vector field, that is,  $\dot{\psi} = f_{\psi}(\psi, r) = f_{\psi}(\psi)$ . The isochrons must preserve this radial symmetry. Then, we have  $\Theta(\psi, r) = \Xi(\psi)$  where  $\Xi : \mathbb{S}^1 \rightarrow \mathbb{S}^1$  is a scalar function to be determined. The function  $\Xi(\cdot)$  is derived from the geometric phase dynamics and we have  $\Xi(\psi) = \omega \int_0^{\psi} \frac{1}{f_{\psi}(\xi)} d\xi$ .

The asymptotic phase map  $\Theta$  that corresponds to a two-dimensional dynamics with radial symmetry of the geometric phase vector field is the change of variable given by

$$\Theta(\psi, r) : (\psi, r) \mapsto \omega \int_0^{\psi} \frac{1}{f_{\psi}(\xi)} d\xi. \quad (3.12)$$

Points  $(0, \bar{r})$  with a geometric phase equal to 0 are mapped to 0, that is,  $\Theta(0, r) = 0$  for all  $r > 0$ .

*Polar symmetry.* We assume the polar symmetry of the vector field, that is,  $\dot{\psi} = f_{\psi}(\psi, r) = f_{\psi}(r)$  and  $\dot{r} = f_r(\psi, r) = f_r(r)$ . The isochrons must preserve this polar symmetry. Then, we have  $\Theta(\psi, r) = \psi - \Xi(r)$  where  $\Xi : \mathbb{R} \rightarrow \mathbb{R}$  is a scalar function to be determined. Differentiating the aforementioned expression with regard to time, we get  $\frac{d\Theta}{dt}(\psi, r) = \frac{d\psi}{dt} - \frac{\partial \Xi}{\partial r}(r) \frac{dr}{dt} = \omega$  since all points on the isochron move with the same frequency  $\omega$ . Rearranging terms, we have  $\frac{\partial \Xi}{\partial r}(r) = [f_{\psi}(r) - \omega] / f_r(r)$  and the scalar function  $\Xi(\cdot)$  is given by  $\Xi(r) =$

$\Xi(\bar{r}) + \int_{\bar{r}}^T \{[f_\psi(\xi) - \omega] / f_r(\xi)\} d\xi$ . Due to the polar symmetry, the geometric phase evolves at a constant speed on the periodic orbit ( $r = \bar{r}$ ). The geometric phase is thus equal to the temporal phase on the periodic orbit ( $r = \bar{r}$ ). So we may enforce  $\Theta(\psi, \bar{r}) = \psi$  on the periodic orbit ( $r = \bar{r}$ ) and it yields  $\Xi(\bar{r}) = 0$ .

The asymptotic phase map  $\Theta$  that corresponds to a two-dimensional dynamics with polar symmetry is the change of variable given by

$$\Theta(\psi, r) : (\psi, r) \mapsto \psi - \int_{\bar{r}}^r \frac{f_\psi(\xi) - \omega}{f_r(\xi)} d\xi. \quad (3.13)$$

### 3.2.3 Response to phase resetting inputs

In many situations, the global knowledge of the asymptotic phase map is not required to study oscillator dynamics. Instead, a local asymptotic phase model may be computed from the information obtained through phase resetting experiments.

A *phase resetting input*  $u(\cdot)$  is such that, for an initial condition  $x_0$ , the perturbed solution starting from  $x_0$  asymptotically converges to a phase shifted periodic solution with initial condition  $x_0^\gamma$  and zero input, that is,

$$\lim_{t \rightarrow \infty} \|\phi(t, x_0, u(\cdot)) - \phi(t + \theta^+ / \omega, x_0^\gamma, \mathbf{0})\|_2 = 0 \quad (3.14)$$

where  $\theta^+ \in \mathbb{S}^1$ .

We define the *basin of attraction of  $\gamma$  under a phase resetting input  $u(\cdot)$*  as the maximal open set from which the periodic orbit  $\gamma$  asymptotically attracts, that is,

$$\mathcal{B}(\gamma; u(\cdot)) := \left\{ x_0 \in \mathcal{X} : \lim_{t \rightarrow +\infty} \text{dist}(\phi(t, x_0, u(\cdot)), \gamma) = 0 \right\}. \quad (3.15)$$

Given a phase resetting input  $u(\cdot)$ , the *asymptotic reset phase map*  $\Theta^+ : \mathcal{B}(\gamma; u(\cdot)) \rightarrow \mathbb{S}^1$  associates with each point  $x$  in the set  $\mathcal{B}(\gamma; u(\cdot))$  its asymptotic reset phase  $\Theta^+(x; u(\cdot)) =: \theta^+$  on the unit circle  $\mathbb{S}^1$ , see (3.14). The notation stresses that this map is a function of the initial condition which also depends on the input  $u(\cdot)$ .

*Remark.* Any input signal converging asymptotically to zero and such that the trajectory stays in the basin  $\mathcal{B}(\gamma)$  is a phase resetting input.

*Remark.* The asymptotic reset phase  $\Theta^+(x; u(\cdot))$  may also be thought of as the initial phase of an unperturbed system from which the reset trajectory appears to resume. It is trivial that

$$\Theta^+(x; u(\cdot)) = \lim_{t \rightarrow +\infty} \Theta(\phi(-t, \phi(t, x, u(\cdot)), \mathbf{0})) \quad (3.16)$$

$$= \lim_{t \rightarrow +\infty} [\Theta(\phi(t, x, u(\cdot))) - \omega t] \pmod{2\pi}. \quad (3.17)$$

For an impulse ( $u(\cdot) = \alpha \delta(\cdot)$ ), we have

$$\Theta^+(x; \alpha \delta(\cdot)) = \lim_{t \rightarrow 0^+} \Theta(\phi(t, x, \alpha \delta(\cdot))). \quad (3.18)$$

For a pulse of finite duration ( $u(\cdot) = \alpha(\cdot) [1_+(\cdot) - 1_+(\cdot - \Delta)]$ ), we have

$$\Theta^+(x; u(\cdot)) = \Theta(\phi(\Delta, x, \alpha(\cdot))) - \omega \Delta \pmod{2\pi}. \quad (3.19)$$

**Definition 1.** Given a phase resetting input  $u(\cdot)$ , the (*finite*) *phase response curve* (PRC) is the map  $Q(\cdot; u(\cdot)) : \mathbb{S}^1 \rightarrow [-\pi, \pi)$  which associates with each phase  $\theta$  a phase shift  $\Delta\theta = Q(\theta; u(\cdot))$  defined as

$$Q(\theta; u(\cdot)) := \Theta^+(x^\gamma(\theta); u(\cdot)) - \theta \pmod{[-\pi, \pi)} \quad (3.20)$$

Similarly, the phase transition curve (PTC) is the map  $R(\cdot; u(\cdot)) : \mathbb{S}^1 \rightarrow \mathbb{S}^1$  which associates with each phase  $\theta$  the new phase  $\theta^+ = R(\theta; u(\cdot))$  defined as

$$R(\theta; u(\cdot)) := \Theta^+(x^\gamma(\theta); u(\cdot)) \quad (3.21)$$

A mathematically more abstract—yet very useful—tool is the infinitesimal phase response curve. It captures the same information in the limit of Dirac delta input with infinitesimally small amplitude (i.e.  $u(\cdot) = \alpha \delta(\cdot)$  with  $\alpha \rightarrow 0$ ).

**Definition 2.** The (*input*) *infinitesimal phase response curve* (iPRC) is the map  $q : \mathbb{S}^1 \rightarrow \mathbb{R}$  defined as the directional derivative

$$q(\theta) := D\Theta(x^\gamma(\theta)) \left[ \frac{\partial f}{\partial u}(x^\gamma(\theta), 0) \right] \quad (3.22)$$

where

$$D\Theta(x)[\eta] := \lim_{h \rightarrow 0} \frac{\Theta(x + h\eta) - \Theta(x)}{h}. \quad (3.23)$$

The directional derivative can be computed as the inner product in  $\mathbb{R}^n$

$$q(\theta) = D\Theta(x^\gamma(\theta)) \left[ \frac{\partial f}{\partial u}(x^\gamma(\theta), 0) \right] = \left\langle \nabla_x \Theta(x^\gamma(\theta)), \frac{\partial f}{\partial u}(x^\gamma(\theta), 0) \right\rangle \quad (3.24)$$

where  $\nabla_x \Theta(x^\gamma(\theta))$  is the gradient of the asymptotic phase map  $\Theta$  at the point  $x^\gamma(\theta)$ . The map  $p : \mathbb{S}^1 \rightarrow \mathbb{R}^n$  which associates with each phase  $\theta$  the gradient of the asymptotic map  $\Theta$  at the point  $x^\gamma(\theta)$ , that is,

$$p(\theta) := \nabla_x \Theta(x^\gamma(\theta)), \quad (3.25)$$

is the *state infinitesimal phase response curve*.

*Remark.* The phase response curve  $Q(\cdot; \alpha \delta(\cdot))$  for impulse of small amplitude (i.e.  $\alpha \ll 1$ ) is, by definition, well approximated by the infinitesimal phase response curve, that is,  $Q(\cdot; \alpha \delta(\cdot)) = \alpha q(\cdot) + \mathcal{O}(\alpha^2)$ .

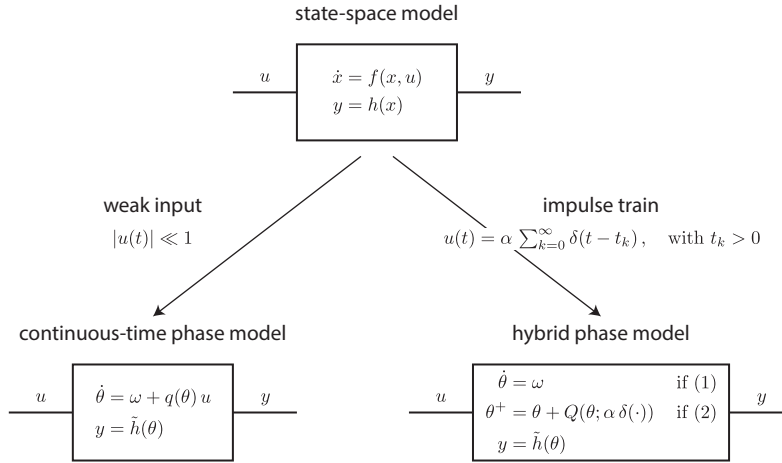


Figure 3.3 – Phase models for single oscillators. For weak inputs, phase reduction methods lead to continuous-time phase models characterized by  $\{\omega, q(\cdot), \tilde{h}(\cdot)\}$ . For impulse trains, phase reduction methods lead to hybrid phase models characterized by  $\{\omega, Q(\cdot; \alpha \delta(\cdot)), \tilde{h}(\cdot)\}$  (where (1) stands for  $t \neq t_k$  and (2) stands for  $t = t_k$ )

### 3.3 Phase response curves in phase models

In this section, we show the utility of the phase response curves in canonical phase models for single oscillators and then for coupled oscillators. Our presentation is informal and we refer to the pioneering papers [43, 100, 126, 193] and the books [60, 85, 89, 155, 195] for further details.

#### 3.3.1 Phase models for single oscillators

We review two popular phase models, which are obtained through phase reduction methods in the case of weak inputs and impulse trains, respectively (see Figure 3.3).

##### Weak input

A popular simplification arises when the input signal is weak, that is,

$$|u(t)| \ll 1, \quad \text{for all } t \geq 0. \quad (3.26)$$

Any solution  $\phi(t, x_0, u(\cdot))$  of the oscillator model which starts in a small neighborhood of the hyperbolic stable periodic orbit  $\gamma$  stays in its neighborhood.

The  $n$ -dimensional state-space model can thus be approximated by a *one-dimensional continuous-time phase model* (see [43, 85, 89, 100, 155, 193, 195])

$$\dot{\theta} = \omega + q(\theta) u \quad (3.27a)$$

$$y = \tilde{h}(\theta) \quad (3.27b)$$

where the phase variable  $\theta$  evolves on the unit circle  $\mathbb{S}^1$ . This continuous-time phase model is fully characterized by the angular frequency  $\omega > 0$ , the infinitesimal phase response curve  $q : \mathbb{S}^1 \rightarrow \mathbb{R}$  and the measurement map  $\tilde{h} : \mathbb{S}^1 \rightarrow \mathcal{Y}$  defined as  $\tilde{h}(\theta) = (h \circ x^\gamma)(\theta)$ .

### Impulse train

Another simplification arises when the input signal is an impulse train, that is,

$$u(t) = \alpha \sum_{k=0}^{\infty} \delta(t - t_k), \quad \text{with } t_k > 0. \quad (3.28)$$

Any solution  $\phi(t, x_0, u(\cdot))$  of the oscillator model which starts from the periodic orbit  $\gamma$  leaves the periodic orbit under the effect of an impulse and converges back to the periodic orbit. If the steady-state of the periodic orbit is recovered between any two successive impulses, the  $n$ -dimensional state-space model can be approximated by a *one-dimensional hybrid phase model* (see [60, 89, 123]), with

1. the (constant-time) flow rule

$$\dot{\theta} = \omega, \quad \text{for all } t \neq t_k, \quad (3.29a)$$

2. the (discrete-time) jump rule (i.e. the kick)

$$\theta^+ = \theta + Q(\theta; \alpha \delta(\cdot)), \quad \text{for all } t = t_k, \quad (3.29b)$$

3. the measurement map

$$y = \tilde{h}(\theta), \quad \text{for all } t, \quad (3.29c)$$

where the phase variable  $\theta$  evolves on the unit circle  $\mathbb{S}^1$ . This hybrid phase model is fully characterized by the angular frequency  $\omega > 0$ , the phase response curve  $Q(\cdot; \alpha \delta(\cdot)) : \mathbb{S}^1 \rightarrow [-\pi, \pi)$  and the measurement map  $\tilde{h} : \mathbb{S}^1 \rightarrow \mathcal{Y}$ .

### 3.3.2 Phase models for coupled oscillators

Most collective phenomena among oscillators in nature arise in large networks of oscillators. Each oscillator dynamics is written, for  $i = 1, \dots, N$ , as

$$\dot{x}_i = f_i(x_i, u_i), \quad (3.30a)$$

$$y_i = h_i(x_i). \quad (3.30b)$$

and the general interconnection is given by

$$u_i = K_i(y_1, \dots, y_N), \quad i = 1, \dots, N, \quad (3.31)$$

where  $K_i(\cdot) : \mathcal{Y}_1 \times \dots \times \mathcal{Y}_N \rightarrow \mathcal{U}_i$  are coupling functions. For presentation convenience, we define the re-parametrized coupling functions  $\tilde{K}_i(\cdot)$  such that

$$u_i = \tilde{K}_i(\theta_1, \dots, \theta_N), \quad i = 1, \dots, N, \quad (3.32)$$

where  $\tilde{K}_i(\cdot) : \mathbb{T}^N \rightarrow \mathcal{U}_i$  is given by  $\tilde{K}_i(\theta_1, \dots, \theta_N) = K_i(\tilde{h}_1(\theta_1), \dots, \tilde{h}_N(\theta_N))$ .

Popular coupling models are particular cases of this general formulation. The diffusive coupling model is such that

$$u_i = \sum_{j \in \mathcal{N}_i} \alpha_{ij} (y_j - y_i) = \sum_{j \in \mathcal{N}_i} \alpha_{ij} (\tilde{h}_j(\theta_j) - \tilde{h}_i(\theta_i)), \quad i = 1, \dots, N, \quad (3.33)$$

where  $\alpha_{ij}$  are positive constant and  $\mathcal{N}_i \subseteq \mathcal{N}$  is the subset of oscillators transmitting their outputs to the  $i$ th oscillator. (The set  $\mathcal{N} = \{1, \dots, N\}$  denotes all oscillators in the network.)

The impulsive coupling model is such that

$$u_i = \sum_{j \in \mathcal{N}_i} \alpha_{ij} \sum_{k=0}^{\infty} \delta(t - t_k^j), \quad \text{with } \theta_j(t_k^j) = 0 \text{ for } j \in \mathcal{N}_i, \quad (3.34)$$

where  $\alpha_{ij}$  is a positive constant for excitatory impulses or a negative constant for inhibitory impulses and  $\mathcal{N}_i \subseteq \mathcal{N} \setminus \{i\}$  is the subset of oscillators transmitting a kick to the  $i$ th oscillator.

In the following, we illustrate how the phase response curve is involved in the phase description of those networks. For simplicity, we consider the case of two coupled oscillators. (The general case can be found in [85, 101, 123] for the weak coupling and in [123, 124, 126] for the impulsive coupling.)

#### Weak coupling

We follow similar lines as in [101] (see also in [85]).

Under weak coupling, it follows from (3.27) and (3.32) that the oscillators are characterized by the continuous-time phase dynamics (note that the coupling does not need to be diffusive)

$$\dot{\theta}_1 = \omega_1 + q_1(\theta_1) \tilde{K}_1(\theta_1, \theta_2), \quad (3.35a)$$

$$\dot{\theta}_2 = \omega_2 + q_2(\theta_2) \tilde{K}_2(\theta_1, \theta_2). \quad (3.35b)$$

The angular frequencies can be decomposed as  $\omega_i = \Omega_i + \Delta_i$ , such that  $\Omega_1 = \Omega_2 = \Omega$  and the phases can be decomposed as  $\theta_i = \Omega_i t + \varphi_i$ , where  $\varphi_i$  are slow phase deviations from the uniform natural oscillation  $\Omega_i t$ . Then, the phase dynamics are rewritten as

$$\dot{\varphi}_1 = \Delta_1 + q_1(\Omega_1 t + \varphi_1) \tilde{K}_1(\Omega_1 t + \varphi_1, \Omega_2 t + \varphi_2), \quad (3.36a)$$

$$\dot{\varphi}_2 = \Delta_2 + q_2(\Omega_2 t + \varphi_2) \tilde{K}_2(\Omega_1 t + \varphi_1, \Omega_2 t + \varphi_2). \quad (3.36b)$$

Note that  $q_i(\cdot)$  and  $\tilde{K}_i(\cdot)$  are considered here as the  $2\pi$ -periodic extension of the infinitesimal phase response curves and of the coupling functions on the real line, i.e.  $q_i(x) \equiv q_i(x \bmod 2\pi)$  and  $\tilde{K}_i(x, y) \equiv \tilde{K}_i(x \bmod 2\pi, y \bmod 2\pi)$ . Next, averaging the above dynamics over the period  $T = 2\pi/\Omega$  and under fixed  $\varphi_1$  and  $\varphi_2$ , we obtain

$$\dot{\varphi}_1 = \Delta_1 + L_1(\varphi_1, \varphi_2), \quad (3.37a)$$

$$\dot{\varphi}_2 = \Delta_2 + L_2(\varphi_1, \varphi_2), \quad (3.37b)$$

where the averaged functions  $L_1(\varphi_1, \varphi_2)$  and  $L_2(\varphi_1, \varphi_2)$  are given by

$$L_1(\varphi_1, \varphi_2) = \frac{1}{T} \int_0^T q_1(\Omega_1 t + \varphi_1) \tilde{K}_1(\Omega_1 t + \varphi_1, \Omega_2 t + \varphi_2) dt, \quad (3.38a)$$

$$L_2(\varphi_1, \varphi_2) = \frac{1}{T} \int_0^T q_2(\Omega_2 t + \varphi_2) \tilde{K}_2(\Omega_1 t + \varphi_1, \Omega_2 t + \varphi_2) dt. \quad (3.38b)$$

Using simple changes of variable, we have

$$\Gamma_1(\varphi_1 - \varphi_2) := L_1(\varphi_1, \varphi_2) = \frac{1}{2\pi} \int_0^{2\pi} q_1(s) \tilde{K}_1(s, s - (\varphi_1 - \varphi_2)) ds, \quad (3.39a)$$

$$\Gamma_2(\varphi_2 - \varphi_1) := L_2(\varphi_1, \varphi_2) = \frac{1}{2\pi} \int_0^{2\pi} q_2(s) \tilde{K}_2(s - (\varphi_2 - \varphi_1), s) ds. \quad (3.39b)$$

Finally, it is convenient to define the phase difference  $\chi = \varphi_2 - \varphi_1$ . The phase difference dynamics is given by

$$\dot{\chi} = \Delta + \Gamma(\chi) \quad (3.40)$$

with  $\Delta := \Delta_2 - \Delta_1$  and  $\Gamma(\chi) := \Gamma_2(\varphi_2 - \varphi_1) - \Gamma_1(\varphi_1 - \varphi_2)$ .

The shape of the phase response curves  $q_1(\cdot)$  and  $q_2(\cdot)$  will affect the shape of the coupling function  $\Gamma(\cdot)$ . They are thus critical to the phase difference dynamics.

*Remark.* The case of entrainment by a periodic signal  $u(\cdot)$  can be seen as a particular case of coupled oscillators. The oscillator 1 plays the role of a periodic signal generator, such that  $u(t) = \tilde{h}_u(\theta_1(t)) = \tilde{h}_1(\theta_1(t))$  with  $\dot{\theta}_1 = \omega_u$ , and the oscillator 2 is the entrained system. The coupling functions are  $K_1(\theta_1, \theta_2) = 0$  and  $K_2(\theta_1, \theta_2) = \tilde{h}_1(\theta_1)$ . The coupling function  $\Gamma$  is thus given by

$$\Gamma(\chi) = \frac{1}{2\pi} \int_0^{2\pi} q_2(s + \chi) \tilde{h}_1(s) ds. \quad (3.41)$$

*Remark.* Note that, in general, the case of resonant frequencies  $m_1 \Omega_1 = m_2 \Omega_2$  may also be considered (see [85] for details).

### Impulsive coupling

We follow similar lines as in [126].

Under impulsive coupling, the oscillators are characterized by the hybrid phase dynamics

$$\dot{\theta}_1 = \omega_1, \quad \text{if } \theta_1 \neq 0 \text{ and } \theta_2 \neq 0, \quad (3.42a)$$

$$\dot{\theta}_2 = \omega_2, \quad \text{if } \theta_1 \neq 0 \text{ and } \theta_2 \neq 0, \quad (3.42b)$$

$$\theta_1^+ = \theta_1 + Q_1(\theta_1; \alpha \delta(\cdot)), \quad \text{if } \theta_2 = 0, \quad (3.42c)$$

$$\theta_2^+ = \theta_2 + Q_2(\theta_2; \alpha \delta(\cdot)), \quad \text{if } \theta_1 = 0. \quad (3.42d)$$

Since the oscillators are uncoupled between two kicks, all the information is retained by considering the oscillator states at the discrete kick times only.

For instance, if the configuration of two coupled oscillators right after a kick of oscillator 2 is  $(\theta, 0)$ , then the oscillators flow until the oscillator 1 reaches 0, that is, for a duration  $\frac{1}{\omega_1}(2\pi - \theta)$ . After this flowing period, the phase of oscillator 2 is equal to  $\frac{\omega_2}{\omega_1}(2\pi - \theta)$ . Then, oscillator 1 sends a kick and the configuration right after the kick is given by  $(0, H_2(\theta))$ , with

$$H_2(\theta) = \frac{\omega_2}{\omega_1}(2\pi - \theta) + Q_2\left(\frac{\omega_2}{\omega_1}(2\pi - \theta); \alpha \delta(\cdot)\right) \pmod{2\pi}. \quad (3.43)$$

And, proceeding similarly for a second flowing period until the phase of oscillator 2 reaches 0, we have that the configuration right after the second next kick (that is, the next kick of oscillator 2) is given by  $(H_1(H_2(\theta)), 0)$ , with

$$H_1(\theta) = \frac{\omega_1}{\omega_2}(2\pi - \theta) + Q_1\left(\frac{\omega_1}{\omega_2}(2\pi - \theta); \alpha \delta(\cdot)\right) \pmod{2\pi}. \quad (3.44)$$

The discrete map  $\theta^+ = R(\theta) := (H_1 \circ H_2)(\theta)$  expresses the phase differences between the two oscillators right after the successive kick times of oscillator 2. Maps  $H_1(\cdot)$  and  $H_2(\cdot)$  are known as the firing maps and the map  $R(\cdot)$  is called the return map.

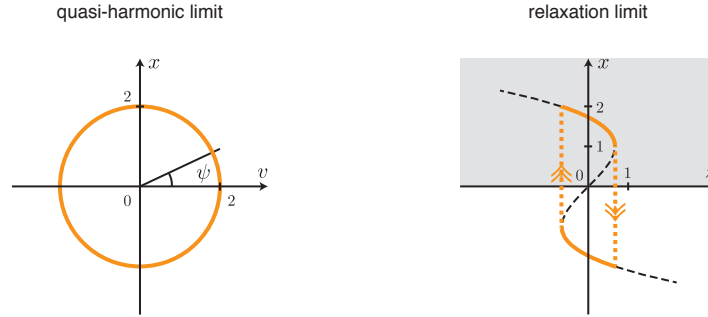


Figure 3.4 – The van der Pol oscillator exhibits two different oscillation regimes: the quasi-harmonic ( $\mu \ll 1$ ) and the relaxation ( $\mu \gg 1$ ) oscillation regimes. Quasi-harmonic and relaxation regimes are displayed in  $(x, v)$  and  $(x, z)$  state-spaces, respectively.

### 3.4 Phase response curves and asymptotic methods

In the following, we derive the phase map and the oscillator dynamics on the circle by exploiting classical asymptotic methods. For presentation convenience, we illustrate the application of the asymptotic methods on the van der Pol oscillator in the quasi-harmonic and relaxation limits (see Figure 3.4). (The general case follows the same steps.)

We consider the van der Pol oscillator forced by an input  $u$

$$\ddot{y} - \mu(1 - y^2)\dot{y} + y = u, \quad u \in \mathbb{R}, \quad y \in \mathbb{R}. \quad (3.45)$$

In both cases, we emphasize the appearance of the infinitesimal phase response curve  $q(\cdot)$  in the phase model.

#### 3.4.1 Averaging theory

To study the van der Pol oscillator in the quasi-harmonic limit, it is convenient to express (2.1) in the state space  $(x, v) = (y, \dot{y})$

$$\dot{x} = v, \quad (3.46a)$$

$$\dot{v} = -x + \mu(1 - x^2)v + u. \quad (3.46b)$$

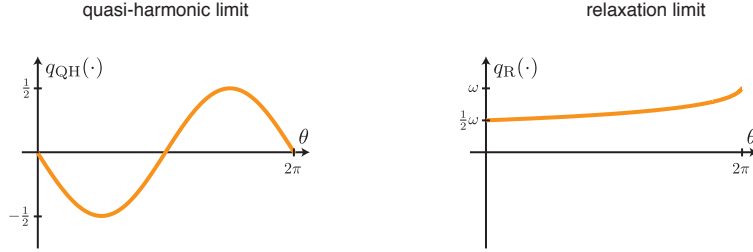


Figure 3.5 – The shape of the infinitesimal phase response curve (for the van der Pol oscillator) is very different in both regimes. Typically, it is harmonic in the weakly nonlinear oscillation regime and monotone (and hence discontinuous) in the relaxation regime.

In polar coordinates  $(x, v) = (r \sin(\psi), r \cos(\psi))$ , dynamics (3.46) read

$$\dot{\psi} = 1 - \frac{\mu}{r} g(r \sin(\psi), r \cos(\psi)) \sin(\psi) - \frac{1}{r} \sin(\psi) u \quad (3.47a)$$

$$\dot{r} = \mu g(r \sin(\psi), r \cos(\psi)) \cos(\psi) + \cos(\psi) u \quad (3.47b)$$

where we denote  $g(y, \dot{y}) = (1 - y^2) \dot{y}$  to simplify notations.

For small values of  $\mu \ll 1$  and for weak inputs  $|u(t)| \ll 1$  for all  $t \geq 0$ , standard averaging theory guarantees that  $r$  stays in a  $\mathcal{O}(\mu, |u(t)|)$ -neighborhood of  $r^* = 2$  (see [92] for details). Substituting  $r$  by  $\tilde{r} = 2 + \mathcal{O}(\mu, |u(t)|)$  into (3.47a) and keeping first-order terms in the equation yield

$$\dot{\psi} \approx 1 - \frac{\mu}{2} g(\tilde{r} \sin(\psi), \tilde{r} \cos(\psi)) \sin(\psi) - \frac{1}{2} \sin(\psi) u. \quad (3.48)$$

The approximately equal sign ( $\approx$ ) means that (3.48) neglects higher order terms in  $(\mu, |u(t)|)$ . This one-dimensional equation describes the dynamics of the angular coordinate  $\psi \in \mathbb{S}^1$ . Note that this (geometric) angular coordinate is different from the (temporal) asymptotic phase defined in (2.8).

Since the angular state dynamics (3.48) are one-dimensional, the asymptotic phase map appears as a bijective change of variable  $\theta = \Theta(\psi)$  given by

$$\Theta(\psi) : \psi \mapsto \omega \int_0^\psi \frac{1}{1 - \frac{\mu}{2} g(\tilde{r} \sin(\xi), \tilde{r} \cos(\xi)) \sin(\xi)} d\xi. \quad (3.49)$$

This change of variable rescales the state-space and the (temporal) phase dynamics are given by

$$\dot{\theta} \approx \frac{\partial \Theta}{\partial \psi} \frac{d\psi}{dt} = \omega + \underbrace{\frac{-\omega \sin(\psi)}{\tilde{r} - \mu g(\tilde{r} \sin(\psi), \tilde{r} \cos(\psi)) \sin(\psi)}}_{=: q_{\text{QH}}(\theta)} u \quad (3.50)$$

where  $\psi = \Theta^{-1}(\theta)$ . The phase dynamics (3.50) are the addition of two terms: the first term represents the autonomous angular frequency and the second term represents the influence of the input on the dynamics. The function  $q_{\text{QH}}(\cdot)$  is the (input) infinitesimal phase response curve. For values of  $\mu$  tending to 0, the asymptotic phase map  $\Theta$  tends to the identity, the angular frequency  $\omega$  tends to 1, and the (input) infinitesimal phase response curve  $q_{\text{QH}}(\theta)$  tends to  $-\frac{1}{2}\sin(\theta)$  (see Figure 3.5, left).

### 3.4.2 Singular perturbation theory

To study the van der Pol oscillator in the relaxation limit, it is convenient to express (2.1) in Liénard's coordinates  $(x, z) = (y, y - y^3/3 - \dot{y}/\mu)$  as

$$\frac{1}{\mu^2}x' = x - x^3/3 - z \quad (3.51a)$$

$$z' = x - u \quad (3.51b)$$

where the symbol  $'$  denotes the derivative with respect to  $s = t/\mu$ .

For large values of  $\mu$  ( $1/\mu^2 \ll 1$ ), standard singular perturbation theory reduces the dynamics (3.51) to (see [92] for details)

$$x' = \frac{x}{1-x^2} - \frac{1}{1-x^2}u \quad (3.52)$$

on the critical manifold defined by  $z = x - x^3/3$  and to instantaneous “jumps” at the folds in the critical manifold. Exploiting the central symmetry of the drift vector field (invariance under point reflection through the origin), we reduce the dynamics to the one-dimensional dynamics on the left branch of the critical manifold: the state  $x$  monotonically increases on  $[-2, -1]$  according to (3.52) and is reset to the lower threshold  $\underline{x} = -2$  when reaching the upper threshold  $\bar{x} = -1$ .

Again, since the state dynamics are one-dimensional, there is a bijective change of variable  $\theta = \Theta(x)$  given by

$$\Theta(x) : x \mapsto \omega \int_{\underline{x}}^x \frac{1-\xi^2}{\xi} d\xi. \quad (3.53)$$

This change of variable rescales in such a way that the lower threshold  $\underline{x} = -2$  is mapped to  $\theta = 0$  and the upper threshold  $\bar{x} = -1$  to  $\theta = 2\pi$ . The (temporal) phase dynamics are then given by

$$\theta' = \frac{\partial\Theta}{\partial x} \frac{dx}{ds} = \omega + \underbrace{\left(-\frac{\omega}{x}\right)}_{=:q_{\text{R}}(\theta)} u \quad (3.54)$$

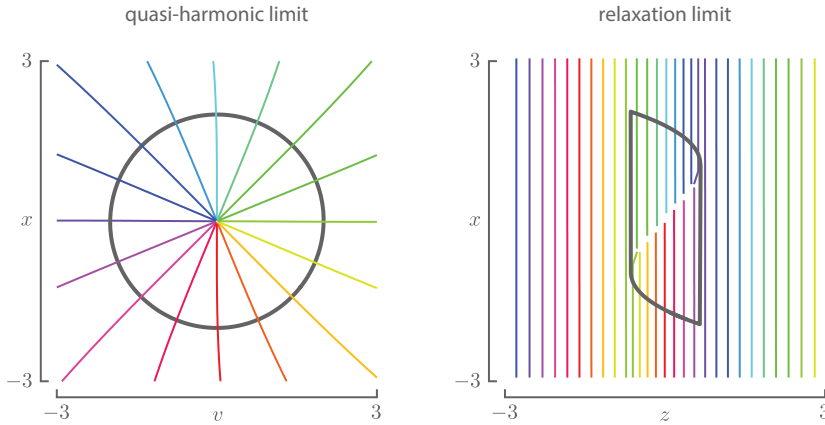


Figure 3.6 – Isochrons of the van der Pol oscillator. (Left) In the quasi-harmonic limit ( $\mu = 0.01$ ), isochrons are radial. (Right) In the relaxation limit ( $\mu = 100$ ), isochrons are parallel to the  $x$ -axis. (The numerical computations have been performed by Alexandre Mauroy [121, 122].)

where  $x = \Theta^{-1}(\theta)$ . Here again, the phase dynamics (3.54) are given by the addition of two terms: the autonomous angular frequency and the coupling term. In this case, the phase sensitivity function (or infinitesimal phase response curve)  $q_R(\cdot)$  is monotone on  $[0, 2\pi)$  (see Figure 3.5, right).

### 3.4.3 Numerical validations

In the following, we validate with numerical computations the geometric intuition of both asymptotic methods.

In the quasi-harmonic limit, the vector field of the geometric phase has a radial symmetry. As a consequence, the isochrons in the state-space  $(x, v)$  must preserve this radial symmetry (see Figure 3.6, left).

In the relaxation limit, the van der Pol oscillator has an instantaneous dynamics in the fast direction (parallel to  $x$ -axis). All trajectories starting with the same initial value  $x_0$  and converging towards the same branch are associated with the same phase. As a consequence, the isochrons in the state-space  $(x, z)$  are parallel to the  $x$ -axis (see Figure 3.6, right). These intuitive arguments are formally stated in Chapter 6.

### 3.5 Computations of phase response curves

For a given state-space model, periodic orbits and phase response curves must be computed numerically. In this section, we review the computation of the periodic orbit and the infinitesimal phase response curve as solutions to boundary value problems. We also provide different methods to compute or approximate the phase response curve associated with a particular phase resetting input.

#### 3.5.1 Periodic orbits

The  $2\pi$ -periodic steady-state solution  $x^\gamma(\cdot)$  and the angular frequency  $\omega$  are calculated by solving the boundary value problem (see [11, 157])

$$\frac{dx^\gamma}{d\theta}(\theta) - \frac{1}{\omega} f(x^\gamma(\theta), 0) = 0 \quad (3.55a)$$

$$x^\gamma(2\pi) - x^\gamma(0) = 0 \quad (3.55b)$$

$$\hat{\varphi}(x^\gamma(0)) = 0 \quad (3.55c)$$

The boundary conditions are given by the periodicity condition (3.55b) which ensures the periodicity of the map  $x^\gamma(\cdot)$  and the phase condition (3.55c) which anchors a reference position  $x^\gamma(0) = x_0^\gamma$  along the periodic orbit. The phase condition  $\hat{\varphi} : \mathcal{X} \rightarrow \mathbb{R}$  is chosen such that it vanishes at an isolated point  $x_0^\gamma$  on the periodic orbit  $\gamma$  (see [157] for details).

Numerical algorithms to solve this boundary value problem are reviewed in Appendix A.

#### 3.5.2 Infinitesimal phase response curves

The (state) infinitesimal phase response curve  $p(\cdot)$  is calculated by solving the boundary value problem (see [43, 70, 101, 117, 118, 132])

$$\frac{dp}{d\theta}(\theta) + \frac{1}{\omega} \frac{\partial f}{\partial x}(x^\gamma(\theta), 0)^\top p(\theta) = 0 \quad (3.56a)$$

$$p(2\pi) - p(0) = 0 \quad (3.56b)$$

$$\langle p(\theta), f(x^\gamma(\theta), 0) \rangle = \omega \quad (3.56c)$$

(where the notation  $A^\top$  stands for the transpose of the matrix  $A$ ). The boundary condition (3.56b) imposes the periodicity of  $p(\cdot)$  and the normalization condition (3.56c) ensures a linear increase at rate  $\omega$  of the phase variable  $\theta$  along zero-input trajectories. The (input) infinitesimal phase response curve  $q(\cdot)$  is then computed by applying (3.24). This method is often called the “adjoint method”.

Numerical methods to solve this boundary value problem as a by-product of the periodic orbit computation are presented in Appendix A.

### 3.5.3 Phase response curves

In the following, we provide an “exact” method (up to numerical errors) to compute the phase response curve  $Q(\cdot; u(\cdot))$  of an oscillator state-space model given a phase resetting input  $u(\cdot)$ . We also give several approximation methods relying on the continuous phase model and its linearization.

#### “Exact” method on the state-space model

The simplest method to compute exactly (up to numerical errors) the phase response curve of an oscillator state-space model is the direct application of Definition 1. It is called the “direct method” (see [18, 60, 102, 173, 194, 195]).

For each point of  $Q(\theta; u(\cdot))$  (that is for  $\theta = \theta_i$ ), the perturbed trajectory  $\phi(t, x^\gamma(\theta_i), u(\cdot))$  is computed by solving the initial value problem (3.3a) from  $x^\gamma(\theta_i)$  up to its convergence back in a neighborhood of the periodic orbit, that is, up to time  $t_*$  such that  $\text{dist}(\phi(t_*, x^\gamma(\theta_i), u(\cdot)), \gamma) < \epsilon$  (where  $\epsilon$  is a chosen error tolerance). The phase  $\theta_* = \Theta(\phi(t_*, x^\gamma(\theta_i), u(\cdot)))$  is estimated using the algorithm

$$\theta_* = \arg \min_{\theta \in \mathbb{S}^1} \|\phi(t_*, x^\gamma(\theta_i), u(\cdot)) - x^\gamma(\theta)\|_2. \quad (3.57)$$

Then, the asymptotic phase shift is measured by direct comparison with the phase of an unperturbed trajectory at time  $t_*$ , that is,

$$Q(\theta_i; u(\cdot)) = \theta_* - (\omega t_* + \theta_i). \quad (3.58)$$

This method can be used for arbitrary phase resetting inputs and only requires a good time integrator. However, it is highly expensive from a computational point of view: each point of the phase response curve requires the time simulation of the  $n$ -dimensional state-space model, up to the asymptotic convergence of the perturbed trajectory towards the periodic orbit.

#### Approximate method based on the phase model

A second method to compute the phase response curve of an oscillator relies on the application of the direct method to the continuous-time phase equation (3.27). The approximation is valid if the input is weak.

Decomposing the phase variable as  $\theta(t) = \omega t + \varphi(t)$  where  $\varphi(t)$  is the phase deviation from the uniform natural oscillation  $\omega t$ , we may rewrite the phase equation (3.27) as follows

$$\dot{\varphi} = q(\omega t + \varphi) u(t), \quad \varphi_0 = \theta_0 \quad (3.59)$$

where  $\theta_0$  is the initial phase condition.

The phase response curve associated with phase  $\theta_0$  may be approximated by the difference between the asymptotic value of the phase deviation variable  $\varphi(t)$  (starting from the initial condition  $\varphi_0 = \theta_0$ ) and the initial phase  $\theta_0$ , that is,

$$Q(\theta_0; u(\cdot)) \approx \lim_{t \rightarrow +\infty} \varphi(t) - \theta_0 \quad (3.60)$$

which tends to a constant value for phase resetting inputs. For phase resetting inputs of finite duration  $\Delta$ , we have  $Q(\theta_0; u(\cdot)) \approx \varphi(\Delta) - \theta_0$ .

### Approximation method based on the linearized phase model

A third method to compute the phase response curve of an oscillator consists in approximating the solution to (3.59) based on the linearization of this equation. Considering the linearization up to the first or zeroth order yields two different approximations.

*First-order approximation.* Linearizing (3.59) around the unperturbed trajectory  $(\varphi^*(t), u^*(t)) = (\varphi_0, \mathbf{0})$  starting from the initial phase deviation  $\varphi_0$ , and defining the perturbations  $\delta\varphi(t) := \varphi(t) - \varphi^*(t)$  and  $\delta u(t) := u(t) - u^*(t)$ , we have

$$\delta\dot{\varphi}(t) \approx \underbrace{\frac{dq}{d\theta}(\omega t + \varphi^*(t))}_{:=A_\varphi(t)} \delta u(t) + \underbrace{q(\omega t + \varphi^*(t))}_{:=b_\varphi(t)} \delta\varphi(t) \quad (3.61)$$

(where the approximately equal sign ( $\approx$ ) means that (3.61) neglects higher order terms in  $\|\delta\varphi(t)\|_2^2$ ). The solution of the linearized equation is given by

$$\delta\varphi(t) = \Phi_\varphi(t, 0) \delta\varphi_0 + \int_0^t \Phi_\varphi(t, s) b_\varphi(s) ds \quad (3.62)$$

where the fundamental solution  $\Phi_\varphi(\tau, \sigma)$  associated with  $A_\varphi(t)$  is the solution of the following equation

$$\frac{\partial \Phi_\varphi(\tau, \sigma)}{\partial \tau} = A_\varphi(\tau) \Phi_\varphi(\tau, \sigma), \quad \Phi_\varphi(\sigma, \sigma) = I. \quad (3.63)$$

As a consequence of uniqueness of solutions of ordinary differential equations, the fundamental solution has the following property [161, Lemma C.4.1(f)]

$$\det \Phi_\varphi(\tau, \sigma) = \exp \left( \int_\sigma^\tau \text{trace } A_\varphi(\rho) d\rho \right), \quad (3.64)$$

and, because the linearized phase equation is one-dimensional, this property reduces to  $\Phi_\varphi(\tau, \sigma) = \exp \left( \int_\sigma^\tau A_\varphi(\rho) d\rho \right)$ . The phase deviation perturbation is

thus given by

$$\delta\varphi(t) = \exp\left(\int_0^t A_\varphi(\rho) d\rho\right) \delta\varphi_0 + \int_0^t \exp\left(\int_s^t A_\varphi(\rho) d\rho\right) b_\varphi(s) ds, \quad (3.65)$$

$$= \int_0^t \exp\left(\int_s^t \frac{dq}{d\theta}(\omega\rho + \varphi_0) u(\rho) d\rho\right) q(\omega s + \varphi_0) u(s) ds. \quad (3.66)$$

*Zeroth-order approximation.* Truncating (3.61) after the independent term (zeroth-order term), we have

$$\delta\dot{\varphi}(t) \approx \underbrace{q(\omega t + \varphi^*(t))}_{:=b_\varphi(t)} \delta u(t) \quad (3.67)$$

(where the approximately equal sign ( $\approx$ ) means that (3.67) neglects all terms in  $\|\delta\varphi(t)\|_2$ ) and the solution is given by

$$\delta\varphi(t) = \delta\varphi_0 + \int_0^t b_\varphi(s) ds = \int_0^t q(\omega s + \varphi_0) u(s) ds. \quad (3.68)$$

In both zero- and first-order approximations, the phase response curve associated with the phase  $\theta_0$  may be approximated by the asymptotic value of the phase deviation perturbation, that is,

$$Q(\theta_0; u(\cdot)) = \lim_{t \rightarrow +\infty} [\varphi^*(t) + \delta\varphi(t)] - \theta_0 = \lim_{t \rightarrow +\infty} \delta\varphi(t). \quad (3.69)$$

The dependence in  $\theta_0$  is hidden behind the fact that  $\delta\varphi(t)$  is computed for the system linearized around the trajectory starting from  $\theta_0$ . The first-order approximation yields

$$Q(\theta_0; u(\cdot)) \approx \lim_{t \rightarrow +\infty} \int_0^t \exp\left(\int_s^t \frac{dq}{d\theta}(\omega\rho + \theta_0) u(\rho) d\rho\right) q(\omega s + \theta_0) u(s) ds \quad (3.70)$$

and the zero-order approximation yields

$$Q(\theta_0; u(\cdot)) \approx \lim_{t \rightarrow +\infty} \int_0^t q(\omega s + \theta_0) u(s) ds. \quad (3.71)$$

## 3.6 Summary

In this chapter, we reviewed the concept of phase response curves, from experiments, from state-space models, and in two popular phase models. We also showed how classical asymptotic methods can be used to reveal the phase

dynamics and thus the phase response curve. We also provided the tools to compute or approximate phase response curves from a state-space model.

Both reduced representations  $\{\omega, q(\cdot), \tilde{h}(\cdot)\}$  and  $\{\omega, Q(\cdot; \alpha \delta(\cdot)), \tilde{h}(\cdot)\}$  of oscillators share similar characteristics with the static gain of transfer function representation of linear time-invariant systems. Both representations capture asymptotic properties of the impulse response. They are independent of the complexity of the internal state-space representation of the oscillators. Moreover, information on such characteristics is available experimentally.

As a consequence, the space of phase response curves is the appropriate space to address input–output systems questions for oscillators.

## Chapter 4

# Metrics in the space of phase response curves

Comparing systems with a proper metric has been central to systems theory (see e.g. Zames [39,197], Georgiou [57,58], Vinnicombe [182,183], Martin [120], or De Cock [29] for exemplative milestones), offering novel frameworks for system identification and robustness analysis.

However, such systems questions have been mainly addressed for linear time-invariant systems or for discrete-time random processes, and surprisingly not for oscillators.

Motivated by the prevalence of input–output descriptions in previous work, we develop a metric in the space of phase response curves for oscillators. We equip the space of phase response curves with the differential structure of a Riemannian manifold. The Riemannian structure is convenient to recast analysis problems in an optimization framework, providing for instance a notion of steepest descent. It also provides a norm in the tangent space and a (geodesic) distance between phase response curves.

This chapter is organized as follows. Section 4.1 presents basic features of differential geometry used in this chapter. Section 4.2 describes two natural equivalence properties in the space of phase response curves. Section 4.3 defines the right metrics in the four spaces resulting from various combinations of these equivalence properties. It also provides the numerics necessary to turn the formal definitions into computable quantities.

*Contributions.* The main contributions of this chapter are (i) the identification of natural equivalence properties and (ii) the definition of the right metrics in the space of phase response curves.

## 4.1 Basics of differential geometry on manifolds

In this section, we briefly recall basic concepts of differential geometry on manifolds. This brief exposition follows the terminology and definitions of [3].

A manifold  $\mathcal{M}$  is endowed with a Riemannian metric  $g_x(\xi_x, \zeta_x)$  which is an inner product of two elements  $\xi_x$  and  $\zeta_x$  of the tangent space  $T_x\mathcal{M}$  at  $x$ . The metric induces a norm on  $T_x\mathcal{M}$  at  $x$ :

$$\|\xi_x\|_x := \sqrt{g_x(\xi_x, \xi_x)}. \quad (4.1)$$

The length of a curve  $\gamma : (a, b) \subset \mathbb{R} \rightarrow \mathcal{M}$  is defined as

$$L(\gamma) := \int_a^b \|\dot{\gamma}(t)\|_{\gamma(t)} dt. \quad (4.2)$$

The geodesic distance between two points  $x$  and  $y$  on  $\mathcal{M}$  is defined as

$$\text{dist}(x, y) = \inf_{\Gamma} L(\gamma) \quad (4.3)$$

where  $\Gamma$  is the set of all curves in  $\mathcal{M}$  joining points  $x$  and  $y$

$$\Gamma = \{\gamma : [0, 1] \rightarrow \mathcal{M} : \gamma(0) = x, \gamma(1) = y\}. \quad (4.4)$$

The curve(s)  $\gamma$  achieving this infimum is called the shortest geodesic between  $x$  and  $y$ . The geodesic distance between two points defines a natural metric. However, the notion of geodesic distance between two points is not obvious. One may define the distance between two points on  $\mathcal{M}$  differently.

The gradient of a smooth scalar function  $F : \mathcal{M} \rightarrow \mathbb{R}$  at  $x \in \mathcal{M}$  is the unique element  $\text{grad}_x F(x) \in T_x\mathcal{M}$  that satisfies

$$DF(x)[\xi] = g_x(\text{grad}_x F(x), \xi), \quad \forall \xi \in T_x\mathcal{M} \quad (4.5)$$

where

$$DF(x)[\eta] = \lim_{t \rightarrow 0} \frac{F(x + t\eta) - F(x)}{t} \quad (4.6)$$

is the standard directional derivative of  $F$  at  $x$  in the direction  $\eta$ .

For quotient manifolds  $\mathcal{M} = \overline{\mathcal{M}} / \sim$ , where  $\overline{\mathcal{M}}$  is the total space and  $\sim$  is the equivalence relation that defines the quotient, the tangent space  $T_{\bar{x}}\overline{\mathcal{M}}$  at  $\bar{x}$  admits a decomposition into its vertical and horizontal subspaces

$$T_{\bar{x}}\overline{\mathcal{M}} = \mathcal{H}_{\bar{x}} \oplus \mathcal{V}_{\bar{x}}. \quad (4.7)$$

A tangent vector  $\xi_x$  at  $x \in \mathcal{M}$  has a unique representation  $\bar{\xi}_{\bar{x}} \in \mathcal{H}_{\bar{x}}$  at  $\bar{x}$ . Provided that the metric  $\bar{g}_{\bar{x}}$  in the total space is invariant along the equivalence classes, it defines a metric on the quotient space

$$g_x(\xi_x, \zeta_x) := \bar{g}_{\bar{x}}(\bar{\xi}_{\bar{x}}, \bar{\zeta}_{\bar{x}}). \quad (4.8)$$

If  $\bar{F}$  is a function on  $\overline{\mathcal{M}}$  that induces a function  $F$  on  $\mathcal{M}$ , then one has

$$\overline{\text{grad}_x F(x)} = \text{grad}_{\bar{x}} \bar{F}(\bar{x}) \quad (4.9)$$

in which  $\text{grad}_{\bar{x}} \bar{F}(\bar{x})$  belongs to the horizontal subspace  $\mathcal{H}_{\bar{x}}$ .

## 4.2 Natural equivalence properties

Because (infinitesimal and finite) phase response curves are signals defined on the unit circle and taking values on the real line, the most obvious Riemannian structure is provided by the infinite-dimensional Hilbert space of square-integrable signals

$$\mathcal{H}^0 := \{q : q(\cdot) \in \mathcal{L}_2(\mathbb{S}^1, \mathbb{R})\} \quad (4.10)$$

(where  $\mathcal{L}_2(\mathbb{S}^1, \mathbb{R}) = \{q : \mathbb{S}^1 \rightarrow \mathbb{R} : (\int_0^{2\pi} |q(\theta)|^2 d\theta)^{\frac{1}{2}} < \infty\}$ ) equipped with the standard inner product

$$\langle \xi(\cdot), \zeta(\cdot) \rangle := \int_0^{2\pi} \xi(\theta) \zeta(\theta)^* d\theta \quad (4.11)$$

and the associated norm

$$\|\xi(\cdot)\|_2 := \sqrt{\langle \xi(\cdot), \xi(\cdot) \rangle}. \quad (4.12)$$

For technical reasons detailed later, we further assume that the first derivative of considered signals is also square-integrable and thus restrict the signal space to

$$\mathcal{H}^1 := \{q : q(\cdot) \in \mathcal{L}_2(\mathbb{S}^1, \mathbb{R}), q'(\cdot) \in \mathcal{L}_2(\mathbb{S}^1, \mathbb{R})\}. \quad (4.13)$$

The space  $\mathcal{H}^1$  is a linear subspace of  $\mathcal{H}^0$  and it inherits its inner product (4.11) and its norm (4.12).

The linear space structure  $\mathcal{H}^1$  is convenient for calculations but it fails to capture important equivalence properties between phase response curves. In many applications, it is not meaningful to distinguish among phase response curves that are related by a scaling factor and/or a phase shift (see Figure 4.1).

**Scaling equivalence** The actual magnitude of the input signal acting on the system is not always well-known. This uncertainty about the input magnitude induces an (inversely proportional) uncertainty about the phase response magnitude. Indeed, the phase model (3.27) is equivalent to

$$\dot{\theta} = \omega + (q(\theta) \alpha) \left( \frac{1}{\alpha} u \right) \quad (4.14a)$$

$$y = \tilde{h}(\theta) \quad (4.14b)$$

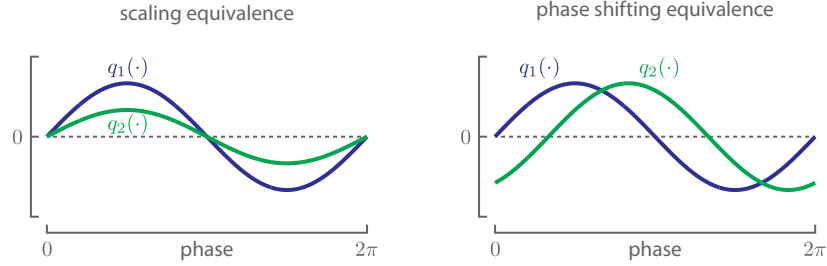


Figure 4.1 – Natural equivalence properties in the space of phase response curves. (Left) The scaling equivalence comes from an uncertainty about the input magnitude that can be compensated by an inversely proportional uncertainty about the phase response magnitude. (Right) The phase shifting equivalence comes from the arbitrary choice of the reference position (associated with the initial phase) along the periodic orbit.

for any scaling factor  $\alpha$ . A scaling of the input magnitude can be counterbalanced by an inverse scaling of the phase response curve. In those cases, we consider a phase response curve  $q$  as the representation of an equivalence class  $\sim$  characterized by (see Figure 4.1, left)

$$q_1 \sim q_2 \Leftrightarrow \exists \alpha > 0 : q_2(\cdot) = q_1(\cdot) \alpha. \quad (4.15)$$

For example, in circadian rhythms, stimuli are pulses of light. They are modeled by scaling the intensity of a parameter but absolute variation this parameter is not known and empirically fitted to experimental data. On the contrary, in neurodynamics, the stimulus is an applied current of controlled magnitude. In this latter case, the scaling equivalence is less appropriate.

**Phase shifting equivalence** The choice of a reference position (associated with the initial phase) along the periodic orbit is often arbitrary. In those cases, we may wish to consider a phase response curve  $q$  as representative of an equivalence class  $\sim$  characterized by (see Figure 4.1, right)

$$q_1 \sim q_2 \Leftrightarrow \exists \sigma \in \mathbb{S}^1 : q_2(\cdot) = q_1(\cdot + \sigma) \quad (4.16)$$

where  $\sigma$  denotes any phase shift.

For example, in circadian rhythms, experimental data are often collected by observing the locomotor activity of the animal. The timing of this locomotor activity is not easily linked to the time-evolution of molecular concentrations. On the contrary, in neurons, the observable events are the action potentials generated in the membrane potential. If the membrane potential is a state variable

	$q(\cdot) \not\sim q(\cdot) \alpha$	$q(\cdot) \sim q(\cdot) \alpha$
$q(\cdot) \not\sim q(\cdot + \sigma)$	$\mathcal{Q}_A := \mathcal{H}^1$	$\mathcal{Q}_B := \mathcal{H}^1 / \mathbb{R}_{>0}$
$q(\cdot) \sim q(\cdot + \sigma)$	$\mathcal{Q}_C := \mathcal{H}^1 / \text{Shift}(\mathbb{S}^1)$	$\mathcal{Q}_D := \mathcal{H}^1 / (\text{Shift}(\mathbb{S}^1) \times \mathbb{R}_{>0})$

Table 4.1 – Four spaces of phase response curves. Combining or not equivalence properties defines four infinite-dimensional spaces: one Hilbert space and three quotient spaces of phase response curves.

of the model, there is no timing ambiguity and the phase shift equivalence is not meaningful.

Those equivalence relations lead to the abstract—yet useful—concept of quotient space. Each point of a quotient space is defined as an equivalence class of signals. Since these equivalence classes are abstract objects, they cannot be explicitly used in numerical computations. Algorithms on quotient space work instead with representatives (in the total space) of these equivalence classes.

### 4.3 Metrics

Combining or not equivalence properties (4.15) and (4.16), we end up with four infinite-dimensional spaces: one Hilbert space and three quotient spaces, respectively, denoted by  $\mathcal{Q}_A$ ,  $\mathcal{Q}_B$ ,  $\mathcal{Q}_C$ , or  $\mathcal{Q}_D$  (see Table 4.1). In the next four subsections, we will equip each space with an appropriate Riemannian metric and provide an expression of tangent vectors, needed for the sensitivity analysis in the subsequent sections

In the following, we denote by  $q$  an element of the considered space. It can be a signal (infinitesimal or finite phase response curve) or an equivalence class of those signals.

#### 4.3.1 Metric on Hilbert space $\mathcal{H}^1$

The simplest space structure is Hilbert space  $\mathcal{Q}_A := \mathcal{H}^1$ . The (flat) Riemannian metric on  $\mathcal{Q}_A$  is given by the inner product

$$g_q(\xi_q, \zeta_q) := \langle \xi_q, \zeta_q \rangle \quad (4.17)$$

with (Euclidean) induced norm

$$\|\xi_q\|_q := \sqrt{g_q(\xi_q, \xi_q)} = \sqrt{\langle \xi_q, \xi_q \rangle} = \|\xi_q\|_2. \quad (4.18)$$

Because the space  $\mathcal{Q}_A$  is a linear space structure, the shortest path between two elements  $q_1$  and  $q_2$  on  $\mathcal{Q}_A$  is the straight line joining those elements. The natural (geodesic) distance between two points  $q_1$  and  $q_2$  on  $\mathcal{Q}_A$  is then given by

$$\text{dist}(q_1, q_2) := \|q_1 - q_2\|_2. \quad (4.19)$$

### 4.3.2 Metric on the quotient space $\mathcal{H}^1/\mathbb{R}_{>0}$

The space capturing the scaling equivalence (4.15) is the quotient space  $\mathcal{Q}_B := \mathcal{H}^1/\mathbb{R}_{>0}$ . Each element  $q$  in  $\mathcal{Q}_B$  represents an equivalence class

$$q = [\bar{q}] := \{\bar{q} \alpha : \alpha > 0\}. \quad (4.20)$$

Those equivalence classes are rays (starting at 0) in the total space  $\bar{\mathcal{Q}}_B := \mathcal{H}^1$ .

The normalized metric on  $\bar{\mathcal{Q}}_B$

$$\bar{g}_{\bar{q}}(\bar{\xi}_{\bar{q}}, \bar{\zeta}_{\bar{q}}) := \frac{\langle \bar{\xi}_{\bar{q}}, \bar{\zeta}_{\bar{q}} \rangle}{\langle \bar{q}, \bar{q} \rangle}, \quad (4.21)$$

is invariant by scaling. As a consequence, it induces a Riemannian metric  $g_q(\xi_q, \zeta_q) := \bar{g}_{\bar{q}}(\bar{\xi}_{\bar{q}}, \bar{\zeta}_{\bar{q}})$  on  $\mathcal{Q}_B$ . The norm in the tangent space  $T_q \mathcal{Q}_B$  at  $q$  is given by

$$\|\xi_q\|_q := \sqrt{g_q(\xi_q, \xi_q)} = \frac{\|\bar{\xi}_{\bar{q}}\|_2}{\|\bar{q}\|_2}. \quad (4.22)$$

A signal representation of a tangent vector at  $q \in \mathcal{Q}_B$  relies on the decomposition of the tangent space  $T_q \bar{\mathcal{Q}}_B$  into its vertical and horizontal subspaces. The vertical subspace  $\mathcal{V}_{\bar{q}}$  is the subspace of  $T_q \bar{\mathcal{Q}}_B$  that is tangent to the equivalence class  $[\bar{q}]$ , that is,

$$\mathcal{V}_{\bar{q}} = \{\bar{q} \beta : \beta \in \mathbb{R}\}. \quad (4.23)$$

The horizontal space  $\mathcal{H}_{\bar{q}}$  is chosen as the orthogonal complement of  $\mathcal{V}_{\bar{q}}$  for the metric  $\bar{g}_{\bar{q}}(\cdot, \cdot)$ , that is,

$$\mathcal{H}_{\bar{q}} = \{\eta \in T_q \bar{\mathcal{Q}}_B : \bar{g}_{\bar{q}}(\eta, \bar{q} \beta) = 0\}. \quad (4.24)$$

The orthogonal projection  $P_{\bar{q}}^h \eta$  of a vector  $\eta \in T_q \bar{\mathcal{Q}}_B$  onto the horizontal space  $\mathcal{H}_{\bar{q}}$  is given by

$$P_{\bar{q}}^h \eta := \eta - \frac{\bar{g}_{\bar{q}}(\eta, \bar{q} \beta)}{\bar{g}_{\bar{q}}(\bar{q} \beta, \bar{q} \beta)} \bar{q} \beta = \eta - \frac{\langle \eta, \bar{q} \rangle}{\langle \bar{q}, \bar{q} \rangle} \bar{q}. \quad (4.25)$$

The distance between two points  $q_1$  and  $q_2$  on  $\mathcal{Q}_B$  is defined as

$$\text{dist}(q_1, q_2) := \cos^{-1} \left( \frac{\langle \bar{q}_1, \bar{q}_2 \rangle}{\|\bar{q}_1\|_2 \|\bar{q}_2\|_2} \right) \quad (4.26)$$

(see [62] for metric on the unit sphere).

### 4.3.3 Metric on the quotient space $\mathcal{H}^1/\text{Shift}(\mathbb{S}^1)$

The space capturing the phase shifting equivalence (4.16) is the quotient space  $\mathcal{Q}_C := \mathcal{H}^1/\text{Shift}(\mathbb{S}^1)$ . Each element  $q$  in  $\mathcal{Q}_C$  represents an equivalence class

$$q = [\bar{q}] = \{\bar{q}(\cdot + \sigma) : \sigma \in \mathbb{S}^1\}. \quad (4.27)$$

Those equivalence classes are closed one-dimensional curves (due to the periodicity of the shift) on the infinite-dimensional hypersphere of radius  $\|\bar{q}\|_2$  in the total space  $\overline{\mathcal{Q}}_C := \mathcal{H}^1$ .

The (flat) metric on  $\overline{\mathcal{Q}}_C$

$$\bar{g}_{\bar{q}}(\bar{\xi}_{\bar{q}}, \bar{\zeta}_{\bar{q}}) := \langle \bar{\xi}_{\bar{q}}, \bar{\zeta}_{\bar{q}} \rangle, \quad (4.28)$$

is invariant by phase shifting along the equivalence classes. As a consequence, it induces a Riemannian metric  $g_q(\xi_q, \zeta_q) := \bar{g}_{\bar{q}}(\bar{\xi}_{\bar{q}}, \bar{\zeta}_{\bar{q}})$  on  $\mathcal{Q}_C$ . The norm in the tangent space  $T_q\mathcal{Q}_C$  at  $q$  is given by

$$\|\xi_q\|_q := \sqrt{g_q(\xi_q, \xi_q)} = \|\bar{\xi}_{\bar{q}}\|_2. \quad (4.29)$$

The vertical space  $\mathcal{V}_{\bar{q}}$  is the subspace of  $T_{\bar{q}}\overline{\mathcal{Q}}_C$  that is tangent to the equivalence class  $[\bar{q}]$

$$\mathcal{V}_{\bar{q}} = \{\bar{q}' \beta : \beta \in \mathbb{R}\} \quad (4.30)$$

(where  $\bar{q}'$  has to belong to  $\mathcal{L}_2(\mathbb{S}^1, \mathbb{R})$  to ensure the regularity of  $\mathcal{V}_{\bar{q}}$ ). We choose the horizontal space  $\mathcal{H}_{\bar{q}}$  as the orthogonal complement of  $\mathcal{V}_{\bar{q}}$  for the metric  $\bar{g}_{\bar{q}}(\cdot, \cdot)$ , that is,

$$\mathcal{H}_{\bar{q}} = \{\eta \in T_{\bar{q}}\overline{\mathcal{Q}}_C : \bar{g}_{\bar{q}}(\eta, \bar{q}' \beta) = 0\}. \quad (4.31)$$

The orthogonal projection  $P_{\bar{q}}^h \eta$  of a vector  $\eta \in T_{\bar{q}}\overline{\mathcal{Q}}_C$  onto the horizontal space  $\mathcal{H}_{\bar{q}}$  is given by

$$P_{\bar{q}}^h \eta := \eta - \frac{\bar{g}_{\bar{q}}(\eta, \bar{q}' \beta)}{\bar{g}_{\bar{q}}(\bar{q}' \beta, \bar{q}' \beta)} \bar{q}' \beta = \eta - \frac{\langle \eta, \bar{q}' \rangle}{\langle \bar{q}', \bar{q}' \rangle} \bar{q}'. \quad (4.32)$$

The distance between two points  $q_1$  and  $q_2$  on  $\mathcal{Q}_C$  is defined as

$$\text{dist}(q_1, q_2) := \min_{\sigma \in \mathbb{S}^1} \|\bar{q}_1(\cdot) - \bar{q}_2(\cdot + \sigma)\|_2 = \|\bar{q}_1(\cdot) - \bar{q}_2(\cdot + \sigma_*)\|_2 \quad (4.33)$$

where  $\sigma_*$  denotes the phase shift achieving this minimization. It corresponds to the phase shift maximizing the circular cross-correlation

$$\sigma_* = \arg \max_{\sigma \in \mathbb{S}^1} \langle \bar{q}_1(\cdot), \bar{q}_2(\cdot + \sigma) \rangle. \quad (4.34)$$

This global optimization problem is solved in two steps. Firstly we compute the circular cross-correlation  $\bar{c} : \mathbb{S}^1 \rightarrow \mathbb{R}$  between the two periodic signals  $\bar{q}_1$  and  $\bar{q}_2$

$$\bar{c}(\sigma) = \langle \bar{q}_1(\cdot), \bar{q}_2(\cdot + \sigma) \rangle. \quad (4.35)$$

The circular cross-correlation  $\bar{c}(\cdot)$  is, by definition, also a periodic signal. An efficient computation of this circular cross-correlation is performed in the Fourier domain. We note that the circular cross-correlation can be expressed as the circular convolution  $\bar{c}(\sigma) = (\bar{q}_1(-\cdot)^* \odot \bar{q}_2(\cdot))(\sigma)$ . Exploiting the properties of Fourier coefficients and the convolution-multiplication duality property, we have

$$\hat{\bar{c}}[k] = \hat{\bar{q}}_1[k]^* \hat{\bar{q}}_2[k] \quad (4.36)$$

where  $\hat{x}[\cdot]$  denotes the discrete signal of Fourier coefficients for the periodic signal  $x(\cdot)$  and where  $x^*$  denotes the complex conjugate of  $x$ . Secondly we identify the optimal phase shift value  $\sigma_* \in \mathbb{S}^1$  achieving the maximal value of the circular cross-correlation. This maximum is global and generically unique (multiplicity of the optimum would mean that one of the signal has a period which is actually equal to  $2\pi/k$  with  $k \in \mathbb{N}_{>0}$ ).

#### 4.3.4 Metric on the quotient space $\mathcal{H}^1/(\mathbb{R}_{>0} \times \text{Shift}(\mathbb{S}^1))$

The space capturing both scaling and phase shifting equivalences (4.15)–(4.16) is the quotient space  $\mathcal{Q}_D := \mathcal{H}^1/(\mathbb{R}_{>0} \times \text{Shift}(\mathbb{S}^1))$ . Each element  $q$  in  $\mathcal{Q}_D$  represents an equivalence class

$$q = [\bar{q}] = \{\bar{q}(\cdot + \sigma) \alpha : \alpha > 0, \sigma \in \mathbb{S}^1\}. \quad (4.37)$$

Based on the individual geometric interpretation of both equivalence properties, those equivalence classes are infinite cones in the total space  $\overline{\mathcal{Q}}_D := \mathcal{H}^1$ , that is, the union of rays that start at 0 and go through the closed one-dimensional curve of phase shifted signals.

Because the metric (4.21) on  $\overline{\mathcal{Q}}_D$  is invariant by scaling and phase shifting along the equivalence classes, it induces a Riemannian metric  $g_q(\xi_q, \zeta_q) := \bar{g}_{\bar{q}}(\bar{\xi}_{\bar{q}}, \bar{\zeta}_{\bar{q}})$  on  $\mathcal{Q}_D$ . The norm in the tangent space  $T_q \mathcal{Q}_D$  at  $q$  is given by (4.22).

The vertical space  $\mathcal{V}_{\bar{q}}$  is the subspace of  $T_{\bar{q}} \overline{\mathcal{Q}}_D$  that is tangent to the equivalence class  $[\bar{q}]$

$$\mathcal{V}_{\bar{q}} = \{\bar{q} \beta_1 + \bar{q}' \beta_2 : \beta_1, \beta_2 \in \mathbb{R}\}. \quad (4.38)$$

It is the direct sum of vertical spaces for equivalence properties individually. We choose the horizontal space  $\mathcal{H}_{\bar{q}}$  as the orthogonal complement of  $\mathcal{V}_{\bar{q}}$  for the metric  $g_q(\cdot, \cdot)$ , that is,

$$\mathcal{H}_{\bar{q}} = \{\eta \in T_{\bar{q}} \overline{\mathcal{Q}}_D : \bar{g}_{\bar{q}}(\eta, \bar{q} \beta_1 + \bar{q}' \beta_2) = 0\}. \quad (4.39)$$

The orthogonal projection  $P_{\bar{q}}^h \eta$  of a vector  $\eta \in T_{\bar{q}} \overline{\mathcal{Q}}_D$  onto the horizontal space  $\mathcal{H}_{\bar{q}}$  is given by

$$P_{\bar{q}}^h \eta := \eta - \frac{\bar{g}_{\bar{q}}(\eta, \bar{q} \beta_1)}{\bar{g}_{\bar{q}}(\bar{q} \beta_1, \bar{q} \beta_1)} \bar{q} \beta_1 - \frac{\bar{g}_{\bar{q}}(\eta, \bar{q}' \beta_2)}{\bar{g}_{\bar{q}}(\bar{q}' \beta_2, \bar{q}' \beta_2)} \bar{q}' \beta_2 \quad (4.40)$$

$$= \eta - \frac{\langle \eta, \bar{q} \rangle}{\langle \bar{q}, \bar{q} \rangle} \bar{q} - \frac{\langle \eta, \bar{q}' \rangle}{\langle \bar{q}', \bar{q}' \rangle} \bar{q}'. \quad (4.41)$$

The distance between two points  $q_1$  and  $q_2$  on  $\mathcal{Q}_D$  is defined as

$$\text{dist}(q_1, q_2) := \min_{\sigma \in \mathbb{S}^1} \cos^{-1} \left( \frac{\langle \bar{q}_1(\cdot), \bar{q}_2(\cdot + \sigma) \rangle}{\|\bar{q}_1\|_2 \|\bar{q}_2\|_2} \right) \quad (4.42)$$

$$= \cos^{-1} \left( \frac{\langle \bar{q}_1(\cdot), \bar{q}_2(\cdot + \sigma_*) \rangle}{\|\bar{q}_1\|_2 \|\bar{q}_2\|_2} \right) \quad (4.43)$$

where  $\sigma_*$  denotes the phase shift achieving this minimization. It corresponds to the phase shift operator maximizing the circular cross-correlation in (4.34).

## 4.4 Summary

In this chapter, we equipped the space of phase response curves with the suitable metrics. In particular, we identified two natural equivalence properties among phase response curves. In many applications, it is not meaningful to distinguish among phase response curves that are related by a scaling factor and/or a phase shift. These equivalence properties lead to four spaces (including or not the equivalences) for which we defined a metric. We also provided the guidelines to turn those abstract definitions into numerically computable quantities.



## Chapter 5

# Sensitivity analysis in the space of phase response curves

Analyzing the sensitivity of a system behavior to changes in the system parameters or in the system architecture has been central to systems theory. It often provides an insight into the nature and function of the system and identifies the important parameters in the system. Sensitivity analyses fall into two main categories: global and local analyses.

Global analysis explores system behaviors in broad regions of the parameter space. It includes methods such as bifurcation analysis [103, 157] or parameter space exploration with a sampling process often guided by statistical methods [152, 153]. This approach provides a description of the effect on the behavior of large deviations in parameter values. The limitation of those approaches is either that they are univariate (only one direction of the parameter space is explored in a particular bifurcation diagram) or that the exploration of the parameter space rapidly becomes formidable as the number of parameters grows.

Local analysis concentrates attention near one particular point in the parameter space and assumes linear dependence on the parameter values around this nominal point (see [32, 53, 141, 174, 175, 181] for details). This assumption simplifies the analysis and provides a complete and elegant description of the effect on the behavior of small perturbations near the operating point.

Both methods are complementary. The local sensitivity analysis may serve as a pre-screening process to guide more efficiently the global parameter space exploration. In the following, we will mainly focus on local sensitivity analysis.

Initially developed for (linear and nonlinear) systems that evolve around a

stable equilibrium, the sensitivity of steady-state state-space features for oscillatory systems (e.g. period and amplitude of oscillations) was early estimated through simulation [22, 95, 104]. More recently, a general theory to treat the sensitivity of oscillatory systems in the state space has emerged [87, 144, 192]. In parallel, the sensitivity of trajectories for oscillatory systems has been decomposed into a contribution due to the “phase-dependent sensitivity” and a contribution due to the “phase-independent sensitivity” [76, 77, 192, 196]. In addition, empirical phase-based performance measures have been proposed in order to quantify the sensitivity of the phase in oscillatory systems [14, 173].

However, those approaches lack the conceptual input–output perspective that we want to pursue in this dissertation. It is thus necessary to develop a sensitivity analysis for oscillators, viewed as open dynamical systems evolving on the circle (i.e. their external representation).

We develop a sensitivity analysis of both essential characteristics of oscillatory systems on the circle, that is, the sensitivity of the period (or equivalently the sensitivity of the angular frequency) and the sensitivity of the infinitesimal phase response curves. We stress that our sensitivity analysis focuses on the sensitivity of the infinitesimal phase response curve appearing in continuous-time phase models for weak inputs. Indeed, only the computation of infinitesimal phase response curves admits an analytical formulation, and the same is true for their sensitivity.

This chapter is organized as follows. Section 5.1 introduces the basic concepts of sensitivity analysis used in this chapter. Section 5.2 derives the sensitivity analysis for periodic orbits, phase response curves, and entrainment behavior. Section 5.3 briefly summarize numerics of sensitivity analysis and Appendix A provides the detailed numerical tools to turn the abstract developments into concrete algorithms.

*Contributions.* The main contribution of this chapter is to introduce the use of sensitivity analysis of infinitesimal phase response curves in the context of biological applications. Although developed independently, the sensitivity formula and the developments in this section are closely related to those in [187] which studies the sensitivity analysis of infinitesimal phase response curves (called perturbation projection vectors) in the context of electronic circuits.

## 5.1 Basics of local sensitivity analysis

In this section, we briefly recall basic concepts of local sensitivity analysis. The brief exposition follows the terminology of [92].

We consider systems described by state-space models

$$\dot{x} = f(x, u, \lambda) \quad (5.1a)$$

$$y = h(x, \lambda) \quad (5.1b)$$

where the constant parameter  $\lambda$  belongs to some subset  $\Lambda \subseteq \mathbb{R}$ . (For presentation convenience, we consider systems with a one-dimensional parameter space. All developments can easily be generalized to systems with a  $l$ -dimensional parameter space.) Most characteristics of this system (defined in the previous sections) depend on the value of this parameter  $\lambda$ . It means that, for each characteristic of the system, there exists a function  $c : \Lambda \rightarrow \mathcal{C}$  that associates with each value of the parameter  $\lambda$  an element  $c(\lambda)$  in the space  $\mathcal{C}$  to which belongs the characteristic.

Under appropriate assumptions, the *sensitivity function*  $S^c : \Lambda \rightarrow T_{c(\lambda)}\mathcal{C}$  of the characteristic  $c(\lambda)$  associates with each value of the parameter  $\lambda$  the element  $S^c(\lambda)$  in the tangent space  $T_{c(\lambda)}\mathcal{C}$  at  $c(\lambda)$ , defined as

$$S^c(\lambda) := \frac{\partial c}{\partial \lambda}(\lambda) = \lim_{h \rightarrow 0} \frac{c(\lambda + h) - c(\lambda)}{h}. \quad (5.2)$$

The sensitivity  $S^c(\lambda)$  provides a first-order estimate of the effect of parameter variations on the characteristic. It can also be used to approximate the characteristic when  $\lambda$  is sufficiently close to its nominal value  $\lambda_0$ . For small  $\|\lambda - \lambda_0\|_2$ , the characteristic  $c(\lambda)$  can be expanded in a Taylor series about the nominal solution  $c(\lambda_0)$  to obtain

$$c(\lambda) = c(\lambda_0) + S^c(\lambda_0) \|\lambda - \lambda_0\|_2 + \mathcal{O}(\|\lambda - \lambda_0\|_2^2). \quad (5.3)$$

This means that the knowledge of the nominal characteristic  $c(\lambda_0)$  and the sensitivity function suffices to approximate the characteristic for all values of  $\lambda$  in a small ball centered at  $\lambda_0$ .

The main difficulty of sensitivity analysis is to formulate the appropriate (analytical) equation to be solved in order to find the characteristic  $c(\lambda)$ . Then, differentiating this (analytical) problem, we obtain the sensitivity equation to be solved in order to find the sensitivity function  $S^c(\lambda_0)$ . It can be an algebraic problem, an initial value problem, a boundary value problem, etc.

*Remark.* If, for a given value of the parameter  $\lambda$ , the characteristic  $c(\lambda)$  is itself a function  $c(\lambda) : A \rightarrow B$  in the space of functions  $\mathcal{C}$ , the sensitivity  $S^c(\lambda)$  is also a function  $S^c(\lambda) : \tilde{A} \rightarrow \tilde{B}$  in the tangent space  $T_{c(\lambda)}\mathcal{C}$ , where  $\tilde{A}$  and  $\tilde{B}$  are the domain and the image of the sensitivity function. For presentation convenience, we write  $c : A \times \Lambda \rightarrow B$  and  $S^c : \tilde{A} \times \Lambda \rightarrow \tilde{B}$ .

## 5.2 Sensitivity analysis for oscillators

In this section, we develop the sensitivity analysis of the periodic orbit, the (infinitesimal) phase response curve, and the (steady-state) phase difference under entrainment.

### 5.2.1 Sensitivity analysis of a periodic orbit

The periodic orbit  $\gamma$  of an oscillator model is characterized by an angular frequency  $\omega(\lambda)$  which measures the “speed” of a solution along the orbit and by a  $2\pi$ -periodic steady-state solution  $x^\gamma(\cdot; \lambda) = \phi(\cdot/\omega(\lambda), x_0^\gamma(\lambda), \mathbf{0}, \lambda)$  which describes the locus of this orbit in the state space.

Given a nominal parameter value  $\lambda_0$ , the sensitivity of the angular frequency is the scalar  $S^\omega(\lambda_0) \in \mathbb{R}$  defined as

$$S^\omega(\lambda_0) := \frac{\partial \omega}{\partial \lambda}(\lambda_0) = \lim_{h \rightarrow 0} \frac{\omega(\lambda_0 + h) - \omega(\lambda_0)}{h}. \quad (5.4)$$

Likewise, the sensitivity of the  $2\pi$ -periodic steady-state solution is the  $2\pi$ -periodic function  $S^{x^\gamma}(\cdot; \lambda_0) : \mathbb{S}^1 \rightarrow \mathbb{R}^n$  defined as

$$S^{x^\gamma}(\cdot; \lambda_0) := \frac{\partial x^\gamma}{\partial \lambda}(\cdot; \lambda_0) = \lim_{h \rightarrow 0} \frac{x^\gamma(\cdot; \lambda_0 + h) - x^\gamma(\cdot; \lambda_0)}{h}. \quad (5.5)$$

From (3.55), we have, taking derivatives with respect to  $\lambda$  (see Appendix B.1),

$$\frac{dS^{x^\gamma}}{d\theta}(\theta; \lambda_0) - \frac{1}{\omega} A(\theta; \lambda_0) S^{x^\gamma}(\theta; \lambda_0) + \frac{1}{\omega^2} v(\theta; \lambda_0) S^\omega(\lambda_0) = \frac{1}{\omega} E(\theta; \lambda_0) \quad (5.6a)$$

$$S^{x^\gamma}(2\pi; \lambda_0) - S^{x^\gamma}(0; \lambda_0) = 0 \quad (5.6b)$$

$$\frac{\partial \hat{\phi}}{\partial x}(x^\gamma(0; \lambda_0); \lambda_0) S^{x^\gamma}(0; \lambda_0) + \frac{\partial \hat{\phi}}{\partial \lambda}(x^\gamma(0; \lambda_0); \lambda_0) = 0 \quad (5.6c)$$

where we use the following short notations

$$A(\theta; \lambda_0) := \frac{\partial f}{\partial x}(x^\gamma(\theta; \lambda_0), 0, \lambda_0), \quad (5.7)$$

$$E(\theta; \lambda_0) := \frac{\partial f}{\partial \lambda}(x^\gamma(\theta; \lambda_0), 0, \lambda_0), \quad (5.8)$$

$$v(\theta; \lambda_0) := f(x^\gamma(\theta; \lambda_0), 0, \lambda_0). \quad (5.9)$$

*Remark.* In the literature, the sensitivity of the period is often preferred to the sensitivity of the angular frequency. It is the scalar  $S^T \in \mathbb{R}$  defined as

$$S^T(\lambda_0) := \frac{\partial T}{\partial \lambda}(\lambda_0) = \lim_{h \rightarrow 0} \frac{T(\lambda_0 + h) - T(\lambda_0)}{h}. \quad (5.10)$$

Both sensitivity measures are equivalent up to a change of sign and a scaling factor, that is,  $S^T(\lambda_0)/T(\lambda_0) = -S^\omega(\lambda_0)/\omega(\lambda_0)$ .

### 5.2.2 Sensitivity analysis of a phase response curve

The (input) infinitesimal phase response curve  $q(\cdot; \lambda)$  is an intrinsic characteristic of an oscillator model.

Given a nominal parameter value  $\lambda_0$ , the sensitivity of (input) infinitesimal phase response curve is the  $2\pi$ -periodic function  $S^q(\cdot; \lambda_0) : \mathbb{S}^1 \rightarrow \mathbb{R}$  defined as

$$S^q(\cdot; \lambda_0) := \frac{\partial q}{\partial \lambda}(\cdot; \lambda_0) = \lim_{h \rightarrow 0} \frac{q(\cdot; \lambda_0 + h) - q(\cdot; \lambda_0)}{h}. \quad (5.11)$$

From (3.24), we have, taking derivatives with respect to  $\lambda$ ,

$$\begin{aligned} S^q(\theta; \lambda_0) = & \left\langle S^p(\theta; \lambda_0), \frac{\partial f}{\partial u}(x^\gamma(\theta; \lambda_0), 0, \lambda_0) \right\rangle \\ & + \left\langle p(\theta; \lambda_0), \frac{\partial^2 f}{\partial x \partial u}(x^\gamma(\theta; \lambda_0), 0, \lambda_0) S^{x^\gamma}(\theta; \lambda_0) \right. \\ & \left. + \frac{\partial^2 f}{\partial \lambda \partial u}(x^\gamma(\theta; \lambda_0), 0, \lambda_0) \right\rangle \end{aligned} \quad (5.12)$$

where the  $2\pi$ -periodic function  $S^p(\cdot; \lambda_0) : \mathbb{S}^1 \rightarrow \mathbb{R}^n$  is the sensitivity of the (state) infinitesimal phase response curve defined as

$$S^p(\cdot; \lambda_0) := \frac{\partial p}{\partial \lambda}(\cdot; \lambda_0) = \lim_{h \rightarrow 0} \frac{p(\cdot; \lambda_0 + h) - p(\cdot; \lambda_0)}{h}. \quad (5.13)$$

From (3.56), we have, taking derivatives with respect to  $\lambda$  (see Appendix B.2),

$$\frac{\partial S^p}{\partial \theta}(\theta; \lambda_0) + \frac{1}{\omega} A(\theta; \lambda_0)^\top S^p(\theta; \lambda_0) = -\frac{1}{\omega} E^p(\theta; \lambda_0)^\top p(\theta; \lambda_0) \quad (5.14a)$$

$$S^p(2\pi; \lambda_0) - S^p(0; \lambda_0) = 0 \quad (5.14b)$$

$$\langle S^p(\theta; \lambda_0), v(\theta; \lambda_0) \rangle + \langle p(\theta; \lambda_0), S^v(\theta; \lambda_0) \rangle = S^\omega(\lambda_0) \quad (5.14c)$$

where we use the following short notation

$$\begin{aligned} E_{ij}^p(\theta; \lambda_0) := & \sum_{k=1}^n \frac{\partial^2 f_i}{\partial x_j \partial x_k}(x^\gamma(\theta; \lambda_0), 0, \lambda_0) S_k^{x^\gamma}(\theta; \lambda_0) \\ & + \frac{\partial^2 f_i}{\partial x_j \partial \lambda}(x^\gamma(\theta; \lambda_0), 0, \lambda_0) - \frac{1}{\omega} \frac{\partial f_i}{\partial x_j}(x^\gamma(\theta; \lambda_0), 0, \lambda_0) S^\omega(\lambda_0), \end{aligned} \quad (5.15)$$

$$S^v(\theta; \lambda_0) := \frac{\partial f}{\partial x}(x^\gamma(\theta; \lambda_0), 0, \lambda_0) S^{x^\gamma}(\theta; \lambda_0) + \frac{\partial f}{\partial \lambda}(x^\gamma(\theta; \lambda_0), 0, \lambda_0). \quad (5.16)$$

### 5.2.3 Sensitivity analysis of entrainment

Given a nominal parameter value  $\lambda_0$ , the sensitivity of the steady-state phase difference  $\chi^*(\lambda_0) \in [-\pi, \pi)$  is the scalar  $S^{\chi^*}(\lambda_0) \in \mathbb{R}$  defined as

$$S^{\chi^*}(\lambda_0) := \frac{\partial \chi^*}{\partial \lambda}(\lambda_0) = \lim_{h \rightarrow 0} \frac{\chi^*(\lambda_0 + h) - \chi^*(\lambda_0)}{h}. \quad (5.17)$$

From  $\Delta(\lambda_0) + \Gamma(\chi^*(\lambda_0); \lambda_0) = 0$ , we have, taking derivatives of with respect to  $\lambda$  and rearranging terms,

$$S^{\chi^*}(\lambda_0) = -\frac{S^\Delta(\lambda_0) + S^\Gamma(\chi^*(\lambda_0); \lambda_0)}{\Gamma'(\chi^*(\lambda_0); \lambda_0)} \quad (5.18)$$

where

$$S^\Delta(\lambda_0) := \frac{\partial \Delta}{\partial \lambda}(\lambda_0) = \lim_{h \rightarrow 0} [\Delta(\lambda_0 + h) - \Delta(\lambda_0)]/h, \quad (5.19)$$

$$S^\Gamma(\cdot; \lambda_0) := \frac{\partial \Gamma}{\partial \lambda}(\cdot; \lambda_0) = \lim_{h \rightarrow 0} [\Gamma(\cdot; \lambda_0 + h) - \Gamma(\cdot; \lambda_0)]/h. \quad (5.20)$$

Considering that  $\omega(\lambda) = \Omega + \Delta(\lambda)$  is the sum of a parameter independent term  $\Omega$  and a parameter dependent term  $\Delta(\lambda)$ , we have that  $S^\omega = S^\Delta$ . In addition, from (3.41), we have, taking derivatives with respect to  $\lambda$ ,

$$S^\Gamma(\cdot; \lambda_0) = \frac{1}{2\pi} \int_0^{2\pi} S^q(s + \cdot; \lambda_0) \tilde{h}_u(s) ds \quad (5.21)$$

(where  $\tilde{h}_u(\Omega_u t) = u(t)$  with  $\Omega_u = \Omega$ ). The sensitivity of the phase difference has thus two distinct contributions:

$$S^{\chi^*}(\lambda_0) = \underbrace{(-S^\omega(\lambda_0)/\Gamma'(\chi^*(\lambda_0); \lambda_0))}_{:=S_\omega^{\chi^*}(\lambda_0)} + \underbrace{(-S^\Gamma(\chi^*(\lambda_0); \lambda_0)/\Gamma'(\chi^*(\lambda_0); \lambda_0))}_{:=S_\Gamma^{\chi^*}(\lambda_0)} \quad (5.22)$$

where  $S_\omega^{\chi^*}(\lambda_0)$  denotes the contribution of the angular frequency sensitivity and  $S_\Gamma^{\chi^*}(\lambda_0)$  denotes the contribution of the coupling function sensitivity at  $\chi^*(\lambda_0)$ , the latter being closely related to the infinitesimal phase response curve through (5.21).

## 5.3 Numerics of sensitivity analysis

Numerical algorithms to solve boundary value problems (5.6) and (5.14) are reviewed in Appendix A. We stress that existing algorithms that compute periodic orbits and infinitesimal phase response curves are easily adapted to compute their sensitivity curves, essentially at the same numerical cost.

## 5.4 Summary

In this chapter, we presented a sensitivity analysis for oscillators viewed as input–output systems evolving on the circle. Starting from a state-space model, we provided accurate derivations of the sensitivity of the period and the sensitivity of the *infinitesimal* phase response curve, that is, the two fundamental characteristics of the circle representation of an oscillator under weak inputs.

The proposed approach is systematic and computationally tractable but it only provides a local sensitivity analysis in the parameter space, around a nominal set of parameter values. It complements more global—but less tractable—tools such as bifurcation analysis or parameter space exploration. Local and global sensitivity analysis techniques provide an valuable tool for probing the behavior of oscillators, leading to insight into their internal nature and predictions of the effect of external perturbations.

Under the assumption of an impulse train, the circle representation (hybrid phase model) is characterized by the period and the *finite* phase response curve. As the finite phase response curve cannot be expressed as the solution of an analytic problem, it is not possible to find an analytic problem to be solved in order to obtain its sensitivity. Finding efficient ways to characterize the sensitivity of finite phase response curves is still an open problem. A first step towards a sensitivity analysis for finite phase response curves could rely on the approximation given in Section 3.5.3.



## Chapter 6

# Singularly perturbed phase response curves

Many oscillators involve dynamics on multiple time scales. They appear in important biological phenomena such as spiking neurons [47, 48, 84, 130], heartbeats [36], mitotic cycles [23], glycolytic oscillations [24, 35, 59], population cycles of predator-prey type [113, 114, 184], but also in many other fields of application. In addition, in most of these oscillators, the input acts on the fast dynamics. Neural action potentials are exemplary of such systems. They exhibit two time-scale dynamics: a fast time scale for the spike generation and a slow time scale for the interspike frequency. The applied current acts directly on the membrane potential fast dynamics [47, 48, 84, 130].

Due to the time-scale separation and to the input acting on the fast dynamics, the reduction of such oscillators to one-dimensional continuous phase models is only valid in a small neighborhood of the periodic orbit. As a consequence, such a phase reduction is informative only for inputs that are much smaller than the singular perturbation parameter [88], therefore, vanishing in the singular limit. For this reason, only the *finite* phase response curve is a meaningful input–output characteristic for oscillator models.

Using geometric methods of singular perturbation theory, we develop the concept of singularly perturbed phase response curves to predict the phase response to finite perturbations from the description of the geometric structure underlying the oscillator dynamics in the singular limit.

This chapter is organized as follows. Section 6.1 summarizes basic concepts of singular perturbation theory used in this chapter and describes the geometry underlying relaxation oscillator dynamics. Section 6.2 stresses the limitations of standard infinitesimal phase response curves in the context of fast-slow oscillators with inputs on the fast variable. Section 6.3 introduces the

novel concepts of singularly perturbed (asymptotic) phase maps and singularly perturbed phase response curves.

*Contributions.* The main contributions of this chapter are to introduce two novel concepts: (i) “singularly perturbed phase maps” and (ii) “singularly perturbed phase response curves” for impulses and pulses of finite duration.

The material of this chapter is the result of a collaboration with Alessio Franci (postdoctoral researcher at the University of Liège). It has not yet been published and should be considered as “work-in-progress”.

## 6.1 Basics of singular perturbation theory

In this section, we briefly recall some classical results of singular perturbation theory and geometric assumptions for relaxation oscillators. This brief exposition follows the terminology and definitions of [91, 99].

### 6.1.1 Classical results of singular perturbation theory

The canonical form of two-dimensional fast-slow systems is

$$\dot{x} = f(x, z, \epsilon), \quad (6.1a)$$

$$\dot{z} = \epsilon g(x, z, \epsilon), \quad (6.1b)$$

where  $x \in \mathcal{X} \subseteq \mathbb{R}$ ,  $z \in \mathcal{Z} \subseteq \mathbb{R}$ , and  $0 < \epsilon \ll 1$  is a small positive parameter explicitly denoting the separation of time scales between the fast variable  $x$  and the slow variable  $z$ . In the slow time scale  $\tau := \epsilon t$ , dynamics (6.1) read

$$\epsilon x' = f(x, z, \epsilon), \quad (6.2a)$$

$$z' = g(x, z, \epsilon), \quad (6.2b)$$

(where the symbol  $'$  denotes differentiation with respect to the rescaled time  $\tau$ ). For  $\epsilon \neq 0$ , the two systems are equivalent and we call (6.1) the fast system and (6.2) the slow system. However, we have to distinguish between the limits for those systems as  $\epsilon \rightarrow 0$ , commonly referred as the singular limit.

Letting  $\epsilon \rightarrow 0$  in the fast system, we obtain the *layer dynamics*

$$\dot{x} = f(x, z, 0), \quad (6.3a)$$

$$\dot{z} = 0, \quad (6.3b)$$

whereas letting  $\epsilon \rightarrow 0$  in the slow system, we obtain the *reduced dynamics*

$$0 = f(x, z, 0), \quad (6.4a)$$

$$z' = g(x, z, 0). \quad (6.4b)$$

The essence of the geometric singular perturbation is to study qualitative properties of the original dynamics (6.1) by a combined analysis of the layer dynamics (6.3) and the reduced dynamics (6.4).

The reduced dynamics (6.4) is a dynamical system on the set

$$\mathcal{S}^0 := \{(x, z) \in \mathcal{X} \times \mathcal{Z} : f(x, z, 0) = 0\}, \quad (6.5)$$

usually called the *critical manifold*. For the layer dynamics, the critical manifold  $\mathcal{S}^0$  corresponds indeed to critical points: pieces of  $\mathcal{S}^0$  on which  $\frac{\partial f}{\partial x}$  is nonvanishing are normally hyperbolic invariant manifolds of equilibria (whose stability is determined by the sign of  $\frac{\partial f}{\partial x}$ ), and points in  $\mathcal{S}^0$  for which  $\frac{\partial f}{\partial x}$  is equal to zero constitute degenerate equilibria.

From Fenichel theory [46], nondegenerate pieces of critical manifolds  $\mathcal{S}^0$  perturb smoothly to normally hyperbolic locally invariant manifolds  $\mathcal{S}^\epsilon$  of (6.1) for  $\epsilon$  sufficiently small.

The analysis near degenerate points is more complex and has been treated in full generality in [97–99]. Here, we focus on phenomena that take place when the critical manifold  $\mathcal{S}^0$  has fold points, which are singularities of the reduced system (6.4). Under certain assumptions (see below), such folded structures of the critical manifold give rise to jumping behavior for solutions.

### 6.1.2 Geometry of relaxation oscillators

Following [97, 99], we impose a few geometric assumptions on the class of systems (6.1) to ensure the existence of a relaxation oscillator in isolation condition. The resulting geometry is illustrated in Figure 6.1 (left).

- (A1) The critical manifold  $\mathcal{S}^0$  is a “cubic” shaped curve. For the layer dynamics, it corresponds to a set of equilibria with a pair of folds,  $\mathcal{F}_- := (x_-, z_-)$  and  $\mathcal{F}_+ := (x_+, z_+)$  and can be broken into pieces as follows

$$\mathcal{S}^0 := \mathcal{S}_-^a \cup \mathcal{F}_- \cup \mathcal{S}^r \cup \mathcal{F}_+ \cup \mathcal{S}_+^a \quad (6.6)$$

where

$$\mathcal{S}_-^a := \{(b_{\mathcal{S}_-^a}(z), z) \in \mathcal{S}^0 : z_- < z\}, \quad (6.7a)$$

$$\mathcal{S}^r := \{(b_{\mathcal{S}^r}(z), z) \in \mathcal{S}^0 : z_- < z < z_+\}, \quad (6.7b)$$

$$\mathcal{S}_+^a := \{(b_{\mathcal{S}_+^a}(z), z) \in \mathcal{S}^0 : z < z_+\}. \quad (6.7c)$$

- (A2) For the layer dynamics, the lower branch  $\mathcal{S}_-^a$  and the upper branch  $\mathcal{S}_+^a$  are attracting, and the branch  $\mathcal{S}^r$  is repelling, that is,

$$\frac{\partial f}{\partial x}(x, z, 0) < 0 \quad \text{on } \mathcal{S}_-^a \cup \mathcal{S}_+^a, \quad \text{and} \quad \frac{\partial f}{\partial x}(x, z, 0) > 0 \quad \text{on } \mathcal{S}^r. \quad (6.8)$$

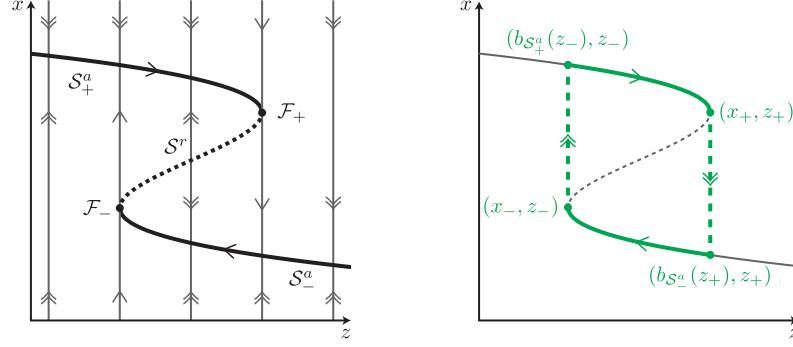


Figure 6.1 – Geometry of relaxation oscillators. (Left) The critical manifold  $\mathcal{S}^0$  is a “cubic” shaped curve and can be broken into pieces as follows  $\mathcal{S}^0 := \mathcal{S}_-^a \cup \mathcal{F}_- \cup \mathcal{S}^r \cup \mathcal{F}_+ \cup \mathcal{S}_+^a$ . (Right) Under assumptions A1–A4, the singular system (6.1) admits a singular periodic orbit  $\gamma^0$  defined as the union of two pieces of the critical manifold associated with a slow evolution (green solid lines) and two critical fibers associated with jumps (green dashed lines).

(A3) Both folds are generic, that is, satisfy the following conditions on  $\mathcal{F}_- \cup \mathcal{F}_+$

$$\frac{\partial^2 f}{\partial x^2}(x, z, 0) \neq 0, \quad \frac{\partial f}{\partial z}(x, z, 0) \neq 0, \quad \text{and,} \quad g(x, z, 0) \neq 0. \quad (6.9)$$

(A4) The set  $\{(x, z) \in \mathcal{X} \times \mathcal{Z} : g(x, z, 0) = 0\}$  intersects  $\mathcal{S}^0$  in only one point located on the repelling branch  $\mathcal{S}^r$ . In addition, the slow flow on  $\mathcal{S}_-^a$  satisfies  $z' < 0$  and the slow flow on  $\mathcal{S}_+^a$  satisfies  $z' > 0$ .

Under the previous assumptions, the singular system (6.1) admits a *singular periodic orbit*  $\gamma^0$  illustrated in Figure 6.1 (right) and defined as the union of

- the two pieces of the critical manifold joining  $(b_{\mathcal{S}_-^a}(z_+), z_+)$  to  $(x_-, z_-)$  and  $(b_{\mathcal{S}_+^a}(z_-), z_-)$  to  $(x_+, z_+)$  (in solid lines); and,
- the two (weakly) unstable critical fibers joining  $(x_-, z_-)$  to  $(b_{\mathcal{S}_+^a}(z_-), z_-)$  and  $(x_+, z_+)$  to  $(b_{\mathcal{S}_-^a}(z_+), z_+)$  (in dashed lines).

Following standard results [99], for all  $\epsilon > 0$  and sufficiently small, there exists a periodic orbit  $\gamma^\epsilon$  near the singular periodic orbit  $\gamma^0$ .

*Remark.* In the slow time scale, the jumps corresponding to critical fibers are instantaneous while the portions of critical manifolds are traveled in finite (slow)

time. The singular period  $T_{\text{slow}}^0$  (in the slow time scale) of the singular periodic orbit  $\gamma^0$  is thus equal to the sum of finite time intervals required to travel both portions of the critical manifold. The singularly perturbed period  $T_{\text{slow}}^\epsilon$  converges towards the singular period  $T_{\text{slow}}^0$ , that is,  $\lim_{\epsilon \rightarrow 0} T_{\text{slow}}^\epsilon = T_{\text{slow}}^0$ . (The associated angular frequency is denoted  $\omega_{\text{slow}}^0 := 2\pi/T_{\text{slow}}^0$ .)

In the fast time scale, the singular period  $T_{\text{fast}}^0$  of the singular periodic orbit  $\gamma^0$  blows up to infinity ( $T_{\text{fast}}^0 = \lim_{\epsilon \rightarrow 0} T_{\text{fast}}^\epsilon = T_{\text{slow}}^\epsilon/\epsilon = +\infty$ ).

## 6.2 Limitations of infinitesimal phase response curves

In this section, we emphasize the limitations of the *infinitesimal* phase response curves for relaxation oscillators with with input acting on the fast dynamics.

Many relaxation oscillators communicate with the environment through their fast variable. Those systems are thus modeled through relaxation oscillators with an input acting on the fast dynamics

$$\dot{x} = f(x, z, u, \epsilon), \quad (6.10a)$$

$$\dot{z} = \epsilon g(x, z, \epsilon), \quad (6.10b)$$

$$y = h(x, z, \epsilon). \quad (6.10c)$$

Neural cells are exemplative of such systems: they receive external information through an external current which acts only on the dynamics of the membrane potential (the fast variable for neural cells).

### Limitations of *infinitesimal* phase response curves

For this class of systems, the classical approximation of phase response curves by a scaling of the infinitesimal phase response curve is only valid for inputs that are much smaller than the singular perturbation parameter [88], that is,

$$Q^\epsilon(\cdot; \alpha \delta(\cdot)) = \alpha q^\epsilon(\cdot) + \mathcal{O}(\alpha^2), \quad \text{with } 0 < |\alpha| \ll \epsilon \ll 1, \quad (6.11)$$

where the singularly perturbed infinitesimal phase response curve  $q^\epsilon(\cdot)$  can be approximated by the singular infinitesimal phase response curve  $q^0(\cdot)$ .

Therefore, the domain of validity of the approximation (6.11) vanishes in the singular limit ( $\epsilon \rightarrow 0$ ). Intuitively, this limitation comes from the fact that, after an impulse of finite magnitude, the singular orbit might jump instantaneously to one branch of the critical manifold or the other, depending on the reset initial condition. This behavior involves a global phenomenon that cannot be captured by a local approximation.

### Singularly perturbed *finite* phase response curves

The main idea underlying our approach is to take advantage of time-scale separation to study the *finite* phase response curve in the singular limit. For a sufficiently small singular parameter  $\epsilon > 0$ , the “*singularly perturbed phase response curve*”  $Q^\epsilon(\cdot; u(\cdot))$  can be approximated by a “*singular phase response curve*”  $Q^0(\cdot; u(\cdot))$ , that is,

$$Q^\epsilon(\cdot; u(\cdot)) = Q^0(\cdot; u(\cdot)) + \mathcal{O}(\epsilon^\beta), \quad \text{with } 0 < \epsilon \ll 1, \quad (6.12)$$

for any phase resetting input  $u(\cdot)$  and with  $0 < \beta \leq 1$  (note that  $\beta$  is usually around 1/2 [97]).

In the following, we show how to exploit the geometry of fast-slow oscillators to predict the singular phase response curve  $Q^0(\cdot; u(\cdot))$  for impulses ( $u(\cdot) = \alpha \delta(\cdot)$ ) and for pulses of finite duration ( $u(\cdot) = \bar{u} [1_+(\cdot) - 1_+(\cdot - \Delta)]$ ).

## 6.3 Singularly perturbed phase response curves

In this section, we introduce two novel concepts: singularly perturbed (asymptotic) phase maps and singularly perturbed phase response curves.

Motivated by applications in neurodynamics, we consider open relaxation oscillators for two-dimensional fast-slow dynamical systems of the form

$$\dot{x} = f(x) - z + u \quad (6.13a)$$

$$\dot{z} = \epsilon g(x, z) \quad (6.13b)$$

$$y = x \quad (6.13c)$$

where the fast variable  $x \in \mathcal{X} \subseteq \mathbb{R}$  is a voltage-like variable, the slow variable  $z \in \mathcal{Z} \subseteq \mathbb{R}$  is a recovery variable, and  $0 < \epsilon \ll 1$ . The slow variable  $z$  provides a slow negative feedback that modulates the total quantity of applied current. The input  $u$  represents the applied current.

To simplify (6.10) to (6.13), we made the following assumptions.

- (A1) The input  $u$  enters the fast dynamics similarly to the slow variable  $z$ , such that its value is subtracted from the value of the slow variable  $z$ , that is, “ $z - u$ ”.
- (A2) The input  $u$  enters the fast dynamics in an affine way such that an impulse will reset the fast variable  $x$  without affecting the slow variable  $z$ .

Those technical assumptions simplify the presentation and are often (if not always) satisfied in models of neural oscillators.

### 6.3.1 Singularly perturbed phase maps and isochrons

A first step towards the prediction of phase response curves is the introduction of (asymptotic) phase maps and isochrons for singularly perturbed systems. The main idea is to define those objects in the singular limit (i.e.  $\epsilon \rightarrow 0$ ) and to rely on standard results to guarantee their persistence for sufficiently small values of  $\epsilon$ .

#### Singularly perturbed phase map

Since the singular periodic orbit  $\gamma^0$  is a one-dimensional manifold in  $\mathcal{X} \times \mathcal{Z}$ , it is naturally parameterized in terms of a single scalar phase on the unit circle  $\mathbb{S}^1$ . As in the nonsingular case (see Section 3.2.2), the phase map will be chosen such that the phase variable linearly increases with time. The construction of the singular phase map is illustrated in Figure 6.2 (left).

We choose to associate with the lower fold  $(x_-, z_-)$  the zero-phase reference position on the singular periodic orbit, that is  $\Theta^0(x_-, z_-) =: \vartheta_- = 0$ . As jumps are instantaneous in the singular limit, all points of the (weakly) unstable critical fiber joining  $(x_-, z_-)$  to  $(b_{\mathcal{S}_+^a}(z_-), z_-)$  are also associated with a phase equal to zero.

Then, the phase  $\theta$  associated with a point  $(x, z)$  is the “normalized” fraction of (slow) time  $\omega_{\text{slow}}^0 \Delta\tau$  needed to reach this point along the periodic orbit starting from the reference initial condition. For a point  $(x_1, z_1)$  on the upper branch, the phase will be given by

$$\Theta^0(x_1, z_1) := \omega_{\text{slow}}^0 \Delta\tau_1. \quad (6.14)$$

For a point  $(x_2, z_2)$  on the lower branch, the phase will be given by

$$\Theta^0(x_2, z_2) := \omega_{\text{slow}}^0 \Delta\tau_+ + \omega_{\text{slow}}^0 \Delta\tau_2 \quad (6.15)$$

where the first term corresponds to the flowing time on the upper branch (up to the upper fold) and the second term corresponds to the remaining flowing time on the lower branch. To simplify notation, it is convenient to denote by  $\Theta^0(x_+, z_+) =: \vartheta_+ = \omega_{\text{slow}}^0 \Delta\tau_+$  the phase associated with the upper fold (and all points of the (weakly) unstable critical fiber joining  $(x_+, z_+)$  to  $(b_{\mathcal{S}_+^a}(z_+), z_+)$ ).

An elegant way to summarize the phase map definition is

$$\Theta^0(x, z) := \begin{cases} \theta_- + \omega_{\text{slow}}^0 \psi_+(z_-, z, \mathbf{0}) & \text{if } (x, z) \in (\gamma^0 \cap \mathcal{S}_+^a) \cup \mathcal{F}_+ \\ \theta_+ + \omega_{\text{slow}}^0 \psi_-(z_+, z, \mathbf{0}) & \text{if } (x, z) \in (\gamma^0 \cap \mathcal{S}_-^a) \cup \mathcal{F}_- \end{cases} \quad (6.16)$$

where  $\psi_{\bullet}(z_0, z_\tau, \mathbf{0})$  (with  $\bullet$  standing for  $+$  or  $-$ ) are functions that measure the time needed to travel along the critical manifold from the initial condition  $z_0$  to final condition  $z_\tau$ .

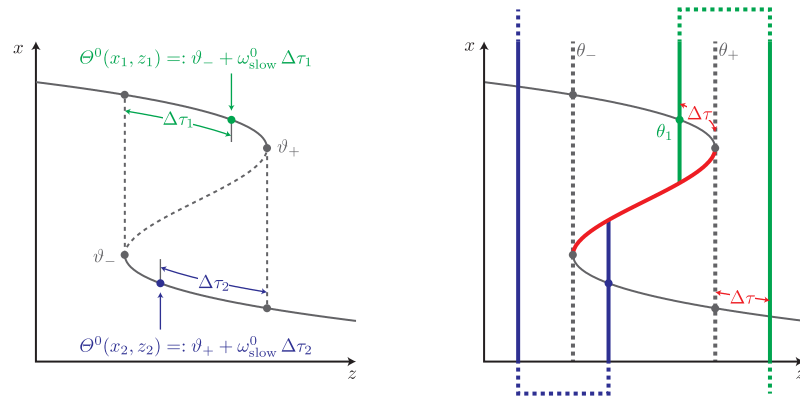


Figure 6.2 – Geometric construction of singular phase and asymptotic phase maps. (Left) The phase map associates with each point on the periodic orbit a phase which corresponds to the normalized time  $\omega_{\text{slow}}^0 \Delta\tau$  required to reach this point from the reference position  $(x_-, z_-)$ . For points on the lower branch, it is convenient to measure the normalized time from  $(x_+, z_+)$  and to add the phase  $\theta_+ := \omega_{\text{slow}}^0 \Delta\tau_+$ . (Right) Because all points on a same vertical ray (in the bistable region) and converging to the same branch instantaneously jump on the branch in the singular limit, the asymptotic phase map associates them with the same asymptotic phase. In addition, other vertical lines (outside the bistable region) are associated with the same phase because these points converge in the same  $\Delta\tau \pmod{T_{\text{slow}}^0}$  to  $(x_+, z_+)$ .

For constant inputs  $u(\cdot) \equiv \bar{u}$ , the function  $\psi_{\bullet}(z_0, z_{\tau}, \bar{u})$  can easily be computed by integrating the reduced dynamics of the system (6.13) on the stable branches of the critical manifold and they read

$$\psi_{\bullet}(z_0, z_{\tau}, \bar{u}) = \int_{z_0}^{z_{\tau}} \frac{1}{g(b_{\mathcal{S}_{\bullet}^a}(\xi - \bar{u}), \xi)} d\xi. \quad (6.17)$$

*Remark.* For constant inputs  $u(\cdot) \equiv \bar{u}$ , the critical manifold is shifted along  $z$ -axis because of Assumption 1 and each branch of the “shifted critical manifold” are described by  $x = b_{\mathcal{S}_{\bullet}^a}(z - u)$ .

### Singularly perturbed asymptotic phase map and isochrons

The notion of singular phase map can be extended to any point  $(x, z)$  in the basin of attraction of the singular periodic orbit by defining the singular asymptotic phase map  $\Theta^0 : \mathcal{B}(\gamma^0) \rightarrow \mathbb{S}^1$ . Because, in the singular limit, any singular trajectory starting from  $(x, z)$  instantaneously jumps from its initial condition (in the basin of attraction) to a branch of the critical manifold, all points on the same vertical line (with the same value of slow variable  $z$ ) and jumping to the same branch will be associated with the same phase. The construction of the singular asymptotic phase map is illustrated in Figure 6.2 (right).

- All points on the line  $z = z_-$  (resp.  $z = z_+$ ) are associated with the phase  $\theta_-$  (resp.  $\theta_+$ ).
- For points with a slow variable in the bistable range, the asymptotic phase  $\theta_1$  of a point  $(x_1, z_1)$  belonging to the basin of attraction of the upper (resp. lower) branch is thus given by the phase  $\vartheta_1$  of the point at the intersection between the line  $z = z_1$  and the upper (resp. lower) branch of the singular periodic orbit  $\gamma^0$ .
- In addition, all points outside the bistable range that converge to the upper fold in the same time interval  $\Delta\tau \pmod{T_{\text{slow}}^0}$  as  $(x_1, z_1)$  are also associated with the asymptotic phase  $\theta_1$ .

An elegant way to summarize the (asymptotic) phase map definition is

$$\Theta^0(x, z) = \begin{cases} \theta_- + \omega_{\text{slow}}^0 \psi_+(z_-, z, 0) \pmod{2\pi}, & \text{if } (x, z) \in \mathcal{B}(\mathcal{S}_+^a) \cup \mathcal{F}_+, \\ \theta_+ + \omega_{\text{slow}}^0 \psi_-(z_-, z, 0) \pmod{2\pi}, & \text{if } (x, z) \in \mathcal{B}(\mathcal{S}_-^a) \cup \mathcal{F}_-, \end{cases} \quad (6.18)$$

where  $\mathcal{B}(\mathcal{S}_{\bullet}^a)$  is the set of points that jumps to the stable branch  $\mathcal{S}_{\bullet}^a$  of the critical manifold.

*Remark.* For presentation convenience, we intentionally do not consider the unstable branch of the critical manifold  $\mathcal{S}^r$  as being part of the basin of attraction of the singular periodic orbit. For small  $\epsilon$ , this repulsive branch is perturbed into a repulsive set which has zero measure.

Isochrons are thus vertical lines for values of  $z$  outside the bistable range and vertical rays for values of  $z$  inside the bistable range. In the bistable region, vertical rays are separated by the repulsive branch  $\mathcal{S}^r$  of the critical manifold. The vertical ray and the vertical lines associated with the same phase join at infinity (see Figure 6.2, right).

This result formalizes the intuitive argument developed in Section 3.4.3 to justify the shape of isochrons for the van der Pol oscillator in the relaxation limit (Figure 3.6).

### 6.3.2 Singularly perturbed phase response curves

We consider the phase response curve for two particular inputs: impulses ( $u(\cdot) = \alpha \delta(\cdot)$ ) and pulses of finite duration ( $u(\cdot) = \alpha [1_+(\cdot) - 1_+(\cdot - \Delta)]$ ). We treat those two cases separately in the following.

#### Impulse

The effect of an impulse ( $u(\cdot) = \alpha \delta(\cdot)$ ) on the system (6.13) is to reset the initial state of the fast variable  $x$  without affecting the slow variable  $z$ . An initial condition  $(x_0, z_0)$  is reset to the new initial condition  $(x_0 + \alpha, z_0)$ . In the singular limit, the singular asymptotic reset phase map is thus given by the singular asymptotic phase associated with the reset state, that is,

$$\Theta^{+,0}(x_0, z_0; \alpha \delta(\cdot)) = \Theta^0(x_0 + \alpha, z_0). \quad (6.19)$$

The value of the asymptotic reset phase map  $\Theta^{+,0}(x_0, z_0; \alpha \delta(\cdot))$  is thus different from the value of the asymptotic phase map  $\Theta^0(x_0, z_0)$  only if the impulse resets an initial condition to a point on the other side of the curve  $\mathcal{C}$  that separates the basin of attraction of each branch (see Figure 6.3).

From this, the reset phase of a point on the upper (resp. lower) branch subjected to a positive (resp. negative) impulse is equal to the phase of the initial point. The phase shift induced by the impulse is thus equal to zero (see Figure 6.3, left).

However, on the lower (resp. upper) branch, there exists a set of points that are reset to the other side of the separatrix  $\mathcal{C}$  by a positive (resp. negative). For simplicity, we assume monotonicity of the separatrix in the bistable region (that is,  $(\partial b_{\mathcal{S}^r} / \partial z)(z) > 0$ ). Given a positive (resp. negative) impulse of amplitude  $\alpha$ , there exists a critical value  $z_c(\alpha)$  of the slow variable such that a trajectory starting on the lower (resp. upper) branch crosses the separatrix under the effect of the impulse for all  $z$ , such that  $z_- \leq z < z_c(\alpha)$  (resp.  $z_c(\alpha) < z \leq z_+$ ). The critical value  $z_c(\alpha)$  is given by

$$z_c(\alpha) = \{z \in \mathcal{Z} : b_{\mathcal{S}^-}(z) + \alpha = b_{\mathcal{S}^r}(z)\} \quad (6.20)$$

$$\text{(resp. } z_c(\alpha) = \{z \in \mathcal{Z} : b_{\mathcal{S}^+}(z) + \alpha = b_{\mathcal{S}^r}(z)\}). \quad (6.21)$$

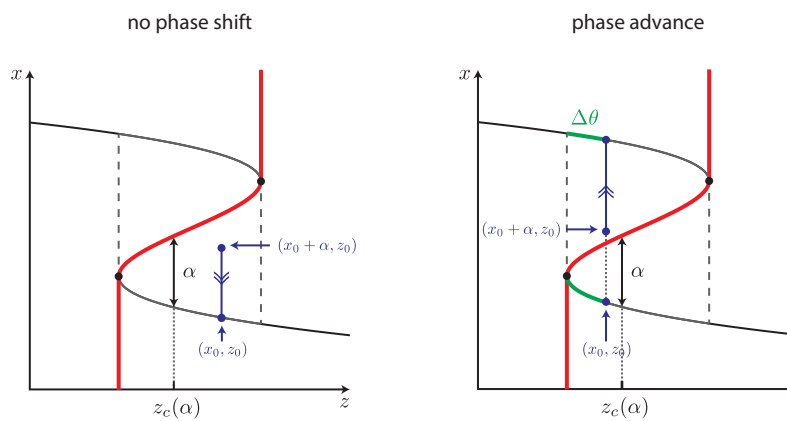


Figure 6.3 – Effect on positive impulses (the case of negative impulses can be treated in a similar way). (Left) Far from the lower fold (on the lower branch) or on the upper branch, the reset state converges back to the initial state instantaneously. As a consequence, no phase shift is produced. (Right) Close enough to the lower fold (on the lower branch), the reset state crosses the separatrix (red curve) and converges toward the upper branch instantaneously. The phase shift corresponds to the phase difference corresponding to the skipped portions of the singular periodic orbit (green).

The asymptotic phase associated with this critical point  $(b_{S^a}(z_c(\alpha)), z_c(\alpha))$  on the stable branch is denoted  $\Theta(b_{S^a}(z_c(\alpha)), z_c(\alpha)) =: \theta_c(\alpha)$ . The phase shift  $\Delta\theta$  induced by an impulse corresponds to the portion of singular periodic orbit skipped due to the impulse.

For positive impulse ( $\alpha > 0$ ), the phase response curve is given by

$$Q^0(\theta; \alpha \delta(\cdot)) = \begin{cases} \theta_- + \omega_{\text{slow}}^0 \psi_+(z_-, z^{\gamma^0}(\theta), \mathbf{0}) - \theta, & \text{if } \theta_c(\alpha) < \theta \leq \theta_-, \\ 0, & \text{otherwise.} \end{cases} \quad (6.22)$$

For negative impulse ( $\alpha < 0$ ), the phase response curve is given by

$$Q^0(\theta; \alpha \delta(\cdot)) = \begin{cases} \theta_+ + \omega_{\text{slow}}^0 \psi_-(z_+, z^{\gamma^0}(\theta), \mathbf{0}) - \theta, & \text{if } \theta_c(\alpha) < \theta < \theta_+, \\ 0, & \text{otherwise.} \end{cases} \quad (6.23)$$

### Pulse of finite duration

The effect of a pulse of finite duration (that is,  $u(\cdot) = \bar{u} [1_+(\cdot) - 1_+(\cdot - \Delta)]$ ) on the system (6.13) is less trivial.

Following the definition of the reset phase and (3.19), the asymptotic reset phase map for a pulse of finite duration is given by

$$\Theta^{+,0}(x_0, z_0; u(\cdot)) = \Theta^0(x_\Delta, z_\Delta) - \omega_{\text{slow}}^0 \Delta_{\text{slow}}^0 \quad (6.24)$$

where  $(x_\Delta, z_\Delta)$  is the state at time  $\Delta_{\text{slow}}^0$  for the reduced dynamics starting from  $(x_0, z_0)$  (where  $\Delta_{\text{slow}}^0$  is the pulse duration in the slow time scale and in the singular limit). It is thus necessary to compute the state  $(x_\Delta, z_\Delta)$  of the trajectory at the end of the pulse in order to compute the reset phase associated with its initial condition.

In the following, we describe how we can compute the state  $(x_\Delta, z_\Delta)$  using only the information contained in the functions  $\psi_-(z_+ + \bar{u}, z, \bar{u})$  and  $\psi_+(z_- + \bar{u}, z, \bar{u})$  (see Figure 6.4).

Starting from the initial condition  $(x_0, z_0)$  on the critical manifold, the trajectory evolves as follows (see Figure 6.4).

- (1) Under a constant input  $\bar{u}$ , the critical manifold of the system is shifted along the  $z$ -axis (because of Assumption 1). The singular trajectory jumps thus instantaneously to the branch of the “shifted critical manifold” corresponding to the basin of attraction to which the initial state belongs.
- (2) Then, the trajectory evolves on the “shifted critical manifold”, sliding slowly on branches and jumping instantaneously when it reaches “shifted folds”.

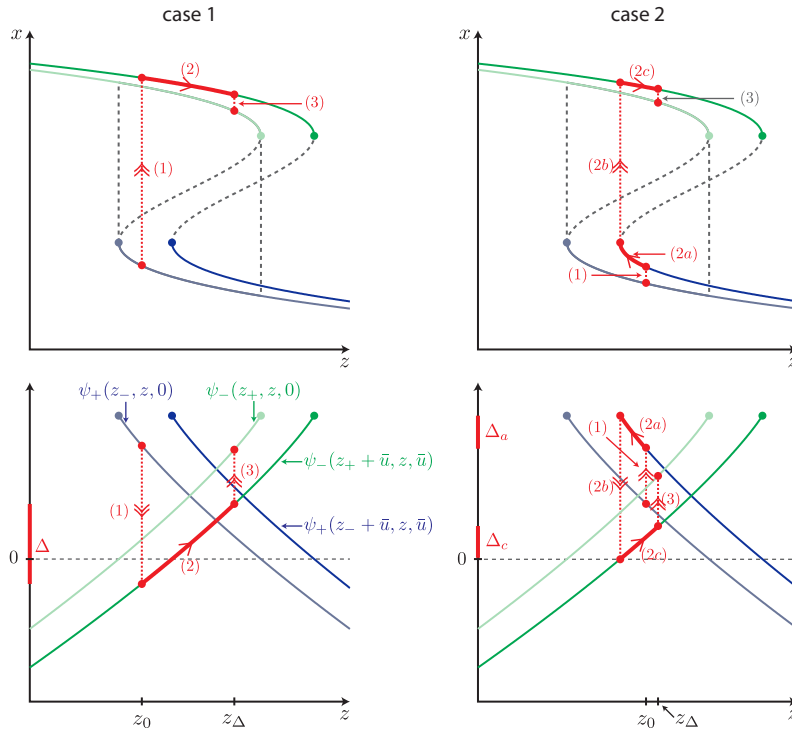


Figure 6.4 – Effect on positive pulses of finite duration (the case of negative pulses can be treated in a similar way). The state  $(x_\Delta, z_\Delta)$  of the trajectory starting from initial condition  $(x_0, z_0)$  (under a pulse of duration  $\Delta$ ) is graphically determined using functions  $\psi_\bullet$  in order to predict the phase response associated with this pulse. The effect of a positive pulse is to shift temporally the critical manifold along the  $z$ -axis to the right. The singular trajectory starting from  $(x_0, z_0)$  evolves as follows: (1) jumps instantaneously on the shifted critical manifold, then (2) evolves around the shifted hysteresis (for a duration  $\Delta = \Delta_a + \Delta_c$ ), and finally (3) jumps back to the initial critical manifold. The main difference between case 1 and case 2 is that during step (1) the trajectory converges to the opposite branch (with respect to the initial point) of the shifted critical manifold (in case 1) or to the same branch (with respect to the initial point) of the shifted critical manifold (in case 2).

- (3) Finally, the trajectory jumps instantaneously back to the critical manifold at the end of the pulse.

Because the slow variable  $z$  is one-dimensional, the evolution of a trajectory under constant input  $\bar{u}$  on an attractive branches is fully characterized by the functions  $\psi_-(z_+ + \bar{u}, z, \bar{u})$  and  $\psi_+(z_- + \bar{u}, z, \bar{u})$  during the flowing time. The total flowing time has to be equal to the duration  $\Delta_{\text{slow}}$ .

In Figure 6.4, we differentiate between two cases.

1. In case 1, the initial condition on the *lower* branch of the critical manifold jumps directly to the *upper* branch of the shifted critical manifold.
2. In case 2, the initial condition on the *lower* branch of the critical manifold jumps on the lower branch of the “shifted critical manifold”.

Case 1 produces larger phase shift than case 2.

The phase response curve is thus given by

$$Q^0(\theta; u(\cdot)) = \Theta^0(x_\Delta(\theta), z_\Delta(\theta)) - \omega_{\text{slow}}^0 \Delta_{\text{slow}} - \theta \quad (6.25)$$

where points  $(x_\Delta(\theta), z_\Delta(\theta))$  have to be computed as described previously for each point  $(x^{\gamma^0}(\theta), z^{\gamma^0}(\theta))$  on the singular periodic orbit  $\gamma^0$ .

*Remark.* The duration  $\Delta$  is expressed in the fast time scale, that is,  $\Delta_{\text{fast}}^\epsilon = \Delta$ . In the slow time scale, the duration is given by  $\Delta_{\text{slow}}^\epsilon = \epsilon \Delta_{\text{fast}}^\epsilon$ . We assume the duration of the pulse  $\Delta_{\text{slow}}^\epsilon$  (in the slow time scale) do not tend to zero in the singular limit and thus that the duration  $\Delta_{\text{fast}}^\epsilon$  tends to infinity. This assumption is motivated by the fact that the duration of the pulse is often a fraction of the period. So we may have  $\lim_{\epsilon \rightarrow 0} \Delta_{\text{fast}}^\epsilon = +\infty$  and  $\lim_{\epsilon \rightarrow 0} T_{\text{fast}}^\epsilon = +\infty$ , and a finite ratio  $\lim_{\epsilon \rightarrow 0} \Delta_{\text{fast}}^\epsilon / T_{\text{fast}}^\epsilon = C$  (with  $C \neq 0$  and  $C \neq \infty$ ).

An example is treated in Section 8.2.

## 6.4 Summary

In this chapter, we showed the limitation of infinitesimal phase response curves in the context of fast-slow oscillators. Then we developed semi-analytical methods to predict (i) the asymptotic phase map (and its isochrons) and (ii) the shape of *finite* phase response curves for impulses and pulses of finite duration in the singular limit.

As a consequence, it shows that geometric methods for systems with strong time-scale separation are powerful and can be exploited to better understand the effect of inputs on the system.

Another class of multiple time-scale systems are bursting oscillators. Those oscillators are characterized by three distinct time scales: a fast time scale

for the spike generation, a slow time scale for the intraburst spike frequency, and an ultra slow time scale for the interburst frequency [51]. In this case, for the two-dimensional layer dynamics, the singular manifold corresponds to a lower branch of equilibria (resting state) and an upper cylinder of stable periodic orbits (bursting state). Using averaging technique, we may “smooth” the dynamics on the cylinder of stable periodic orbits and apply a similar approach to predict the shape of the singular phase response curve for this kind of systems. We may investigate the dependence of this shape on the type of singularities that induce the jumps between resting and bursting states, leading to a classification of bursters.



## Chapter 7

# Systems analysis of circadian rhythm models in the space of phase response curves

Circadian rhythm is a biological process at the core of most living organisms which need to adapt their physiological activity to the 24 hours environmental cycle associated with earth's rotation (e.g. variations in light or temperature condition) [140]. Circadian entrainment is thus by nature an exogenous phenomenon because it involves the periodic forcing by the external environment.

Historically, the core mechanism responsible for circadian rhythms was based on the delayed negative feedback motif [64, 106, 110, 145]. More recently, detailed models with additional positive and negative loops have been proposed to describe circadian rhythms in *Drosophila* [49, 108]. In these systems, the input corresponds to the effect of light that increases or decreases the rate of transformation of some biochemical species.

In circadian rhythms, the phase response curve is used to study the effect of light (and sometimes the effect of drugs as melatonin) on the rhythm. A vast quantity of experimental phase response curves for circadian rhythms has been compiled in an atlas by Johnson [90]. Most of these phase response curves have a typical shape: it contains a so-called dead-zone, which is an interval of zero sensitivity during the subjective day of the studied organism.

From a systems analysis perspective, phase response curves are mainly used a posteriori in order to validate state-space models by comparing finite phase response curves from simulations and from experimental data [107]. Surpris-

ingly, only few studies really exploit the predictive nature of phase response curves to study the robustness of these rhythms and their entrainment [138]. Because of the smooth nature of circadian oscillations (relying on the delayed negative feedback motif), the infinitesimal phase response curve offers particularly valuable information that needs to be exploited in systems analysis. In addition, in most of these studies [109], the values of the parameters are often chosen empirically using trial-and-error or parameter exploration techniques due to few quantitative experimental data. Yet, with the increasing dimensionality of models in biology, these methods become quickly computationally intractable.

We apply the metric and sensitivity tools developed in Chapters 4 and 5 to analysis the parametric robustness of the rhythms through the robustness of the infinitesimal phase response curve and to guide the parametric system identification in the space of phase response curves.

This chapter is organized as follows. Section 7.1 proposes a parametric robustness analysis in the space of phase response curves. We develop scalar robustness measures to quantify the sensitivity of the angular frequency and the sensitivity of the infinitesimal phase response curves. We apply those measures to a detailed model. Section 7.2 provides a parametric system identification in the space of phase response curves. We introduce a gradient-descent algorithm to identify a set of parameter values which gives a phase response curve close to an experimental phase response curve (in our metric).

*Contributions.* The main contributions of this chapter are (i) to develop and apply scalar robustness measures for oscillators in the space of phase response curve and (ii) to propose a gradient-descent algorithm to perform parametric system identification in the space of phase response curves.

## 7.1 Parametric robustness analysis

Testing the robustness of a model against parameter variations is a basic systems question. In a number of situations, the very purpose of modeling is to identify those parameters that influence a given system property.

In the literature, robustness analysis of circadian rhythms mostly studies the zero-input steady-state behavior (period, amplitude of oscillations, etc.) [66, 168, 191] and (empirical) phase-based performance measures [14, 77, 78, 173].

In this section, we propose scalar robustness measures to quantify the sensitivity of the angular frequency (or the period) and the sensitivity of the infinitesimal phase response curve to parameters. We apply those measures to a model of the circadian rhythm.

### Scalar robustness measures

The angular frequency  $\omega$  is a positive scalar number. The sensitivity of  $\omega$  with respect to the parameter  $\lambda$  is thus also a scalar number  $S^\omega$ , leading to the scalar robustness measure  $R^\omega := |S^\omega|$ .

In contrast, the infinitesimal phase response curve (or its equivalence class)  $q$  belongs to a (nonlinear) space  $\mathcal{Q}$ . The sensitivity of  $q$  is thus a vector  $S^q$  which belongs to the tangent space  $T_q\mathcal{Q}$  at  $q$ . A scalar robustness measure  $R^q$  is defined as

$$R^q := \|S^q\|_q = \sqrt{g_q(S^q, S^q)} \quad (7.1)$$

where  $\|\cdot\|_q$  denotes the norm induced by the Riemannian metric  $g_q(\cdot, \cdot)$  at  $q$ . It is the natural extension of robustness measures to a (nonlinear) space  $\mathcal{Q}$ .

When  $\mathcal{Q}$  is a quotient space, the element  $q$  and the tangent vector  $S^q$  are abstract objects. The evaluation of the robustness measure relies on the sensitivity  $S^{\bar{q}}$  of the signal  $\bar{q}$  defining the equivalence class in the total space

$$R^q = \|P_{\bar{q}}^h S^{\bar{q}}\|_{\bar{q}} = \sqrt{\bar{g}_{\bar{q}}(P_{\bar{q}}^h S^{\bar{q}}, P_{\bar{q}}^h S^{\bar{q}})} \quad (7.2)$$

where  $P_{\bar{q}}^h$  is the projection operator onto the horizontal space  $\mathcal{H}_{\bar{q}}$ . The projection removes the component of the sensitivity which is tangent to the equivalence class.

The stable phase difference  $\chi^*$  is a scalar phase on the unit circle  $\mathbb{S}^1$ . The sensitivity of  $\chi^*$  with respect to the parameter  $\lambda$  is a scalar number  $S^{\chi^*}$ , leading to a scalar robustness measure  $R^{\chi^*} := |S^{\chi^*}|$ .

When analyzing a model with several parameters ( $\lambda \in \Lambda \subseteq \mathbb{R}^l$ ), all robustness measures  $R^x$  (where  $x$  stands for any characteristic of the oscillator) collect in a  $l$ -dimensional vector the scalar robustness measure corresponding to each parameter. This vector is often normalized as follows

$$\rho^x = \frac{R^x}{\|R^x\|_\infty} \quad (7.3)$$

where  $\|\cdot\|_\infty$  denotes the maximum norm such that elements of  $\rho^x$  belongs to the unit interval  $[0, 1]$ . This measure allows to rank model parameters according to their ability to influence the characteristic  $x$ .

In addition, it is often meaningful to compute relative sensitivity measures, that is, relative changes in the model characteristic to relative changes in parameter values.

### Quantitative circadian oscillator model

We illustrate our parametric robustness analysis on a quantitative circadian rhythm model for mammals developed by Leloup and Goldbeter [108] (see Figure 7.1). The model describes the regulatory interactions between the products

of several genes (*Per*, *Cry*, and *Bmal1*). A negative autoregulatory feedback loop established by the *per* (period) and *cry* (cryptochrome) genes is at the heart of the circadian oscillator. The PER and CRY proteins form a complex PER–CRY that indirectly represses the activation of the *Per* and *Cry* genes. The PER–CRY complexes exert their repressive effect by binding to a complex of two proteins CLOCK–BMAL1. This latter, formed by the products of *Clock* and *Bmal1* genes, activates *Per* and *Cry* transcription. In addition to this negative autoregulation, an (indirect) positive regulatory feedback loop is also involved. Indeed, the *Bmal1* expression is subjected to negative autoregulation by CLOCK–BMAL1, through the product of the *Rev-Erba* gene. The complex PER–CRY enhances *Bmal1* expression in an indirect manner by binding to CLOCK–BMAL1, and thereby reducing the transcription of the *Rev-Erba* gene. Finally, environmental periodic cycles associated with earth’s rotation are mediated through light–dark cycles. Light acts on the system by inducing the expression of the *Per* gene.

The detailed computational model of [108] possesses 16 state variables and 52 parameters. State-space model equations and nominal parameter values are available in [108, Supporting Text]. The effect of light is incorporated through periodic square-wave variations in the maximal rate of *Per* expression (i.e. the value of the parameter  $v_{sP}$  goes from a constant low value during dark phase to a constant high value during light phase). Parameters values remain to be determined experimentally and have been chosen semiarbitrarily in physiological ranges in order to satisfy experimental observations. This model has been extensively studied through unidimensional bifurcation analyses and various numerical simulations of entrainment [108, 109].

Each parameter of the model describes a single regulatory mechanism such as transcription and translation control of mRNAs, degradation of mRNAs or proteins, transport reaction, and phosphorylation/dephosphorylation of proteins. The analysis of single-parameter sensitivities thus reveals the importance of individual regulatory processes on the function of the oscillator.

In order to emphasize the potential role of circuits rather than single-parameter properties, we group model parameters according to the mRNA loop to which they belong. In the graphical plots, each group of parameters is associated with a different color: *Per*-loop in blue, *Cry*-loop in red, and *Bmal1*-loop in green. In addition, we gathered parameters associated with interlocked loops in a last group represented in gray.

We develop our robustness analysis in the space  $\mathcal{Q}_D$  incorporating both scaling and phase shifting equivalence properties. This is motivated by the uncertainty about the exact magnitude of the light input on the circadian oscillator and by the absence of precise experimental state trajectories preventing from defining a precise reference position (corresponding to the initial phase).

In the following, we consider sensitivities to relative parameter variations.

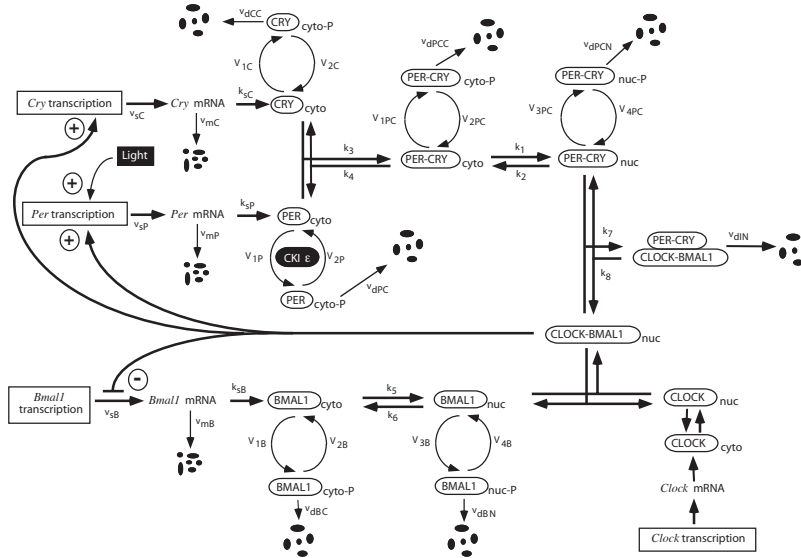


Figure 7.1 – The Leloup-Goldbeter model accounts for several regulatory processes identified in circadian rhythms of mammals. Figure taken from [108].

### Sensitivity analysis of the period and the phase response curve

The period and the phase response curve are two intrinsic characteristics of the circadian oscillator with physiological significance. We study the sensitivity analysis of the period and the phase response curve to measure the influence of regulatory processes on tuning the period and shaping the phase response curve.

A two-dimensional  $(\rho^\omega, \rho^q)$  scatter plot in which each point corresponds to a parameter of the model reveals the shape and strength of the relationship between both normalized robustness measures  $\rho^\omega$  (angular frequency or, equivalently, period) and  $\rho^q$  (phase response curve). It enables to identify which characteristic is primarily affected by perturbations in individual parameters: parameters below the dashed bisector mostly influence the period; those above the dashed bisector mostly influence the phase response curve (see Figure 7.2).

At a coarse level of analysis, the scatter plot reveals that most parameters exhibit both low sensitivities of the period and of the phase response curve (most points are close to the origin); only few parameters display a medium or high sensitivity either of period or of phase response curve.

At a finer level of analysis, the scatter plot reveals a qualitative difference of sensitivity for the parameters associated with each of the three mRNA loops (materialized for each loop by a least-square regression line passing through

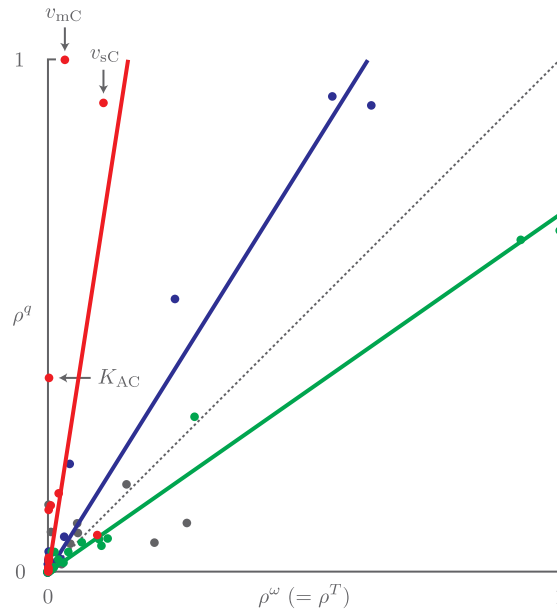


Figure 7.2 – Local parametric robustness analysis in the space of infinitesimal phase response curves. Normalized robustness measures  $\rho^\omega$  (angular frequency) and  $\rho^q$  (infinitesimal phase response curve) reveal the distinct sensitivity of three distinct genetic circuits (*Cry*, *Per*, and *Bmal1*). Each point is associated to a particular parameter. The three lines are regression over the parameters of the three gene loops. The dashed bisector indicates the positions at which both measures of robustness are identical. Only parameters associated with the *Cry*-loop exhibit low angular frequency and high infinitesimal phase response curve sensitivities. The color code corresponds to different subsets of parameters associated to different loops (see the text for details).

the origin):

- the *Bmal1*-loop parameters are associated with a high sensitivity of the period and a medium sensitivity of the phase response curve (regression line below the bisector);
- the *Per*-loop parameters are associated with a medium sensitivity of the period and a high sensitivity of the phase response curve (regression line above the bisector);
- the *Cry*-loop parameters are associated with a low sensitivity of the period and a high sensitivity of the phase response curve (regression line above the bisector, close to the vertical axis).

In each feedback loop, the three most sensitive parameters represent the three same biological functions: the maximum rates of mRNA synthesis ( $v_{sB}$ ,  $v_{sP}$ , and  $v_{sC}$ ), the maximum rate of mRNA degradation ( $v_{mB}$ ,  $v_{mP}$ , and  $v_{mC}$ ), and the inhibition (I) or activation (A) constants for the repression or enhancement of mRNA expression by BMAL1 ( $K_{IB}$ ,  $K_{AP}$ , and  $K_{AC}$ ). Those three parameters primarily govern the sensitivity tendency associated to each loop.

The small number of highly sensitive parameters is in agreement with the robust nature of the circadian clock and the concentration of fragilities in some specific locations of the architecture [168]. Our analysis suggests that the transcriptional and translational control of mRNA (i.e. the control of both biological steps required to synthesize a protein) has to be regulated by specific mechanisms (not included in the model) in order to avoid failures in the clock function. While the topology of *Per*- and *Cry*-loops are identical, the asymmetry introduced by the choice of parameter values leads to different sensitivity curve for those loops. Both loops have a similar high sensitivity of the phase response curve (while the light acts only on the maximum rate of *Per* mRNA synthesis) but a different sensitivity of the period, the *Per*-loop being more sensitive than the *Cry*-loop. The high sensitivity of the period for parameters associated with the *Bmal1*-loop has also been identified in [109]. However, this last prediction of the model (high sensitivity of the period to *Bmal1*-loop) is not in agreement with experimental observations in [21, 186]. This observation may encourage the biologist and the modeler to design of new experiments to enlighten biological mechanisms responsible for this discrepancy between the experiment and the model.

Two of the three sensitive parameters of the *Cry*-loop emphasized by our sensitivity analysis have been identified by numerical simulations as important for entrainment properties of the model without affecting the period ( $K_{AC}$  in [108] and  $v_{mC}$  in [109]). Our approach supports the importance of those two parameters and identifies the potential importance of a third one ( $v_{sC}$ ).

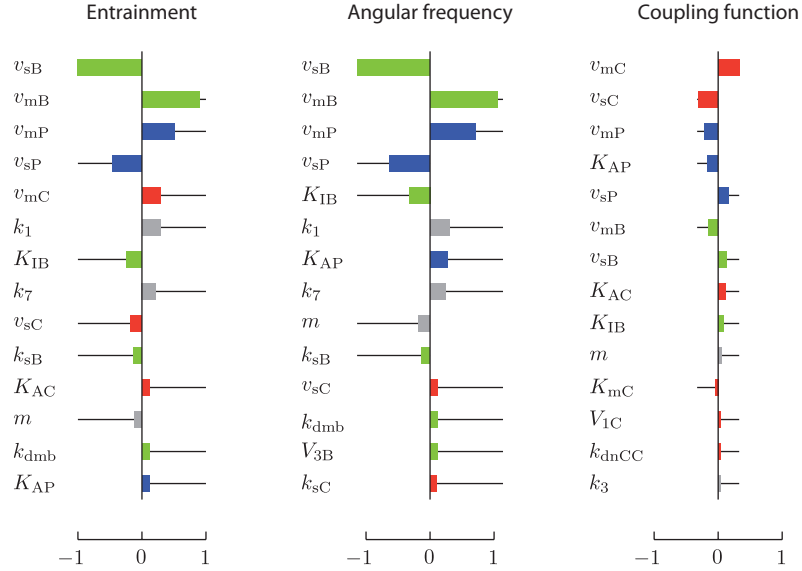


Figure 7.3 – Normalized sensitivity measures  $S^{x^*} / \|S^{x^*}\|_{\infty}$  (entrainment) are due to two contributions:  $S_{\omega}^{x^*} / \|S^{x^*}\|_{\infty}$  (angular frequency) and  $S_{\Gamma}^{x^*} / \|S^{x^*}\|_{\infty}$  (coupling function). Each (thick) horizontal bar corresponds to a sensitivity measure with respect to a particular parameter. The (thin) horizontal lines indicate (in absolute value) the maximal sensitivity (among all parameters) and may be useful to compare the sensitivity of a parameter to the maximal sensitivity. The color code corresponds to different subsets of parameters associated to different loops (see the text for details).

### Sensitivity analysis of the entrainment

Entrainment is an important characteristic of the circadian model. In Section 5.2.3, we have seen that the entrainment sensitivity  $S^{x^*}$  is mathematically given by the summation of two terms: a term  $S_{\omega}^{x^*}$  proportional to the period sensitivity and a term  $S_{\Gamma}^{x^*}$  proportional to the coupling function sensitivity at  $\chi^*$ . Those two terms correspond to two biologically distinct mechanisms by which the entrainment properties of the circadian clock can be regulated: a modification of the period or a modification of the coupling function (resulting from the modification of the infinitesimal phase response curve or the input signal).

Bar plots of  $S^{x^*} / \|S^{x^*}\|_{\infty}$ ,  $S_{\omega}^{x^*} / \|S^{x^*}\|_{\infty}$ , and  $S_{\Gamma}^{x^*} / \|S^{x^*}\|_{\infty}$  in which each bar corresponds to a parameter allows to identify the most sensitive parameters

for entrainment and to quantify the respective contribution of both mechanisms in the entrainment sensitivity (see Figure 7.3). The entrainment sensitivity and the contributing terms are normalized by  $\|S^{x^*}\|_\infty$  (the same maximal value of the entrainment sensitivity) such that the summation of normalized terms is equal to the normalized entrainment sensitivity. For each bar plot, we sorted parameters by absolute magnitude and restricted the plot to the 14 parameters with the highest sensitivity measure (the number 14 results from our choice to keep the parameters with an entrainment sensitivity greater than 0.1). Those plots allow to identify the parameters which play an important role in the entrainment sensitivity. We note that the parameter orders for  $S^{x^*} / \|S^{x^*}\|_\infty$  and  $S_\omega^{x^*} / \|S^{x^*}\|_\infty$  are almost identical, except for parameters associated with the *Cry*-loop. Those parameters appear in the highest ones for  $S_T^{x^*} / \|S^{x^*}\|_\infty$ .

Figure 7.4 (top) reveals the competitive and complementary nature of both contributions to entrainment sensitivity. For most parameters, both contributions have opposite signs, that is, points are located in the second and fourth quadrants. In addition, both mechanisms are well decoupled such that, when one mechanism is active, the other is almost inactive (points are located close to the horizontal and vertical axes). Parameters associated with *Cry*-loop seem to influence the entrainment sensitivity through a modification of the coupling function (points close to the vertical axis); others parameters associated with *Per*-loop and *Bmal1*-loop seem to influence the entrainment sensitivity through a modification of the period (points close to the horizontal axis).

The different mechanisms leading to entrainment sensitivity are also observed in both other scatter plots (see Figure 7.4 bottom-left and -right). In those plots, parameters associated with points close to the bisector of the first and third quadrants influence the entrainment sensitivity through a modification of the period (bottom-left) or the coupling function (bottom-right), respectively. Again, only parameters associated with the *Cry*-loop seem to affect the entrainment through a variation of the phase response curve.

Two of the parameters belonging to the *Cry*-loop (with high coupling function and low period sensitivities) have been identified by numerical simulations as important for entrainment properties of the model without affecting the period:  $K_{AC}$  in [108] and  $v_{mC}$  in [109]. Our approach supports the importance of those two parameters and identifies the potential importance of a third one ( $v_{sC}$ ).

**Remark** We stress that the conclusions in [108, 109] rely on extensive simulations of the model to simulate entrainment conditions while varying one parameter at a time. In contrast, the proposed analysis is systematic and allows a computationally cheap screening of all parameters. The plots in Figure 7.2–7.4 are generated in less than a minute with our MATLAB code.

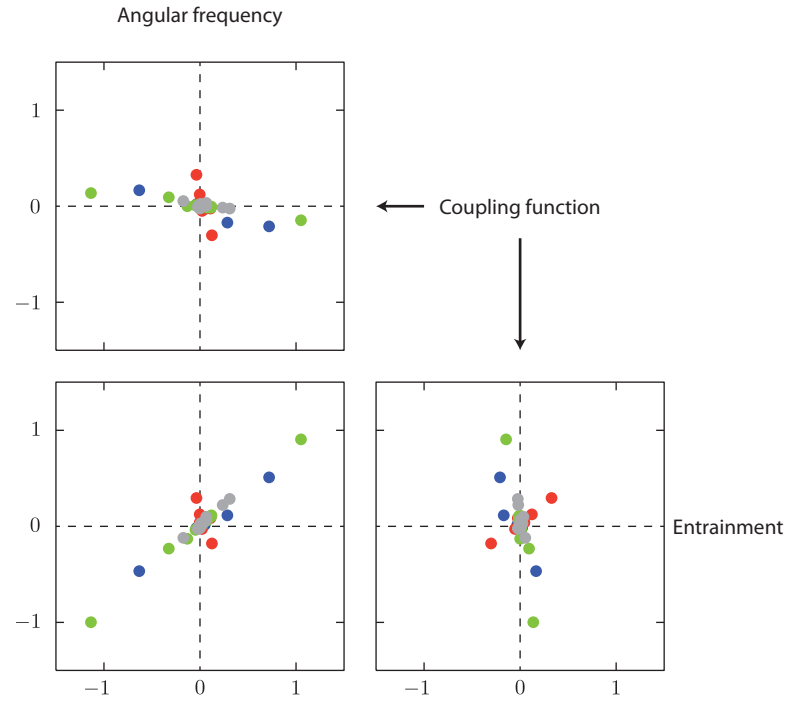


Figure 7.4 – Normalized scalar sensitivity measures  $S^{x^*} / \|S^{x^*}\|_\infty$  (entrainment),  $S_\omega^{x^*} / \|S^{x^*}\|_\infty$  (angular frequency contribution to entrainment), and  $S_\Gamma^{x^*} / \|S^{x^*}\|_\infty$  (coupling function contribution to entrainment) exhibit particular correlation shapes. The top graph represents the  $(S_\omega^{x^*} / \|S^{x^*}\|_\infty, S_\Gamma^{x^*} / \|S^{x^*}\|_\infty)$ -plan; the bottom-left graph represents the  $(S_\omega^{x^*} / \|S^{x^*}\|_\infty, S^{x^*} / \|S^{x^*}\|_\infty)$ -plan; and the bottom-right graph represents the  $(S_\Gamma^{x^*} / \|S^{x^*}\|_\infty, S^{x^*} / \|S^{x^*}\|_\infty)$ -plan. Each point is associated to a particular parameter. The color code corresponds to different subsets of parameters associated to different loops (see the text for details). Those correlations support the competitive nature of both mechanisms (modification of the period or the coupling function) leading to the entrainment sensitivity.

### Nonlocal sensitivity analysis

To evaluate the nonlocal nature of our local predictions, we plot in Figure 7.5 the time behavior of solutions for different finite (nonlocal) parameter changes. The left plots illustrate the autonomous oscillation of the isolated oscillator whereas the right plots illustrate the steady-state solution entrained by a periodic light input. Parameter perturbations are randomly taken in a range of  $\pm 10\%$  around the nominal parameter value. Each panel corresponds to the perturbation of a different group of parameters (the black time-plot corresponds to the nominal system behaviors for nominal parameter values).

- A. Perturbations of three most sensitive parameters of *Cry*-loop ( $v_{sC}$ ,  $v_{mC}$ , and  $K_{AC}$ ) lead to small variations (mostly shortening) of the autonomous period and (not structured) large variations of the phase-locking. This observation is consistent with the low sensitivity of the period and the high sensitivity of the phase response curve.
- B. Perturbations of three most sensitive parameters of *Bmal1*-loop ( $v_{sB}$ ,  $v_{mB}$ , and  $K_{IB}$ ) lead to medium variations of the autonomous period and medium variations of the phase-locking. The variations of the phase-locking exhibit the same structure as variations of the period, suggesting that the change in period is responsible for the change of phase-locking for those parameters. This observation is consistent with the high sensitivity of the period and the medium sensitivity of the phase response curve.
- C. Perturbations of three most sensitive parameters of *Per*-loop ( $v_{sP}$ ,  $v_{mP}$ , and  $K_{AP}$ ) exhibit an intermediate behavior between the situations A and B.
- D. Perturbations of parameters of interlocked loops lead to small variations of the autonomous period and the phase-locking, which is consistent with their low sensitivity.

Those (nonlocal) observations are thus well predicted by the classification of parameters suggested by the (local) sensitivity analysis (see Figure 7.2).

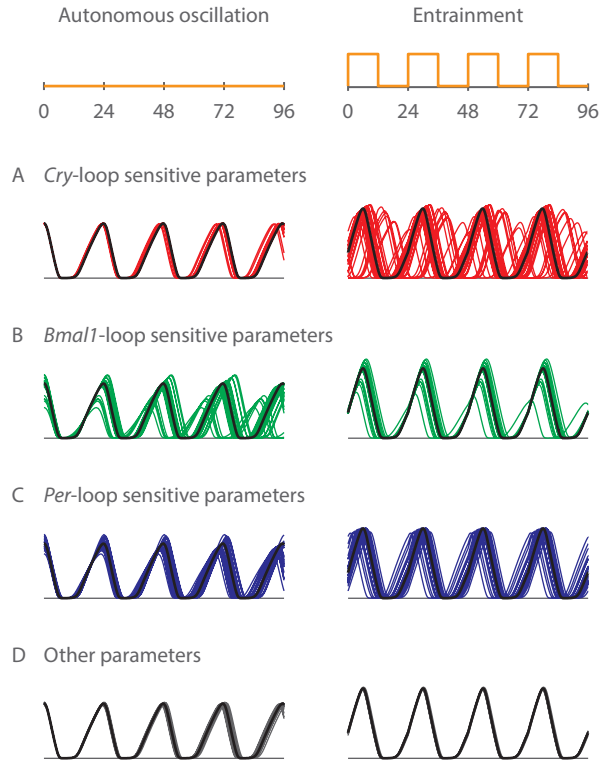


Figure 7.5 – Validation of the local parametric robustness analysis for finite (non-local) parameter perturbations. Steady-state behaviors for the nominal model and different finite (nonlocal) parameter perturbations are illustrated by time-plots of the state variable  $M_P$  under constant environmental conditions (autonomous oscillation, left) and periodic environmental conditions (entrainment, right). Each panel (or row) corresponds to the perturbation of a different group of parameters, the black time-plot corresponding to system behaviors for nominal parameter values. Perturbations are randomly taken in a range of  $\pm 10\%$  around the nominal parameter value (for one parameter at a time). **A.** Perturbations of three most sensitive parameters of *Cry*-loop ( $v_{sC}$ ,  $v_{mC}$ , and  $K_{AC}$ ) lead to small variations of the autonomous period and (not structured) large variations of the phase-locking. **B.** Perturbations of three most sensitive parameters of *Bmal1*-loop ( $v_{sB}$ ,  $v_{mB}$ , and  $K_{IB}$ ) lead to larger variations of the autonomous period and medium variations of the phase-locking. **C.** Perturbations of three most sensitive parameters of *Per*-loop ( $v_{sP}$ ,  $v_{mP}$ , and  $K_{AP}$ ) exhibit an intermediate behavior between the situations A and B. **D.** Perturbations of parameters of interlocked loops lead to small variations of the autonomous period and the phase-locking.

## 7.2 Parametric system identification

System identification deals with the problem of building mathematical models of dynamical systems based on observed data from the systems. In particular, parametric system identification aims at finding a set of parameter values in agreement with observed data for a given state-space model structure.

In the literature, parameter values for circadian rhythm models are often determined empirically by trial-and-error methods due to the few pieces of experimental information about parameter values.

In this section, we aim at providing a gradient-descent algorithm to identify a set of parameter values which gives a phase response curve close to an experimental phase response curve (in our metric). We illustrate this algorithm on a qualitative circadian oscillator model.

### Gradient-descent algorithm

A standard method to tackle the system identification problem is to recast it into an optimization framework. The minimization of an empirical cost  $\tilde{V}(\lambda)$  yields the parameter estimate

$$\hat{\lambda} = \arg \min_{\lambda \in \Lambda} \tilde{V}(\lambda) \quad (7.4)$$

where  $\tilde{V}(\lambda) : \Lambda \rightarrow \mathbb{R}_{\geq 0}$  penalizes the discrepancy between observed data from the system and prediction from the model. Local minimization is usually achieved with a gradient-descent algorithm requiring the computation of the gradient  $\nabla_{\lambda} \tilde{V}(\lambda)$ .

Given an ‘experimental-like’ phase response curve  $\bar{q}_0$  (or its equivalence class  $q_0 = [\bar{q}_0]$ ), a natural cost function  $\tilde{V}(\lambda)$  is defined as

$$\tilde{V}(\lambda) := V(q(\lambda)) = \frac{1}{2} \text{dist}(q(\lambda), q_0)^2 \quad (7.5)$$

where  $\text{dist}(\cdot, \cdot)$  is the distance in the (nonlinear) space  $\mathcal{Q}$ . The gradient (in the parameter space  $\Lambda$ ) of this cost function with respect to the parameter  $\lambda_j$  is given by

$$\nabla_{\lambda_j} \tilde{V}(\lambda) = g_q \left( \text{grad}_q V(q(\lambda)), S_j^q(\lambda) \right) \quad (7.6)$$

where  $\text{grad}_q V(q(\lambda))$  and  $S_j^q(\lambda)$  are elements in the tangent space  $T_q \mathcal{Q}$ .

When  $\mathcal{Q}$  is a quotient space, the evaluation of the gradient  $\nabla_{\lambda_j} \tilde{V}(\lambda)$  relies on representatives in the total space

$$\nabla_{\lambda_j} \tilde{V}(\lambda) = \bar{g}_{\bar{q}} \left( \text{grad}_{\bar{q}} \bar{V}(\bar{q}(\lambda)), P_{\bar{q}}^h S_j^{\bar{q}}(\lambda) \right) \quad (7.7)$$

where  $\bar{V}(\bar{q}) = V([\bar{q}])$  for all  $\bar{q} \in [\bar{q}]$ .

*Remark.* Actual experimental phase response curves are finite discrete sets of measurements. The comparison of the model prediction to those measurements would require a discretized version of our distances. We do not consider this in this paper. The illustration problem can be seen as the second step of a procedure in which a continuous curve have been fitted in a first step to experimental data. We can also see this problem as fitting the parameter of a reduced model to reproduce the phase response curve of a quantitative model.

### Qualitative circadian oscillator model

We illustrate the system identification on a qualitative circadian rhythm model. The Goodwin oscillator is a cyclic feedback system where metabolites repress the enzymes which are essential for their own synthesis by inhibiting the transcription of the molecule DNA to messenger RNA (mRNA) [68]. It can be described as the cyclic interconnection of three first-order subsystems and a monotone static nonlinearity

$$\tau_m \dot{m} = -m + K_m \frac{1}{1 + [(p + u)/\kappa]^\nu} \quad (7.8a)$$

$$\tau_e \dot{e} = -e + K_e m \quad (7.8b)$$

$$\tau_p \dot{p} = -p + K_p e \quad (7.8c)$$

$$y = e. \quad (7.8d)$$

A dimensionless form of this system is equivalent to impose  $K_e = K_p = \tau_m = \kappa = 1$ . For notational convenient, the remaining static gain is denoted  $K_m = K$ .

To simplify the analysis (but without loss of generality), we reduce the parameter space to two dimensions: we impose equal time constants ( $\tau_e = \tau_p = \tau$ ) and we fix the Hill coefficient  $\nu = 20$ . This high coefficient is justified for the purpose of the illustration by the necessity to get periodic orbits ( $\nu > 8$ ) and strong enough differences between infinitesimal phase response curve shapes in the parameter space. The results for weaker coefficient are similar but less marked. The parameter space reduces to  $(K, \tau) \in \mathbb{R}_{>0}^2$ .

An ‘experimental-like’ infinitesimal phase response curve is chosen as the infinitesimal phase response curve computed for a quantitative circadian rhythm model of *Drosophila* which agrees with experimental data [107, 110].

In this context, it is meaningful to perform the identification in the space  $\mathcal{Q}_D$  incorporating both scaling and phase shifting equivalence properties for the same reasons as in the previous illustration.

### System identification

The Goodwin model exhibits stable oscillations in a region of the reduced parameter space (Figure 7.6, top). The border of this region corresponds to a

supercritical Andronov-Hopf bifurcation through which the model single equilibrium loses its stability. The contour levels of the cost function—which have been computed in the whole region to make results interpretation easier—reveal two local minima of the cost function.

Picking initial guess values for model parameters, the gradient-descent algorithm minimizes the cost function following a particular path in the parameter space (Figure 7.6, top). The cost function value decreases at each step of the algorithm along this path (Figure 7.6, bottom). The optimal infinitesimal phase response curve (blue or red) fits very well the ‘experimental’ one (gray), in contrast to the initial infinitesimal phase response curve.

Due to the nonconvexity of the cost function, two paths starting from different initial points may evolve towards different local minima. In the present example, the cost function happens to be (nearly) symmetric with respect to a unitary time-constant  $\tau$  and both local minima correspond to similar infinitesimal phase response curves (up to a scaling factor and a phase shift).

To evaluate the consistency of our identification procedure in the space of infinitesimal phase response curves with prediction on finite phase response curves, we compare in Figure 7.7 the finite phase response curves for both optimally identified parameters to the finite phase response curve of the quantitative circadian rhythm model. The finite phase response curve have been computed through direct numerical simulations of the model. The magnitude of the input and the reference point used to evaluate the finite phase response curve are chosen appropriately based on the phase shift and the scaling factor computed in the optimization procedure on infinitesimal phase response curves. The shape of (finite) phase response curves matches. It suggests that (finite) phase response curves are well captured by the (local) infinitesimal phase response curves.

## 7.3 Summary

In this chapter, we performed a (local) robustness analysis of a detailed circadian rhythm model and a (local) parametric systems identification with a gradient-descent algorithm. Both local analyses have been validated with non-local investigations.

The results suggest that a local analysis is useful to study those oscillators without facing the curse of dimensionality obstacle associated with numerical exploration of the parameter space.

The sensitivity analysis can be a first step to identify a reduced parameter space in which to perform the system identification. It would be of interest to apply the system identification on the detailed oscillator model.

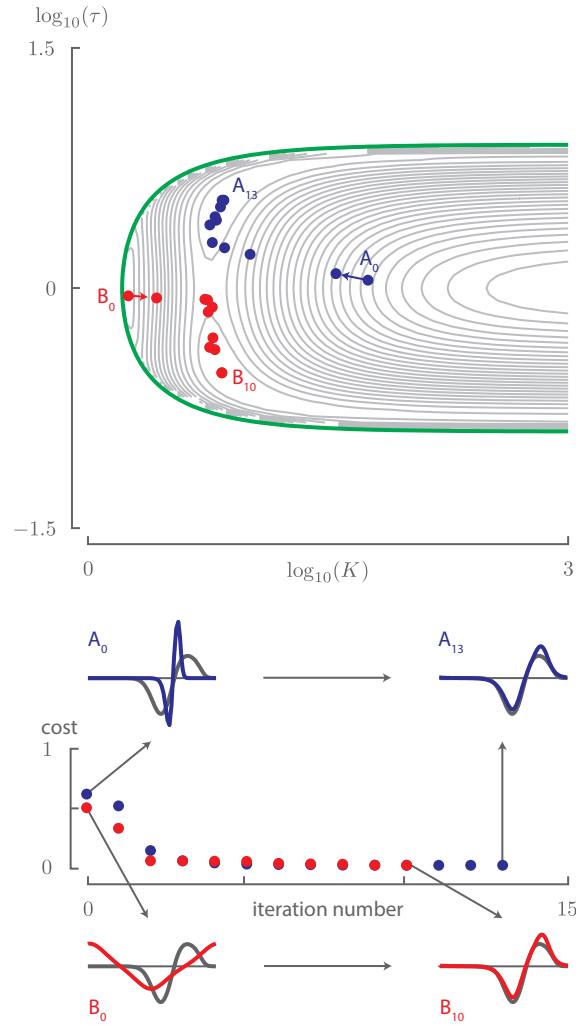


Figure 7.6 – Parametric system identification in the space of infinitesimal phase response curves. (Top) The cost function (gray levels) between an experimental infinitesimal phase response curve and the (input) infinitesimal phase response curves exhibits a nonconvex behavior in the reduced parameter space. The gradient-descent algorithm follows the path indicated by dots. (Bottoms) The cost along the path followed by the gradient-descent algorithm decreases with the iteration number. The shape of the optimal infinitesimal phase response curve (blue or red) is closer to the reference infinitesimal phase response curve (gray) than the initial infinitesimal phase response curve (blue or red).

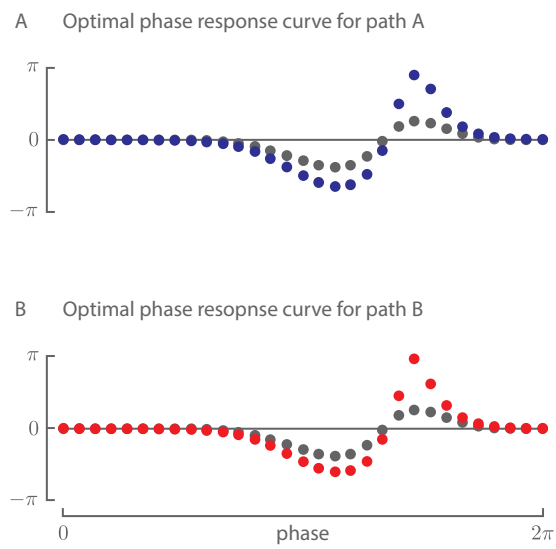


Figure 7.7 – Validation of the parametric system identification for finite phase response curves. The (finite) phase response curves computed at optimally identified parameters (blue and red) in the parameter space match well with the (finite) phase response curve of the quantitative circadian rhythm model (gray). The magnitude of the input and the reference point have been chosen based on the results of the optimization procedure in the space of infinitesimal phase response curves.



## Chapter 8

# Systems analysis of neural oscillator models in the space of phase response curves

Neural oscillators are essential building blocks in neurodynamics. They play a key role in many neural functions.

Historically, the core mechanism responsible for neural oscillators was based on the hysteresis-and-adaptation motif [47, 48, 84, 130]. Nowadays, this architecture is still at the heart of all neural oscillator systems [51, 52].

In neural (or cardiac) excitable cells, the phase response curve is used to study ensemble behavior in a network. In particular, synchronization in coupled neurons and entrainment in uncoupled neurons subject to correlated inputs (also known as stochastic synchronization). The recent book [155] compiles several applications of phase response curves in neuroscience.

An important fraction of applications of phase response curves in neurodynamics focuses on infinitesimal phase response curves. In particular, they aim at studying the behavior of networks in which each oscillator is characterized by a canonical infinitesimal phase response curve, that is, the infinitesimal phase response curve in a close neighborhood of the bifurcation giving birth to the oscillator. Two main classes of canonical phase response curves are the following. Class-I phase response curves exhibit only primarily positive or primarily negative phase shift; class-II phase response curves exhibit a sinusoidal phase shift.

However, due to time-scale separation, the domain of validity of infinitesimal

phase response curves vanishes in the singular limit.

We apply the metric developed in Chapter 4 to investigate the fragility of the classification of neural oscillator models based on the bifurcation giving birth to the oscillator and we apply the singular perturbation theory developed in Chapter 6 to predict the shape of *finite* phase response curves.

This chapter is organized as follows. Section 8.1 propose a model classification directly based on a distance in the space of response curves. Section 8.2 provide geometric predictive tools of the shape of *finite* phase response curves.

*Contributions.* The main contributions of this chapter are (i) to emphasize that the current classification method based on the bifurcation giving birth to the oscillator makes little sense and to propose a new classification based directly on the shape of phase response curve and (ii) to predict, through a novel geometric approach, the shape of *finite* phase response curves.

## 8.1 Model classification

Model classification aims at separating models in groups which share respectively common qualitative and/or quantitative characteristics.

In the literature, models of neurons are often grouped into two classes based on the bifurcation that gives birth to periodic firing [81]. Class-I excitable neurons arise from saddle-node on invariant circle bifurcations and can theoretically fire at arbitrarily low finite frequencies. Class-II excitable neurons arise from a subcritical or supercritical Andronov-Hopf bifurcations and possess a nonzero minimum frequency of firing. Recently several papers have suggested that class-II neurons display a higher degree of stochastic synchronization than class-I neurons [2, 54–56, 83, 119]. All those studies analyze phase models using canonical phase response curves associated with each class (see below) and the role played by the shape of the infinitesimal phase response curves for this property. As we will see later the shape of the infinitesimal phase response curve can change quickly as the oscillator model is away from the bifurcation and thus the qualitative synchronization behavior may also change.

In this section, we compare this model classification to a classification directly based on the distance to canonical infinitesimal phase response curves in the space of infinitesimal phase response curves.

### Model classification scheme in the space of phase response curves

A strong relationship between the bifurcation type and the shape of the infinitesimal phase response curve has been demonstrated [18, 41, 81]: near the bifurcation, the infinitesimal phase response curve of class-I excitable neurons

is nonnegative or nonpositive and approximated by

$$q_{\text{I}}(\theta) := [1 - \cos(\theta)], \quad (8.1)$$

whereas the infinitesimal phase response curve of class-II excitable neurons has both positive and negative parts and is approximated by

$$q_{\text{II}}(\theta) := \sin(\theta + \pi). \quad (8.2)$$

We propose to classify models in the parameter space based on the distance between the model infinitesimal phase response curve and canonical infinitesimal phase response curves

$$q \in \begin{cases} \text{class-}q_{\text{I}} & \text{if } \text{dist}(q, q_{\text{I}}) < \text{dist}(q, q_{\text{II}}) \\ \text{class-}q_{\text{II}} & \text{if } \text{dist}(q, q_{\text{I}}) > \text{dist}(q, q_{\text{II}}) \end{cases} \quad (8.3)$$

where  $\text{dist}(\cdot, \cdot)$  is the distance in the space  $\mathcal{Q}$ .

*Remark.* Recently, it has been shown that, arbitrary close to a saddle-node on invariant circle bifurcation, the phase response curve continuously depends on model parameters and its shape can be not only primarily positive or primarily negative but also nearly sinusoidal [42]. However, it remains true that many neural oscillators undergoing a saddle-node on invariant circle bifurcation are such that they exhibit a primarily positive (or primarily negative) phase response curve.

### Neural oscillator model

We illustrate the model classification on a simple neuron model developed by Morris and Lecar [127]. This model is a popular two-dimensional reduced model of excitable neurons

$$C \dot{V} = -\bar{g}_{\text{Ca}} m_{\infty}(V) (V - V_{\text{Ca}}) - \bar{g}_{\text{K}} w (V - V_{\text{K}}) - \bar{g}_{\text{L}} (V - V_{\text{L}}) + I_{\text{app}} \quad (8.4a)$$

$$\dot{w} = \phi(w_{\infty}(V) - w) / \tau_w(V) \quad (8.4b)$$

where

$$m_{\infty}(V) = 0.5 [1 + \tanh((V - V_1)/V_2)] \quad (8.5)$$

$$w_{\infty}(V) = 0.5 [1 + \tanh((V - V_3)/V_4)] \quad (8.6)$$

and

$$\tau_w(V) = 1 / \cosh((V - V_3)/(2V_4)). \quad (8.7)$$

The applied current  $I_{\text{app}}$  plays the role of input.

This model exhibits both classes of excitability for different parameter values [143, 176]. In particular, the calcium conductance  $\bar{g}_{Ca}$  modifies the nature of the bifurcation giving birth to the periodic orbit. For large values of  $\bar{g}_{Ca}$ , the model exhibits a class-I excitability (saddle-node on invariant circle bifurcation). For smaller value of  $\bar{g}_{Ca}$ , the model exhibits a class-II excitability (Andronov-Hopf bifurcation).

In this context, it is meaningful to classify model based on a distance in the space  $\mathcal{Q}_D$  incorporating both scaling and phase shifting equivalence properties. We are indeed interested only in comparing the qualitative shape of infinitesimal phase response curves.

## Results

Standard classification scheme is unidimensional and defines an horizontal separation in the two-dimensional parameter space  $(I_{app}, \bar{g}_{Ca})$  (Figure 8.1, left). Indeed, a model is classified based on the bifurcation giving birth to periodic firing while varying the applied current  $I_{app}$ .

However, the shape of the infinitesimal phase response curve close to the bifurcation can be different from the ideal shape predicted at the bifurcation boundary (Figure 8.1, right).

The classification scheme based on the infinitesimal phase response curve shape provides a different separation in the parameter space (Figure 8.1, right). The new classification scheme allows one neuron (for one value of  $\bar{g}_{Ca}$ ) to pass from one class to another (crossing of the separation) for different values of applied current  $I_{app}$ . Infinitesimal phase response curves computed for several points close to the bifurcation boundary confirm the classification based on the qualitative shape of infinitesimal phase response curves. In particular, parameter set B belongs to the new class-I.

For class-II oscillators, we observe that the correspondence between the bifurcation-based classification and the phase response curve-based classification is limited to a narrow region in the neighborhood of the bifurcation.

To verify the predictive value of our classification, we plot in Figure 8.2 the time evolution of a uncoupled neuron network in which all neurons are entrained by the same stochastic input (i.e. stochastic synchronization). For each neuron (one horizontal line), we plot a point when the neuron fires (raster plot). Each panel (from A to C) corresponds to a different point in the parameter space. The synchronization level is quantified by the time-evolution of the spike distance in panel D [96]. This distance is equal to 0 for perfect synchronization and to 1 for perfect desynchronization.

The stronger synchronization observed for parameter set C than for both parameter sets A and B supports the better prediction given by a classification scheme based on the shape of the phase response curve rather than on the bifurcation at the origin of the periodic firing.

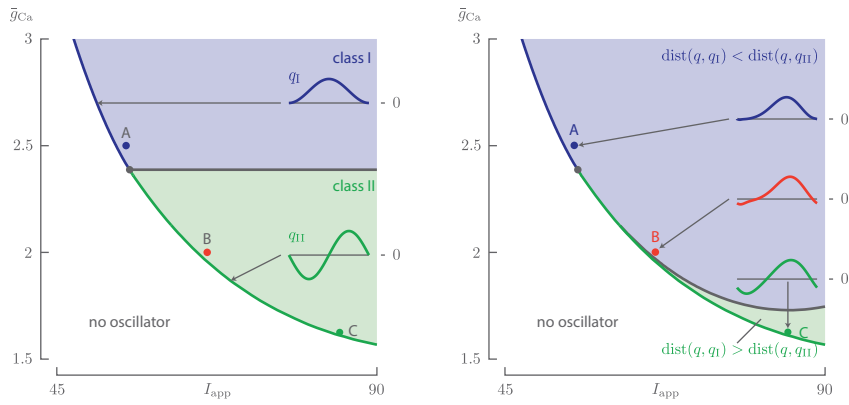


Figure 8.1 – Parametric model classification based on a distance in the space of infinitesimal phase response curves. (Left) Standard classification relies on the bifurcation giving birth to the periodic orbit while varying the applied current  $I_{app}$  (class-I in blue and class-II in green). This unidimensional classification defines an horizontal separation in the parameter space. Ideal phase response curves at the bifurcation are shown. (Right) Our classification relies on the distance to nearest ideal phase response curves (class-I in blue and class-II in green). This classification in the two-dimensional parameter space determines very different subsets. Parameter set A (resp. C) belongs to class-I (resp. class-II) and its phase response curve is closest to the class-I ideal phase response curve (resp. class-II ideal phase response curve). However, parameter set B (in red) belongs to class-II and its phase response curve is closest to the class-I ideal phase response curve. (Parameter values:  $C = 20 \mu\text{F}/\text{cm}^2$ ,  $\bar{g}_K = 8 \text{ mS}/\text{cm}^2$ ,  $\bar{g}_L = 2 \text{ mS}/\text{cm}^2$ ,  $V_{Ca} = 120 \text{ mV}$ ,  $V_K = -80 \text{ mV}$ ,  $V_L = -60 \text{ mV}$ ,  $V_1 = -1.2 \text{ mV}$ ,  $V_2 = 18 \text{ mV}$ ,  $V_3 = 12 \text{ mV}$ ,  $V_4 = 17.4 \text{ mV}$ ,  $\phi = 1/15 \text{ s}^{-1}$ .)

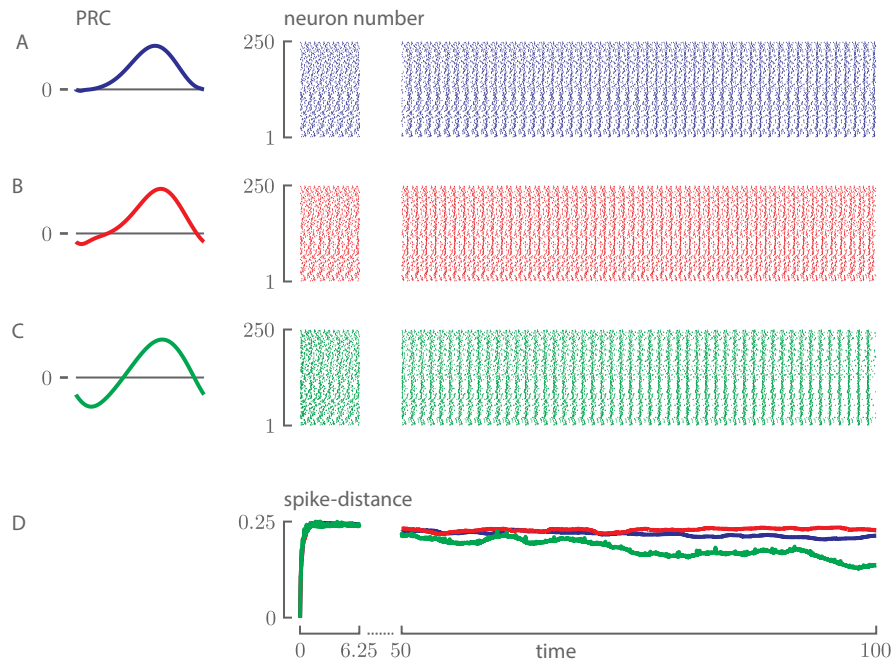


Figure 8.2 – Validation of the parametric model classification for stochastic synchronization. Stochastic synchronization for uncoupled network of state-space models are illustrated by time-plots of firing times (one line corresponds to one neuron). Each panel (from A to C) corresponds to a point in the parameter space (see Figure 8.1). In panel D, the spike-distance quantifies the synchronization level of the network (it is equal to 0 for perfect synchronization and to 1 for perfect desynchronization). Parameter sets A and B exhibit a lower stochastic synchronization (higher values of the spike-distance) than parameter set C, consistent with the fact that the phase response curve of parameter set B is shapewise closer to the phase response curve of parameter set A than to the one of parameter set C.

## 8.2 Geometric prediction

Neural oscillators exhibit multiple time-scale dynamics. Motivated by the inherent limitations of the *infinitesimal* phase response curves for relaxation oscillators, it is of interest to predict the shape of the *finite* phase response curve.

### Neural oscillator model

We illustrate our geometric approach on a simple neuron model developed by FitzHugh and Nagumo [48, 130]. This model is a popular two-dimensional simplification of the Hodgkin-Huxley model of spike generation in squid giant axons

$$\dot{v} = v - v^3/3 - w + u \quad (8.8a)$$

$$\tau \dot{w} = a - b w + v \quad (8.8b)$$

$$y = v \quad (8.8c)$$

where  $v$  is the voltage variable,  $w$  is the recovery variable, and  $\epsilon := 1/\tau$  is a small parameter.

The critical manifold of the system under a constant input  $\bar{u}$  is illustrated in Figure 8.3 (top). The critical manifold of the system under a constant step input is identical to the critical manifold of the zero-input system, but shifted along  $w$ -axis.

The functions  $\psi_+$  and  $\psi_-$  describing the time spent on the critical manifold from a initial condition  $z_0$  to a final condition  $z_\tau$  may be computed numerical and are illustrated in Figure 8.3 (bottom). We note that the dependence of the function on the input value  $\bar{u}$  is more complex than a simple shift. This is due to the direct dependence of the slow vector field on the slow variable  $w$ .

### Phase response curves for excitatory or inhibitory impulses

Figure 8.4 illustrates the phase response curve of the FitzHugh-Nagumo model for excitatory and inhibitory impulses  $u(\cdot) = \alpha \delta(\cdot)$ , with  $\alpha > 0$  and  $\alpha < 0$ . The solid lines are the geometric predictions computed in the singular limit. Dots represent the phase response computed through numerical time-simulations of trajectories of the model for different values of the parameter  $\epsilon$ .

The singular phase response curve is equal to zero except in one region of the periodic orbit which corresponds to the region right before the initiation (resp. termination) of the upper part of the periodic orbit for an excitatory (resp. inhibitory) impulse. In this region, an impulse advances the initiation (resp. termination) of the upper part of the periodic orbit. The phase advance decreases monotonically to zero until the phase corresponding to the lower (resp. upper) fold.

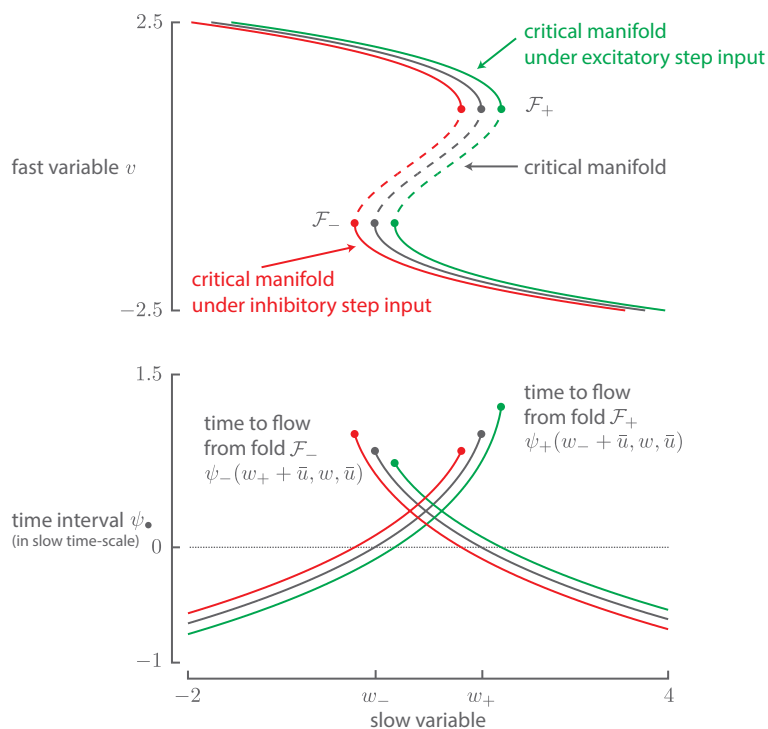


Figure 8.3 – Geometry of FitzHugh-Nagumo model. (Top) The critical manifold of FitzHugh-Nagumo model under zero-input (gray) exhibits bistability for a wide range of slow variable values. Excitatory step input (green) and inhibitory step input (red) shift the critical manifold along  $w$ -axis on the right and on the left, respectively. (Bottom) Time intervals  $\psi_+(w_- + \bar{u}, w, \bar{u})$  spent on the upper branch of the critical manifold (for  $\bar{u} < 0$ ,  $\bar{u} = 0$ , or  $\bar{u} > 0$ ) are increasing functions of the slow variable  $w$  and equal to 0 for  $w = w_- + \bar{u}$ . Time intervals  $\psi_-(w_+ + \bar{u}, w, \bar{u})$  spent on the lower branch of the critical manifold (for  $\bar{u} < 0$ ,  $\bar{u} = 0$ , or  $\bar{u} > 0$ ) are decreasing functions of the slow variable  $w$  and equal to 0 for  $w = w_+ + \bar{u}$ . (Parameter values:  $a = 0.7$ ,  $b = 0.8$ ,  $I = 1$ .)

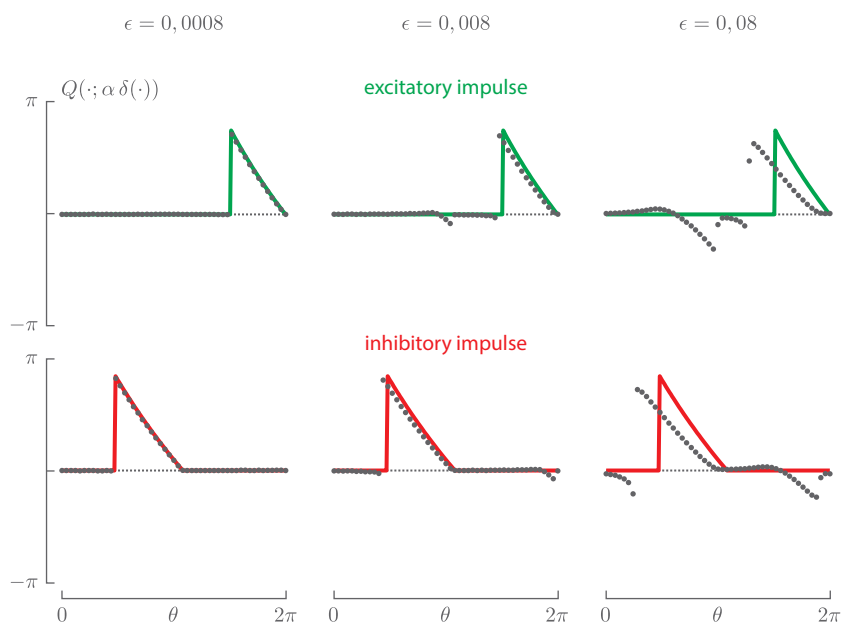


Figure 8.4 – Phase response curves for excitatory and inhibitory impulses: singular prediction (solid line) and simulations (dots). (Parameter values: see Figure 8.3. The impulse input is such that  $|\alpha| = 1.5$ .)

For small values of  $\epsilon$ , the geometric prediction matches very well the actual phase response curves. For larger values of  $\epsilon$ , the prediction still matches (qualitatively) the larger phase shifts arising before the lower (resp. upper) fold but do not capture the small phase shifts arising before the upper (resp. lower) fold.

### Phase response curves for excitatory or inhibitory pulses

Figure 8.5 illustrates the phase response curve of the FitzHugh-Nagumo model for excitatory and inhibitory pulses of finite duration. The solid lines are the geometric predictions computed in the singular limit. Dots represent the phase response computed through numerical time simulations of trajectories of the model for different values of the parameter  $\epsilon$ .

The singular phase response curve is equal to zero except in two regions of the periodic orbit. The first region which exhibits the highest phase shifts corresponds to same region as for the impulse case. The phase shifts in this region follow a piecewise law: the breaking point in the phase shifts corresponds to the separation between points that continues to evolve on the shifted ini-

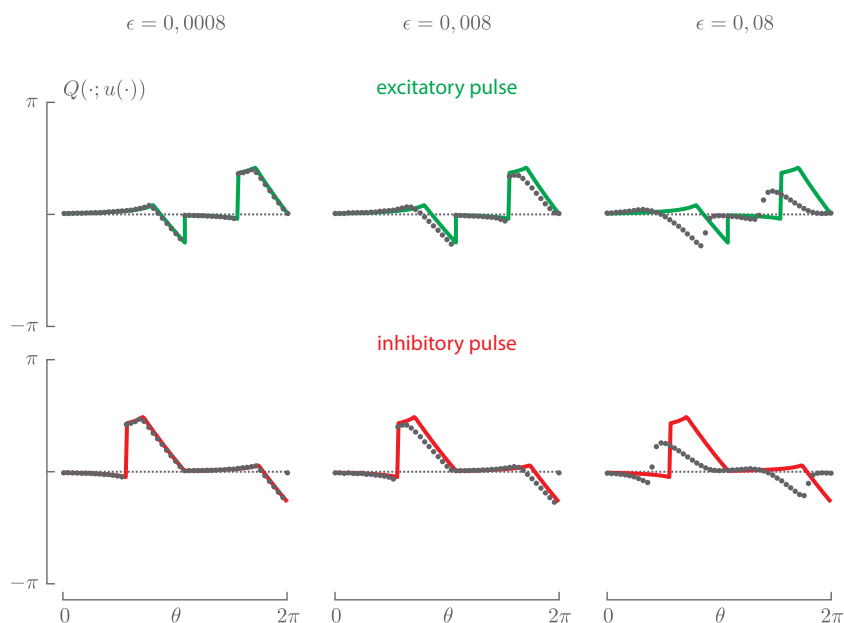


Figure 8.5 – Phase response curves for excitatory and inhibitory pulses of finite duration: singular prediction (solid line) and simulations (dots). (Parameter values: see Figure 8.3. The pulse input is such that  $|\bar{u}| = 0.25$  and  $\Delta = 0.1 T$ .)

tial branch and those that directly jump to the opposite branch. The second region corresponds to point close to the other fold (see case 1 and case 2 in Figure 6.4). An excitatory (resp. inhibitory) pulse may delay the termination (resp. initiation) of the upper part.

Once again, for small values of  $\epsilon$ , the geometric prediction matches very well the actual phase response curves. For larger values of  $\epsilon$ , the prediction matches qualitatively both non-zero regions of the phase response curve.

The main difference between the phase response curve for an impulse and for a pulse is that a positive (resp. negative) pulse may delay the termination (resp. advance the initiation) of the behavior on the upper branch, while a positive (resp. negative) impulse may not.

In Table 8.1, we summarize the capacity of an input to create a phase shift.

Input	Initiates upper part	Terminates upper part
excitatory impulse	yes	no
inhibitory impulse	no	yes
excitatory pulse	yes (++)	yes (+)
inhibitory pulse	yes (+)	yes (++)

Table 8.1 – Capacity of an input to create a phase shift by advancing or delaying the initiation or termination of the evolution on the upper branch of the critical manifold. The main difference between the phase response curve for an impulse and for a pulse is that a positive (resp. negative) pulse may delay the termination (resp. advance the initiation) of the behavior on the upper branch, while a positive (resp. negative) impulse may not.

### 8.3 Summary

In this chapter, we investigated the current classification method of neural oscillator models based on the bifurcation giving birth to the oscillator and we stressed that the shape of the phase response curve (and thus the input–output behavior the neuron) can change quickly away from the bifurcation. We also predicted the geometric shape of the *finite* phase response curves (better suited for fast-slow oscillators).

As a consequence, it means that the input–output systems analysis of fast-slow neural oscillators should advantageously be performed in the space of the *finite* phase response curves.



## Chapter 9

# Phase oscillator control in the space of phase response curves

The last decades have witnessed a growing interest in the analysis and the synthesis of oscillators [50, 72, 164]. Global and local stability analysis of oscillators but also the generation of oscillators with large basin of attraction in stabilizable nonlinear systems were widely addressed in the control theory literature (see [165, and references therein]). Here, we focus on a different problem. Any periodic oscillation can be characterized by its amplitude, frequency (or frequencies spectrum), and phase. Several strategies have been proposed to control each of these characteristics [12, 16, 37, 94].

Many design and control problems arising for oscillators are related to characteristics of the dynamics on the circle. It makes thus sense to develop the design and control strategies directly on the circle (and not in the state space). Yet, few approaches have been proposed so far.

We investigate some elementary strategies based on the phase response curve to control the phase of a large class of oscillators. Our control objective is to drive an oscillator to track the phase of a reference trajectory evolving at the natural frequency of the system. While this problem can be found in many applications, it has been motivated by biological applications in the study of circadian rhythm. Recent work addressing the phase control using model predictive control includes [13, 15]. An independent but closely related idea has been proposed in [27] in the context of a neuronal model.

This chapter is organized as follows. Section 9.1 reviews several design and control problems arising for oscillators and emphasizes the phase nature of the design or control objectives. Section 9.2 introduces a biological toy motivating

example, focuses on phase control map and phase response curve-based control strategies, and applies these control laws to the motivating example.

*Contributions.* The main contribution of this chapter is to develop control strategies to drive an oscillator to track the phase of a reference trajectory evolving at the natural frequency of the system.

The material of this chapter is the result of a collaboration with Denis Efimov (former postdoctoral researcher at the University of Liège).

## 9.1 Design and control of phase oscillator

In this section, we review several phase oscillator design and control problems arising in engineering. In these applications, the design or control objectives concern the frequency or the phase of the oscillator which emphasizes the pertinence to study such problems on the circle (and not in the state space). This section does not intend to be exhaustive.

In nuclear fusion engineering, oscillatory phenomena are observed in current carrying magnetically confined plasmas. It corresponds to a periodic crash-like reorganization of the plasma core known as the sawtooth instability. Experimental evidence has shown that the sawtooth period may follow the modulation frequency of an external control signal [105], leading to the phase-locking phenomenon.

In electronic engineering, oscillatory systems are commonly needed to generate precise clock signals that translate data to desired frequency band in receivers or trigger events in digital circuits. In those oscillators, noise mainly appears as phase noise (or timing jitter) and degrades the performance of those electronic devices. Therefore, the design of low-noise oscillators is an critical aspect of circuit design in many applications [79, 188]. The conversion of the noise from circuit components into phase noise is characterized by the so-called perturbation projection vector [31].

In neural engineering, the desire to control the spiking behavior of neural oscillators and, by extension, the level of synchronization in neural populations appears naturally in the context of Parkinson's disease, which has been associated with pathological synchronization of motor control neurons. A popular therapeutic procedure, known as deep brain stimulation, consists in injecting current signals directly into the brain through an implanted electrode in order to desynchronize the neural population. Several control strategies have been proposed to choose the injected signal: event-based feedback control (e.g. charge-balanced [26, 28], minimum-time [129], or minimum-energy [128]).

In aerospace engineering, the optimal control problem of a spacecraft rendezvous with a satellite is frequent. The optimum can be in the sense of minimum-time, minimum fuel consumption, or a rational combination of both.

Due to the circular nature of the satellite orbit, it is very tempting to regard this problem as a phase control problem.

## 9.2 Phase oscillator control strategies

In this section, we introduce a biological toy motivating example. Then we provides the phase control map and phase response curve-based control strategies. Finally we apply these control laws to the motivating example.

### 9.2.1 A motivating example

A common illustration of phase assignment is the jet-lag that most scientists experience when traveling to conferences. The organism needs some time to “reset” the phase of its initial circadian rhythm to shifted environmental light conditions. This problem prompts biologists to study phase resetting and entrainment mechanisms in simple models of circadian oscillations.

The fundamental mechanism in the Goldbeter model of *Neurospora* circadian rhythms is the auto-inhibition of the transcription of the gene *frq* [67, 110]. This inhibition is through a feedback loop that involves nuclear translocation. Light (modeled by input  $u$ ) controls the circadian system by enhancing the rate of *frq* gene expression.

Corresponding to these assumptions, one obtains an ordinary differential equation (ODE) system for concentrations as follows:

$$\dot{M} = (v_s + u) \frac{K_I^n}{K_I^n + F_N^n} - v_m \frac{M}{K_m + M}, \quad (9.1a)$$

$$\dot{F}_C = k_s M - v_d \frac{F_C}{K_d + F_C} - k_1 F_C + k_2 F_N, \quad (9.1b)$$

$$\dot{F}_N = k_1 F_C - k_2 F_N, \quad (9.1c)$$

where  $M > 0$  denotes the concentration of *frq* mRNA, and  $F_C > 0$  and  $F_N > 0$  are used to indicate the concentrations of FRQ in the cytoplasm and in the nucleus, respectively.

The parameters used by Goldbeter are given in Section 9.2.3. With these parameters, there are periodic orbit oscillations (a unique unstable equilibrium and an asymptotically stable periodic orbit). If  $v_s$  is used as a bifurcation parameter, a Hopf bifurcation occurs at  $v_s \approx 0.60$ .

Periodic excitation by light input results in phase and frequency entrainment of the natural circadian oscillations [67, 110, 172]. This means that the application of a suitable input  $u$  over a periodic time window close to the natural periodic orbit period  $T$  may entrain the phase of the system. This phenomenon is illustrated for the specific model in [67, 110]. The input is usually modeled as a sequence of pulses of limited duration and amplitude (for

instance, one unique pulse of duration  $T_w = 12$  h and amplitude  $\Delta = v_s/4$  is applied every 24 hours).

## 9.2.2 Design of control strategies

In this section, we start with the derivation of the phase control map. Next, we propose three control strategies: feedforward (FF), proportional feedback (P) and proportional-integral feedback (PI) control.

### Phase control map

For control purposes, we consider the application of a fixed input  $w(t)$  of finite duration  $0 < T_w \ll T$  at different time instants  $t_0 < t_1 < \dots$ . The time instants  $t_i$ ,  $i \in \mathbb{N}$ , are the control parameters. For an initial phase  $\theta$ , the input  $w(t)$  (asymptotically) causes a phase shift approximately measured by (see the zeroth order approximation in Section 3.5)

$$Q(\theta; w(\cdot)) = \int_0^{T_w} q(\omega s + \theta) w(s) ds. \quad (9.2)$$

The phase difference  $\chi = \theta - \theta_r \pmod{2\pi}$  between a reference oscillator

$$\theta_r(t) = \omega t + \theta_r(0) \pmod{2\pi} \quad (9.3)$$

and a controlled oscillator evolving according to

$$\dot{\theta} = \omega + q(\theta) w(t - t_0), \quad \theta(0) = \theta_0, \quad (9.4)$$

thus satisfies

$$\chi(t) = \chi(0) = \theta(0) - \theta_r(0), \quad \text{for } 0 \leq t < t_0, \quad (9.5)$$

and

$$\chi(t_0 + T_w) = \chi(0) + Q(\theta(t_0); w(\cdot)) \quad (9.6)$$

$$= \chi(0) + Q(\omega t_0 + \theta_r(0) + \chi(0); w(\cdot)). \quad (9.7)$$

If the input signal is no longer an isolated application of  $w(t)$  but instead a train of such finite-duration inputs

$$u(t) = \sum_{i=0}^{+\infty} w(t - t_i), \quad (9.8)$$

the equations (9.5)–(9.7) suggest to study the evolution of the phase difference via the discrete map

$$\chi_{i+1} = \chi_i + Q(\omega t_i + \theta_r(0) + \chi_i; w(\cdot)) \quad (9.9)$$

where  $\chi_i$  denotes the phase error  $\chi(t_i)$ . This discrete map rests on the assumption that the (asymptotic) phase shift  $Q(\theta(t_i); w(\cdot))$  has been reached after the (finite) duration  $t_{i+1} - t_i$ . To validate the assumption, one must impose

$$t_{i+1} - t_i \geq T_s \quad \forall i \in \mathbb{N} \quad (9.10)$$

where the minimal ‘‘sampling’’ time  $T_s$  is typically chosen according to the periodic orbit attractivity.

The discrete map (9.9) is a first-order discrete-time control system whose control parameters are the pulse timings  $t_i$ ,  $i \in \mathbb{N}$ . Equivalently, one may rewrite (9.9) as

$$\chi_{i+1} = \chi_i + Q(\theta_i; w(\cdot)) \quad (9.11)$$

(where  $\theta_i$  denotes the phase  $\theta(t_i)$ ) and treat  $\theta_i$  as the control variable.

In the remaining, we discuss three elementary control strategies to select these control parameters: a feedforward control, a proportional feedback control, and a proportional-integral feedback control.

### Feedforward control of the phase control map

The feedforward control strategy is based on the model (9.9) and does not require any measurement about the current phase of the system. As the phase variable  $\theta$  evolves on the unit circle  $\mathbb{S}^1$ , phase shifts in both directions can be used to modify the phase.

For the ease of exposition, we assume that the phase response curve has particular properties (it is similar to type-II phase response curve from [81]). The corresponding control strategies for other types of phase response curves can be easily deduced from this main case.

**Assumption 1.** The phase response curve is continuous and it has one zero  $\theta_s^0 \in \mathbb{S}^1$  with negative slope and another  $\theta_u^0 \in \mathbb{S}^1$  with positive slope,  $\theta_s^0 < \theta_u^0$ .

Since the phase response curve is  $2\pi$ -periodic (from Definition 1), the zeros can be arranged in the required order  $\theta_s^0 < \theta_u^0$  changing the initial point on the periodic orbit. Define

$$\theta_{\max} = \arg \max_{\theta \in \mathbb{S}^1} Q(\theta; w(\cdot)), \quad Q_{\max} = Q(\theta_{\max}; w(\cdot)), \quad (9.12)$$

$$\theta_{\min} = \arg \min_{\theta \in \mathbb{S}^1} Q(\theta; w(\cdot)), \quad Q_{\min} = Q(\theta_{\min}; w(\cdot)), \quad (9.13)$$

with  $\theta_s^0 < \theta_{\min} < \theta_u^0 < \theta_{\max}$ ,  $Q_{\max} > 0$ , and  $Q_{\min} < 0$ .

The integer part of the numbers

$$n_+ = (2\pi - \chi_0)/Q_{\max}, \quad n_- = -\chi_0/Q_{\min}, \quad (9.14)$$

determine the number of steps required to drive the initial phase error  $\chi_0$  into a neighborhood of zero applying positive or negative phase shift, respectively. These numbers are minimal since for their calculation we use the maximum amplitudes of shift ( $Q_{\max}$  or  $Q_{\min}$ ). Defining  $N = \text{floor}[\min(n_+, n_-)]$ , where the function  $\text{floor}[n]$  returns the greatest integer not bigger than  $n$ , a natural feedforward control is to apply  $N$  pulses of maximal phase shift ( $0 \leq i < N$ )

$$\theta_i = \begin{cases} \theta_{\max}, & \text{for } n_+ \leq n_- \\ \theta_{\min}, & \text{for } n_+ > n_- \end{cases} . \quad (9.15)$$

A last pulse is needed to annihilate the residual error. The corresponding phase  $\theta_N$  is thus the solution of the following equation (obtained by annihilating the phase error  $\chi_{N+1}$  in (9.11))

$$\theta_N : \begin{cases} Q(\theta_N; w(\cdot)) + \chi_N = 2\pi, & \text{for } n_+ \leq n_- \\ Q(\theta_N; w(\cdot)) + \chi_N = 0, & \text{for } n_+ > n_- \end{cases} . \quad (9.16)$$

Following this control strategy, the phase error evolves as

$$\chi_i = \begin{cases} \chi_0 + i Q_{\max}, & \text{for } n_+ \leq n_- \\ \chi_0 + i Q_{\min}, & \text{for } n_+ > n_- \end{cases} , \quad (9.17)$$

for  $0 \leq i \leq N$  and we have  $\chi_{N+1} = 0 (= 2\pi)$ .

The sequence of phases  $\theta_i$ ,  $0 \leq i \leq N$ , determines the sequence of times  $t_i$  as follows:  $t_0$  is chosen as the first  $t \geq 0$  such that

$$\theta_0 = (\theta(0) + \omega t) \pmod{2\pi} . \quad (9.18)$$

For  $i = 0, \dots, n$ , one assumes

$$\theta(t_i + T_s) = (\theta_i + Q(\theta_i; w(\cdot)) + \omega T_s) \pmod{2\pi} . \quad (9.19)$$

Since

$$\dot{\theta} = \omega, \quad \text{for } t_i + T_s \leq t \leq t_{i+1}, \quad (9.20)$$

one defines  $t_{i+1}$  as the first time  $t \geq t_i + T_s$  such that

$$\theta_{i+1} = (\theta(t_i + T_s) + \omega(t - (t_i + T_s))) \pmod{2\pi} . \quad (9.21)$$

This strategy is called “feedforward” since it does not require any measurement of the phase variable.

### Proportional feedback control of the phase control map

The proportional feedback control strategy assumes on-line measurements of the current phase variable after each “pulse” application. To realize this strategy it is enough to replace in (9.21) the values  $\theta(t_i + T_s)$  computed from (9.19)

with measurement values. By measurements we mean the calculation of the phase based on measurements of the state vector  $x(t_i + T_s)$ . The phase of  $x(t)$  can be computed using the following algorithm:

$$\theta(t) = \arg \inf_{\vartheta \in \mathbb{S}^1} \|x(t) - x^\gamma(\vartheta)\|_2. \quad (9.22)$$

Of course the application of (9.22) is valid only in the neighborhood of the periodic orbit.

The overall strategy for proportional feedback control is similar to the feedforward one. The desired phases  $\theta_i$  are computed by

$$n_+^i = (2\pi - \chi_i)/Q_{\max}, \quad n_-^i = -\chi_i/Q_{\min}, \quad (9.23)$$

$$\theta_i = \begin{cases} \theta_{\max}, & \text{for } 1 \leq n_+^i \leq n_-^i, \\ \theta_{\min}, & \text{for } 1 \leq n_-^i < n_+^i, \\ \ell(\chi_i), & \text{otherwise,} \end{cases} \quad (9.24)$$

where the function  $\ell(\chi)$  represents a solution of the equation

$$\ell(\chi) : \begin{cases} Q(\ell(\chi); w(\cdot)) + \chi = 2\pi, & \text{for } n_+^i \leq n_-^i \\ Q(\ell(\chi); w(\cdot)) + \chi = 0, & \text{for } n_+^i > n_-^i \end{cases}. \quad (9.25)$$

The time instants  $t_i$  are given by (9.18) and (9.21).

### Proportional-integral feedback control of the phase control map

In the previous sections, it was assumed that the phase response curve is exactly known, but the map (9.2) is an approximation only valid for infinitesimal inputs. Suppose, that the static uncertainty on the model (9.11) is modeled by

$$\chi_{i+1} = \chi_i + Q(\theta_i; w(\cdot)) + d \quad (9.26)$$

where  $Q_{\min} < d < Q_{\max}$  is an unknown constant additive disturbance. The presence of  $d$  results in a steady state error for both the feedforward and the proportional feedback control.

For proportional-integral feedback control, the desired phases  $\theta_i$  are given by a solution of the following equation

$$Q(\theta_i; w(\cdot)) := \text{sat}(-\hat{d}_i - \kappa \chi_i), \quad (9.27)$$

with

$$\hat{d}_{i+1} = \hat{d}_i + \gamma [\chi_{i+1} - (1 - \kappa) \chi_i], \quad \hat{d}_0 = 0. \quad (9.28)$$

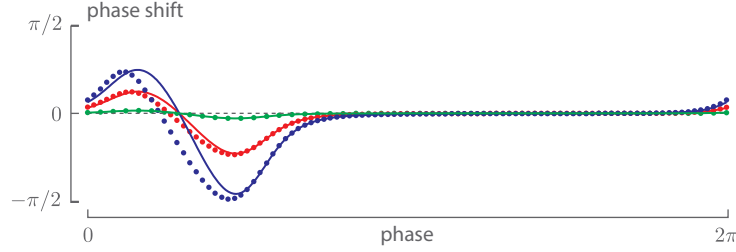


Figure 9.1 – Analytical (lines) and numerical (dots) phase response curves of the Goldbeter model for inputs with  $T_w = 1$  and increasing  $\Delta$ . The amplitude of the phase response curve increases with the amplitude of the input (respectively  $\Delta = 0.1$ ,  $\Delta = 0.8$ , and  $\Delta = 1.6$ ). (Parameter values:  $v_m = 0.505$ ,  $v_d = 1.4$ ,  $v_s = 1.6$ ,  $k_s = 0.5$ ,  $k_1 = 0.5$ ,  $k_2 = 0.6$ ,  $K_m = 0.5$ ,  $K_d = 0.13$ ,  $K_I = 1$ ,  $n = 4$ .)

The parameters  $\kappa$  and  $\gamma$  are chosen such that  $0 < \kappa < 1$  and  $0 < \gamma < 1$ . The function  $\text{sat}(\cdot)$  is defined as

$$\text{sat}(u) = \begin{cases} u & \text{for } Q_{\min} \leq u \leq Q_{\max}, \\ Q_{\max} & \text{for } u > Q_{\max}, \\ Q_{\min} & \text{for } u < Q_{\min}. \end{cases} \quad (9.29)$$

The time instants  $t_i$  are given by (9.18) and (9.21).

Note that the proportional-integral feedback control is implemented with an anti-wind up compensator.

### 9.2.3 Application to motivating example

In this section, we apply our control strategies to the circadian oscillator model presented in Section 9.2.1. We choose the parameters used by Goldbeter [110].

We use a very simple pulse input defined as

$$w(t) = \begin{cases} \Delta & \text{for } t < T_w \\ 0 & \text{otherwise} \end{cases} \quad (9.30)$$

with  $T_w = 1$  and with different values of  $\Delta$ . Figure 9.1 represents analytical and numerical phase response curve. The “analytical” phase response curve is obtained from (9.2) while the “numerical” phase response curve is computed by simulating the nonlinear model. The analytical and the numerical phase response curves are very similar for small inputs (the first-order approximation is valid) but differ for larger inputs.

The simulation results in Figure 9.2 are for the input with the largest magnitude ( $\Delta = 1.6$ ). For the control design, we only use the analytical phase

response curve over the domain  $[\theta_{\max}, \theta_{\min}]$ . In this region, the phase model has a clear and robust response to the stimulation. We observe the existence of a disturbance  $d$  (not exactly constant) between the analytical phase response curve and the numerical one. The discrete-time evolution of the phase error  $\chi$  is shown for four cases:  $\chi_{\text{FF}}$  is for the feedforward reference (9.17),  $\chi_{\text{OL}}$  presents the phase error for the feedforward control,  $\chi_{\text{P}}$  shows the error of the proportional feedback control, and  $\chi_{\text{PI}}$  is the error when applying the proportional-integral feedback control strategy. Input curves correspond to the control signal in feedforward, proportional feedback, and proportional-integral feedback control cases (they almost all overlap). The algorithm (9.22) is used to compute the phase based on measurement of the state vector. The curve  $\chi_{\text{FF}}$  indicates the reference behavior for the variable  $\chi_{\text{OL}}$ . We choose  $T_s = T$  such that the discrete model (9.17) captures the main behavior of the nonlinear model and  $\chi_{\text{OL}}$  accurately follows  $\chi_{\text{FF}}$ . The phase error  $\chi_{\text{P}}$  of the proportional feedback control evolves almost as the phase error  $\chi_{\text{OL}}$ . As expected, we observe a steady state error for both the feedforward and the proportional feedback control. The proportional-integral feedback asymptotically reject this constant error.

Figure 9.3 illustrates the time-evolution of the output variable  $M$  for the reference oscillator ( $M_{\text{REF}}$ ) and for the initially shifted oscillator controlled with the proportional-integral feedback control strategy ( $M_{\text{PI}}$ ). The timing difference of the maxima in  $M$  between those trajectories is a measure of the phase difference for the full-dimensional model. The proportional-integral feedback control strategy (asymptotically) annihilates this difference.

### 9.3 Summary

We presented basic control strategies to ensure the convergence of an oscillator phase to that of a reference phase trajectory with the same natural frequency. The control laws are based on a first-order discrete control system computed from the infinitesimal phase response curve of the model. Three control laws were considered: feedforward, proportional feedback and proportional-integral feedback strategies. The control algorithms developed in this paper were illustrated on the original Goldbeter model of *Neurospora* circadian rhythm.

As a consequence, it emphasizes the importance to develop control strategies directly on the circle representation if the control objective concerns the frequency or the phase of the oscillator.

The proposed approach is basic but it opens several interesting questions including a formal proof of convergence and its potential use in addressing more challenging engineering questions such as the rendezvous problem in satellite orbital control.

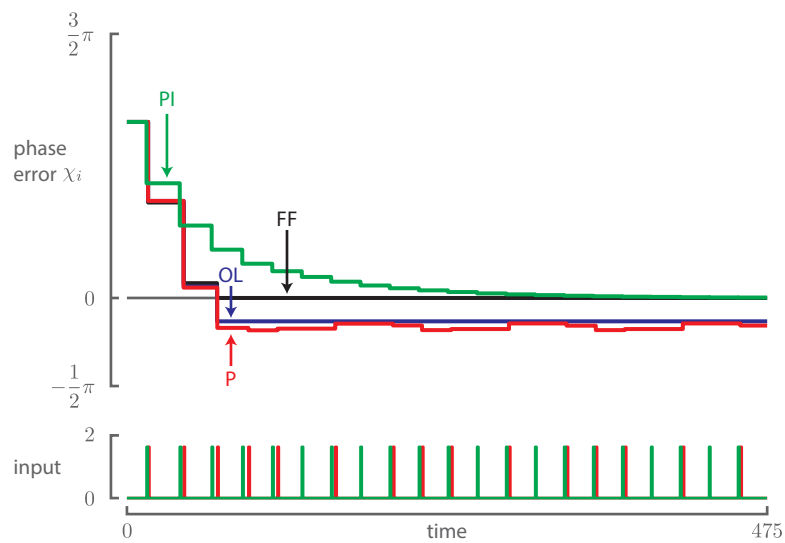


Figure 9.2 – Discrete-time evolution of the phase error  $\chi$  for four cases:  $\chi_{FF}$  is for the feedforward reference (9.17),  $\chi_{OL}$  presents the phase error for the feedforward control,  $\chi_P$  shows the error of the proportional feedback control, and  $\chi_{PI}$  is the error when applying the proportional-integral feedback control strategy ( $\kappa = 0.25$  and  $\gamma = 0.9$ ). Input curves correspond to the control signal in feedforward, proportional feedback, and proportional-integral feedback control cases (they almost all overlap).

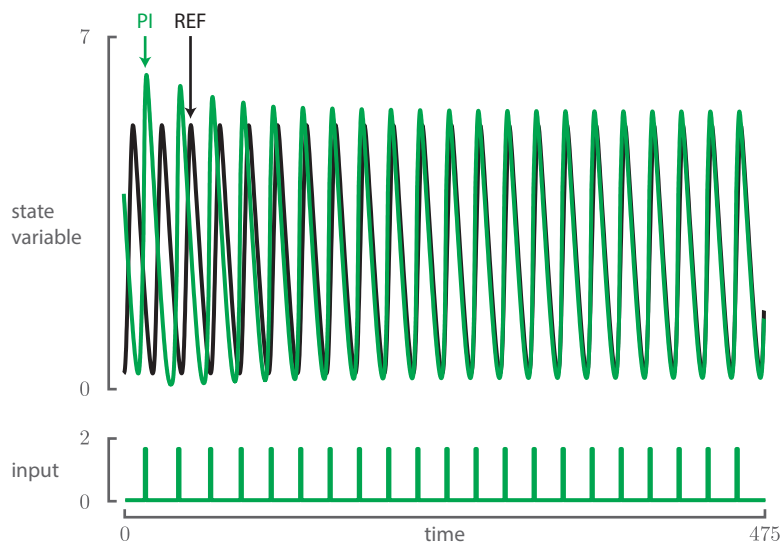


Figure 9.3 – Time-evolution of the output variable  $M$  for the reference oscillator ( $M_{\text{REF}}$ ) and for the initially shifted oscillator controlled with the proportional-integral feedback control strategy ( $M_{\text{PI}}$ ). The input curve corresponds to the control signal in proportional-integral feedback control case.



# Chapter 10

## Conclusion

The present dissertation is a story about systems models of rhythms at the interface between (internal) state-space and (external) circle representations. While the existing literature is relatively separated in two distinct areas, this dissertation recasts input–output systems questions in the space of phase response curves, contributing to bridge the gap between both descriptions.

The conclusion is organized as follows. The first section summarizes the main outcomes of this dissertation and their implications. The second section broadens the view with further perspectives.

### 10.1 Summary

#### **Two fundamental classes of oscillator systems**

A conceptual contribution of the present dissertation is to discriminate between *two fundamental classes of oscillators* (Chapter 2). Oscillators are regarded as globally dissipative systems whose stable equilibrium is transformed into a periodic orbit by a local destabilizing mechanism. One destabilizing mechanism is through delay in the feedback loop, the other is through hysteresis created by autocatalysis. The two classes of oscillators differ both in their analysis and synthesis.

This fundamental classification is watermarked throughout the dissertation. The two main biological systems studied in this dissertation are exemplary of each class: (i) the core architecture of circadian rhythms is a delayed negative-feedback loop and (ii) the basic building block of neural oscillators relies on a dynamical hysteresis induced by autocatalysis.

### Classical systems questions in the space of phase response curves

To address input–output systems questions for oscillators, the main conceptual contribution of the present dissertation is to formulate those questions in the space of phase response curves.

A first theoretical contribution of this thesis is to develop *metrics* to compare oscillators in the space of phase response curves (Chapter 4). We identify two natural equivalence properties, that is, scaling and phase shifting, and we propose a metric in the four spaces resulting from various combination of these equivalence properties. These metrics are valid to compare oscillators characterized by continuous-time circle representations (weak input) or hybrid circle representations (impulse train).

A main theoretical contribution of this thesis is to develop a *local sensitivity analysis* for oscillators in the space of phase response curves (Chapter 5). This sensitivity analysis focuses on infinitesimal phase response curves which locally describe the oscillator behavior around the periodic orbit and which can be characterized analytically (through the adjoint linear equation). This sensitivity analysis is systematic and computationally tractable but it only provides a local sensitivity analysis in the parameter space, around a nominal set of parameter values. It complements more global—but less tractable—tools such as bifurcation analysis or parameter space exploration.

In addition to the abstract developments, we provide the *numerical tools* required to turn those developments into concrete algorithms (Appendix A).

### Circadian rhythms, neural oscillators, and phase oscillator control

A methodological contribution is to illustrate the pertinence of those analysis tools to study systems questions about models of circadian rhythms and neural oscillators (exemplative of each class).

- The systems analysis of circadian rhythm models focuses on parametric robustness analysis and parametric system identification (Chapter 7). The robustness analysis emphasizes the important parameters of the model. The system identification finds a set of parameter values that matches experimental phase response curve.
- The systems analysis of neural oscillator model focuses on model classification (Section 8.1). In contrast with standard classification relying on the bifurcation which gives birth to the oscillator, this approach is directly linked to the shape of the phase response curve in the whole parameter space.

In addition, as a side contribution, we also investigate phase oscillator control (Chapter 9). In particular, we design some elementary control strategies

to assign the phase of an oscillator based on the shape of the phase response curve.

### Singularly perturbed phase response curves

Finally, motivated by the limitation of *infinitesimal* phase response curves for relaxation oscillators (due to the time-scale separation), an “ongoing” contribution of the dissertation is to develop the novel geometric concept of “singularly perturbed phase response curve” to predict the phase response to finite perturbations (Chapter 6). We take advantage of the time-scale separation to rely on the geometric structure underlying the oscillator. We illustrate this approach a neural oscillator and we show that those oscillators are sensitive only in the regions of the periodic orbit that precede jumps (Section 8.2).

## 10.2 Perspectives

The present dissertation is a first step that contributes to bridging the gap between input–output systems theory in the state space and on the circle. It opens the door to further steps.

### Implications for systems analysis of oscillator networks

In this dissertation, we developed methods for the analysis of single oscillators. A natural extension is to develop tools to analyze networks of interconnected oscillators.

- *Metrics for interconnections.*  
In previous works on metrics for systems, many metrics go further than comparing systems “in open loop”. For example, Zames [39,197] and then Vinnicombe [182,183] developed the gap metric which compares systems behavior under feedback condition. The behavior of two systems can be very close in open loop condition, but very far in closed loop condition (and vice versa). It would be of interest to develop metrics conceptually similar to the gap metric for oscillators, that is, metrics that are focused on an interconnection theory.
- *Sensitivity analysis of networks.*  
The collective behavior of an oscillator network may be sensitive (or robust) to perturbations of some individual oscillators. Sensitivity analysis at the network level would probably allow to identify those oscillators that play a critical role in the collective behavior.
- *Phase response curves of networks.*  
The collective behavior of an oscillator network may be regarded as one

“global” oscillator with its own input and output. The phase response curve of this global oscillator would likely depend on the phase response curve of each individual oscillator belonging to the network. Analyzing this dependence would provide valuable information to study interconnections of oscillator networks (e.g. populations of neural oscillators).

### **Singularly perturbed phase response curves for bursting oscillators**

In this dissertation, we studied singularly perturbed phase response curves for two time-scale systems. Another class of multiple time-scale systems are bursting oscillators. Those oscillators are characterized by three distinct time scales: a fast time scale for the spike generation, a slow time scale for the intraburst spike frequency, and an ultra slow time scale for the interburst frequency [51].

The underlying geometry of bursting oscillators is conceptually similar to the one of relaxation oscillators. In this case, for the two-dimensional layer dynamics, the singular manifold corresponds to a lower branch of equilibria (resting state) and an upper cylinder of stable periodic orbits (bursting state). Using averaging technique, we may “smooth” the dynamics on the cylinder of stable periodic orbits and apply a similar approach to predict the shape of the singular phase response curve for this kind of systems. We may investigate the dependence of this shape on the type of singularities that induce jumps between resting and bursting states, leading to a classification of bursters.

The predicted singularly perturbed phase response curve may then be exploited to analyze synchronization of coupled singularly perturbed oscillators. In particular, it would likely provide a phase-based interpretation to the fast-threshold modulation phenomenon [160].

# Appendix A

## Numerical tools

Several numerical algorithms exist for the numerical computation of periodic orbits [11, 115, 157]. Most algorithms recast the periodic orbit computation as a two-point boundary value problems. Numerical boundary value methods fall into two classes:

1. *shooting methods* generate trajectory segments using a numerical time integration and match segment end points with each other and the boundary conditions;
2. *global methods* project the differential equations onto a finite dimensional space of discrete closed curves that satisfy the boundary conditions.

Both methods yield a set of (nonlinear) equations that are solved with root finding algorithms, usually Newton's method.

In this appendix, we summarize popular simple algorithms for the computation of periodic orbits. Then we emphasize how the computation of the (state) infinitesimal phase response curve is a cheap by-product of this computation. Finally we extend those algorithms for the computation of oscillator sensitivities: angular frequency, steady-state periodic solution, and infinitesimal phase response curve sensitivities. More sophisticated algorithms can be found in the literature and adapted similarly (see [70, 73, 115]).

### A.1 Numerical computation of periodic orbits

A periodic orbit  $\gamma$  is characterized by the  $2\pi$ -periodic steady-state solution  $x^\gamma : \mathbb{S}^1 \rightarrow \gamma$  describing a closed curve in the state space and the angular frequency  $\omega \in \mathbb{R}_{>0}$  (or equivalently the period  $T$ ) which solve the boundary value problem (3.55).

Introducing a (nonuniform) partition  $\Pi$  of the unit circle  $\mathbb{S}^1$

$$\Pi : 0 = \theta_0 < \theta_1 < \dots < \theta_N = 2\pi, \quad (\text{A.1})$$

the  $2\pi$ -periodic steady-state solution  $x^\gamma(\cdot)$  is numerically approximated by a closed discrete curve in the state space  $\mathcal{X}$ . A discrete curve is a set of points  $\{x_0^\gamma, x_1^\gamma, \dots, x_N^\gamma\}$  associated to the set of phases such that  $x_i^\gamma$  approximates  $x^\gamma(\theta_i)$  for all  $i = 0, 1, \dots, N$ . This discrete curve is closed, that is,  $x_N^\gamma = x_0^\gamma$ , which reflects the periodicity of the solution  $x^\gamma(\cdot)$ . In the following, the circle partition  $\Pi$  is fixed and the discrete curve is numerically represented by the vector  $x_\Pi^\gamma = [x_0^{\gamma\top}, x_1^{\gamma\top}, \dots, x_N^{\gamma\top}]^\top$ . We denote  $h_i = \theta_{i+1} - \theta_i$ .

Equations for approximate periodic orbits take then the form of  $N$   $n$ -dimensional vector equations

$$r_i(x_\Pi^\gamma, \omega) = 0, \quad i = 0, 1, \dots, N-1, \quad (\text{A.2})$$

where different residual maps  $r_i$  lead to different numerical methods (Table A.1). Those equations are completed by the periodicity condition

$$r_N(x_\Pi^\gamma, \omega) := x_N^\gamma - x_0^\gamma = 0 \quad (\text{A.3})$$

and the phase condition

$$r_\varphi(x_\Pi^\gamma, \omega) := \hat{\varphi}(x_\Pi^\gamma; \lambda) = 0. \quad (\text{A.4})$$

We solve this set of (nonlinear) equations  $r(x_\Pi^\gamma, \omega) = 0$  with the root finding Newton's method. Starting from an initial guess  $((x_\Pi^\gamma)^{(0)}, \omega^{(0)})$ , this method iteratively update the solution

$$(x_\Pi^\gamma)^{(k+1)} = (x_\Pi^\gamma)^{(k)} + (\Delta x_\Pi^\gamma)^{(k)} \quad \text{and} \quad \omega^{(k+1)} = \omega^{(k)} + \Delta \omega^{(k)}. \quad (\text{A.5})$$

Correction terms are computed by solving the linear problem

$$\begin{bmatrix} A & b^{x^\gamma} \\ c^{x^\gamma\top} & d^{x^\gamma} \end{bmatrix} \begin{bmatrix} \Delta x_\Pi^\gamma \\ \Delta \omega \end{bmatrix} = - \begin{bmatrix} r_\Pi(x_\Pi^\gamma, \omega) \\ r_\varphi(x_\Pi^\gamma, \omega) \end{bmatrix} \quad (\text{A.6})$$

where  $A$  has a particular block structure for one-step schemes and  $b^{x^\gamma}$ ,  $c^{x^\gamma}$ , and  $d^{x^\gamma}$  are also defined by blocks

$$A = \begin{bmatrix} G_0 & -H_0 & & & \\ & \ddots & \ddots & & \\ & & G_{N-1} & -H_{N-1} & \\ -I_n & & & I_n & \end{bmatrix}, \quad b^{x^\gamma} = \begin{bmatrix} b_0^{x^\gamma} \\ \vdots \\ b_{N-1}^{x^\gamma} \\ 0_{n \times 1} \end{bmatrix}, \quad (\text{A.7})$$

$$c^{x^\gamma\top} = \begin{bmatrix} \frac{\partial \hat{\varphi}}{\partial x_0} & \dots & \frac{\partial \hat{\varphi}}{\partial x_{N-1}} & \frac{\partial \hat{\varphi}}{\partial x_N} \end{bmatrix}, \quad d^{x^\gamma} = \begin{bmatrix} \frac{\partial \hat{\varphi}}{\partial \omega} \end{bmatrix}. \quad (\text{A.8})$$

	Forward multiple shooting	Trapezoidal scheme
$r_i$	$\phi(\frac{h_i}{\omega}, x_i^\gamma, \mathbf{0}, \lambda) - x_{i+1}^\gamma$	$x_{i+1}^\gamma - x_i^\gamma - \frac{1}{2} \frac{h_i}{\omega} [f(x_i^\gamma, 0, \lambda) + f(x_{i+1}^\gamma, 0, \lambda)]$
$G_i$	$\frac{\partial \phi}{\partial x_0}(\frac{h_i}{\omega}, x_i^\gamma, \mathbf{0}, \lambda)$	$-I_n - \frac{1}{2} \frac{h_i}{\omega} \frac{\partial f}{\partial x}(x_i^\gamma, 0, \lambda)$
$H_i$	$I_n$	$-I_n + \frac{1}{2} \frac{h_i}{\omega} \frac{\partial f}{\partial x}(x_{i+1}^\gamma, 0, \lambda)$
$b_i^{x^\gamma}$	$-\frac{h_i}{\omega^2} \frac{\partial \phi}{\partial t}(\frac{h_i}{\omega}, x_i^\gamma, \mathbf{0}, \lambda)$	$-\frac{1}{2} \frac{h_i}{\omega^2} [f(x_i^\gamma, 0, \lambda) + f(x_{i+1}^\gamma, 0, \lambda)]$
$\tilde{G}_i$	$I_n$	$-I_n + \frac{1}{2} \frac{h_i}{\omega} \frac{\partial f}{\partial x}(x_i^\gamma, 0, \lambda)^\top$
$\tilde{H}_i$	$\frac{\partial \phi}{\partial x_0}(\frac{h_i}{\omega}, x_i^\gamma, \mathbf{0}, \lambda)^\top$	$-I_n - \frac{1}{2} \frac{h_i}{\omega} \frac{\partial f}{\partial x}(x_{i+1}^\gamma, 0, \lambda)^\top$
$E_i$	$\frac{\partial \phi}{\partial \lambda}(\frac{h_i}{\omega}, x_i^\gamma, \mathbf{0}, \lambda)$	$\frac{1}{2} \frac{h_i}{\omega} [E(\theta_i; \lambda) + E(\theta_{i+1}; \lambda)]$
$E_i^p$	$[\frac{d}{d\lambda} \frac{\partial \phi}{\partial x_0}(\frac{h_i}{\omega}, x_i^\gamma, \mathbf{0}, \lambda)]^\top p_{i+1}$	$-\frac{1}{2} \frac{h_i}{\omega} [E^p(\theta_i; \lambda)^\top p_i + E^p(\theta_{i+1}; \lambda)^\top p_{i+1}]$
$P$	$\frac{1}{N+1} I_{(N+1)n}$	$\frac{1}{2\pi} \text{diag}(\frac{h_0}{2}, \frac{h_0+h_1}{2}, \dots, \frac{h_{N-1}+h_N}{2}, \frac{h_N}{2}) \otimes I_n$

Table A.1 – Residual maps  $r_i$ , linear block elements  $G_i$ ,  $H_i$ , and  $b_i^{x^\gamma}$ , adjoint linear block elements  $\tilde{G}_i$  and  $\tilde{H}_i$ , and sensitivity block elements  $E_i$ ,  $E_i^p$ , and  $P$  for two one-step numerical algorithms ( $i = 0, 1, \dots, N-1$ ).

Expressions of block elements  $G_i$ ,  $H_i$ , and  $b_i^{x^\gamma}$  depend on the methods used to generate residual maps  $r_i(x_\Pi^\gamma, \omega) = 0$ , with  $i = 0, 1, \dots, N-1$ , for approximate periodic orbits (TableA.1).

The main computational effort in one iteration arises from the evaluation of the  $(N+1)n \times (N+1)n$  structured matrix  $A$  whose block elements are computed through fundamental solution time integrations or Jacobian matrix evaluations.

## A.2 Numerical computation of infinitesimal phase response curves

The (state) infinitesimal phase response curve  $p : \mathbb{S}^1 \rightarrow \mathbb{R}^n$  of a periodic orbit is the solution of the boundary value problem (3.56).

The (state) infinitesimal phase response curve is numerically approximated by a set of points  $\{p_0, p_1, \dots, p_N\}$  associated to the phases in the partition  $\Pi$  such that  $p_N = p_0$ .

Following the same procedure as for approximate periodic orbits, equations for approximate infinitesimal phase response curves take the form of  $(N+1)n$  linear equations

$$\tilde{A} p_\Pi = 0 \quad (\text{A.9})$$

where the matrix  $\tilde{A}$  has the same structure as the matrix  $A$

$$\tilde{A} = \begin{bmatrix} \tilde{G}_0 & -\tilde{H}_0 & & & \\ & \ddots & \ddots & & \\ & & \tilde{G}_{N-1} & -\tilde{H}_{N-1} & \\ -I_n & & & I_n & \end{bmatrix}. \quad (\text{A.10})$$

Block elements of  $\tilde{A}$  can be constructed based on numerical computations done for the periodic orbit computation (TableA.1).

The matrix  $\tilde{A}$  is by construction singular with a simple rank deficiency. This rank deficiency is overcome by adding a normalization condition for  $p_\Pi$ . Using (3.56c), we have

$$v_\Pi^\top P p_\Pi = \omega \quad (\text{A.11})$$

where  $v_\Pi$  is the approximate tangent vector to the periodic orbit and  $P$  is a ponderation matrix which depends on the method class. We seek a system of defining equations that is square and regular. A standard way to tackle this issue is to border the matrix  $\tilde{A}$  as follows (see [157, Theorem 5.8] for details)

$$\begin{bmatrix} \tilde{A} & b^p \\ c^{p^\top} & d^p \end{bmatrix} \begin{bmatrix} p_\Pi \\ \xi \end{bmatrix} = \begin{bmatrix} 0 \\ \omega \end{bmatrix} \quad (\text{A.12})$$

with  $d^p \neq 0$ ,  $c^{p^\top} = v_\Pi^\top P$ , and  $b^p \notin \text{range}(\tilde{A})$  (for example  $b^p = v_\Pi$ ).

### A.3 Numerical computation of sensitivities

The angular frequency sensitivity  $S^\omega \in \mathbb{R}^{1 \times l}$  and the sensitivity of the  $2\pi$ -periodic steady-state solution  $S^{x^\gamma} : \mathbb{S}^1 \rightarrow \mathbb{R}^{n \times l}$  are the solutions of the linear boundary value problem (5.6). Equations for approximate periodic orbit sensitivities take the form of a system of linear equations

$$\begin{bmatrix} A & b^{x^\gamma} \\ c^{x^\gamma \top} & d^{x^\gamma} \end{bmatrix} \begin{bmatrix} S_{\Pi}^{x^\gamma} \\ S^\omega \end{bmatrix} = \begin{bmatrix} E_{\Pi} \\ E_{\varphi} \end{bmatrix} \quad (\text{A.13})$$

where  $E_{\varphi} = -\frac{\partial \hat{\varphi}}{\partial \lambda}$  and  $E_i$  depends on the numerical method used (Table A.1).

The sensitivity of the (state) infinitesimal phase response curve  $S^p : \mathbb{S}^1 \rightarrow \mathbb{R}^{n \times l}$  is the solution of the linear boundary value problem (5.14). Equations for approximate infinitesimal phase response curve sensitivities take the form of a system of linear equations

$$\begin{bmatrix} \tilde{A} & b^p \\ c^p \top & d^p \end{bmatrix} \begin{bmatrix} S_{\Pi}^p \\ \xi \end{bmatrix} = \begin{bmatrix} E_{\Pi}^p \\ E_{\omega}^p \end{bmatrix} \quad (\text{A.14})$$

where  $E_{\omega}^p = S^\omega - p_{\Pi}^{\top} P S_{\Pi}^v$  and  $E_i^p$  depends on the numerical method used (Table A.1).

In both cases, square matrices in left hand sides are identical to the matrices used for the computation of the periodic orbit and the infinitesimal phase response curve, respectively. The only additional computation effort arises from the evaluation of the right hand side.



# Appendix B

## Omitted derivations

### B.1 Sensitivity of the periodic orbit

Let  $\lambda_0$  be a nominal value of the parameter  $\lambda$ , and suppose that the nominal boundary value problem

$$\frac{dx^\gamma}{d\theta}(\theta; \lambda_0) - \frac{1}{\omega(\lambda_0)} f(x^\gamma(\theta; \lambda_0), 0, \lambda_0) = 0 \quad (\text{B.1a})$$

$$x^\gamma(2\pi; \lambda_0) - x^\gamma(0; \lambda_0) = 0 \quad (\text{B.1b})$$

$$\hat{\varphi}(x^\gamma(0; \lambda_0), \lambda_0) = 0 \quad (\text{B.1c})$$

has unique periodic solution  $x^\gamma(\theta; \lambda_0) = \phi(\theta/\omega(\lambda_0), x_0^\gamma(\lambda_0), \mathbf{0}, \lambda_0)$  over  $[0, 2\pi]$  and angular frequency  $\omega(\lambda_0)$ . Under technical assumptions (see [92, Theorem 3.5] for details), we know that for all  $\lambda$  sufficiently close to  $\lambda_0$ , that is,  $\|\lambda - \lambda_0\|_2$  sufficiently small, the boundary value problem

$$\frac{dx^\gamma}{d\theta}(\theta; \lambda) - \frac{1}{\omega(\lambda)} f(x^\gamma(\theta; \lambda), 0) = 0 \quad (\text{B.2a})$$

$$x^\gamma(2\pi; \lambda) - x^\gamma(0; \lambda) = 0 \quad (\text{B.2b})$$

$$\hat{\varphi}(x^\gamma(0; \lambda), \lambda) = 0 \quad (\text{B.2c})$$

has also unique periodic solution  $x^\gamma(\theta; \lambda) = \phi(\theta/\omega(\lambda), x_0^\gamma(\lambda), \mathbf{0}, \lambda)$  over  $[0, 2\pi]$  and angular frequency  $\omega(\lambda)$  that are close to the nominal  $x^\gamma(\theta; \lambda_0)$  and the nominal angular frequency  $\omega(\lambda_0)$ . The continuous differentiability of  $f$  with respect to  $x$  and  $\lambda$  implies the additional property that the solution  $x^\gamma(\theta; \lambda)$  is differentiable with respect to  $\lambda$  near  $\lambda_0$ . To see this, write

$$x^\gamma(\theta; \lambda) = x^\gamma(0; \lambda) + \frac{1}{\omega(\lambda)} \int_0^\theta f(x^\gamma(s; \lambda), 0, \lambda) ds. \quad (\text{B.3})$$

Taking partial derivatives with respect to  $\lambda$  yields

$$\begin{aligned} S^{x^\gamma}(\theta; \lambda) &= \frac{\partial x^\gamma}{\partial \lambda}(0; \lambda) \\ &+ \frac{1}{\omega(\lambda)} \int_0^\theta \left[ \frac{\partial f}{\partial x}(x^\gamma(s; \lambda), 0, \lambda) S^{x^\gamma}(s; \lambda) + \frac{\partial f}{\partial \lambda}(x^\gamma(s; \lambda), 0, \lambda) \right] ds \\ &- \frac{1}{\omega(\lambda)^2} \left[ \int_0^\theta f(x^\gamma(s; \lambda), 0, \lambda) ds \right] S^\omega(\lambda) \end{aligned} \quad (\text{B.4})$$

where  $S^{x^\gamma}(\theta; \lambda) := \frac{\partial x^\gamma}{\partial \lambda}(\theta; \lambda)$  and  $S^\omega(\lambda) := \frac{\partial \omega}{\partial \lambda}(\lambda)$ . Differentiating with respect to  $\theta$ , it can be seen that  $S^{x^\gamma}(\theta; \lambda)$  satisfies the differential equation

$$\frac{dS^{x^\gamma}}{d\theta}(\theta; \lambda) = \frac{1}{\omega(\lambda)} A(\theta; \lambda) S^{x^\gamma}(\theta; \lambda) + \frac{1}{\omega(\lambda)} E(\theta; \lambda) - \frac{1}{\omega(\lambda)^2} v(\theta; \lambda) S^\omega(\lambda) \quad (\text{B.5})$$

where

$$A(\theta; \lambda) := \frac{\partial f}{\partial x}(x^\gamma(\theta; \lambda), 0, \lambda), \quad (\text{B.6})$$

$$E(\theta; \lambda) := \frac{\partial f}{\partial \lambda}(x^\gamma(\theta; \lambda), 0, \lambda), \quad (\text{B.7})$$

$$v(\theta; \lambda) := f(x^\gamma(\theta; \lambda), 0, \lambda). \quad (\text{B.8})$$

For  $\lambda$  sufficiently close to  $\lambda_0$ , the matrices  $A(\theta; \lambda)$  and  $E(\theta; \lambda)$ , and the vector  $v(\theta; \lambda)$  are defined on  $[0, 2\pi]$ . Hence,  $S^{x^\gamma}(\theta; \lambda)$  is defined on the same interval. In addition, taking partial derivative of (B.2b) and (B.2c) with respect to  $\lambda$  yields

$$S^{x^\gamma}(2\pi; \lambda) - S^{x^\gamma}(0; \lambda) = 0 \quad (\text{B.9})$$

$$\frac{\partial \hat{\varphi}}{\partial x}(x^\gamma(0; \lambda), \lambda) S^{x^\gamma}(0; \lambda) + \frac{\partial \hat{\varphi}}{\partial \lambda}(x^\gamma(0; \lambda), \lambda) = 0. \quad (\text{B.10})$$

Then the sensitivity functions  $S^{x^\gamma}(\theta; \lambda)$  and  $S^\omega(\lambda)$  are the unique solutions of the boundary value problem

$$\frac{dS^{x^\gamma}}{d\theta}(\theta; \lambda) - \frac{1}{\omega(\lambda)} A(\theta; \lambda) S^{x^\gamma}(\theta; \lambda) + \frac{1}{\omega(\lambda)^2} v(\theta; \lambda) S^\omega(\lambda) = \frac{1}{\omega(\lambda)} E(\theta; \lambda), \quad (\text{B.11a})$$

$$S^{x^\gamma}(2\pi; \lambda) - S^{x^\gamma}(0; \lambda) = 0, \quad (\text{B.11b})$$

$$\frac{\partial \hat{\varphi}}{\partial x}(x^\gamma(0; \lambda), \lambda) S^{x^\gamma}(0; \lambda) + \frac{\partial \hat{\varphi}}{\partial \lambda}(x^\gamma(0; \lambda), \lambda) = 0. \quad (\text{B.11c})$$

## B.2 Sensitivity of the phase response curve

Let  $\lambda_0$  be a nominal value of the parameter  $\lambda$ , and suppose that the nominal boundary value problem

$$\frac{dp}{d\theta}(\theta; \lambda_0) + \frac{1}{\omega} \frac{\partial f}{\partial x}(x^\gamma(\theta; \lambda_0), 0, \lambda_0)^\top p(\theta; \lambda_0) = 0 \quad (\text{B.12a})$$

$$p(2\pi; \lambda_0) - p(0; \lambda_0) = 0 \quad (\text{B.12b})$$

$$\langle p(\theta; \lambda_0), f(x^\gamma(\theta; \lambda_0), 0, \lambda_0) \rangle = \omega \quad (\text{B.12c})$$

has a unique  $2\pi$ -periodic solution  $p(\theta; \lambda_0) = \nabla_x \Theta(x^\gamma(\theta; \lambda_0); \lambda_0)$  over  $[0, 2\pi]$ . Under appropriate technical assumptions (see [92, Theorem 3.5] for details), we know that for all  $\lambda$  sufficiently close to  $\lambda_0$ , that is,  $\|\lambda - \lambda_0\|_2$  sufficiently small, the boundary value problem

$$\frac{dp}{d\theta}(\theta; \lambda) + \frac{1}{\omega} \frac{\partial f}{\partial x}(x^\gamma(\theta; \lambda), 0, \lambda)^\top p(\theta; \lambda) = 0 \quad (\text{B.13a})$$

$$p(2\pi; \lambda) - p(0; \lambda) = 0 \quad (\text{B.13b})$$

$$\langle p(\theta; \lambda), f(x^\gamma(\theta; \lambda), 0, \lambda) \rangle = \omega \quad (\text{B.13c})$$

has also a unique  $2\pi$ -periodic solution  $p(\theta; \lambda) = \nabla_x \Theta(x^\gamma(\theta; \lambda); \lambda)$  over  $[0, 2\pi]$  that is close to the nominal  $p(\theta; \lambda_0)$ . The continuous differentiability of  $\frac{\partial f}{\partial x}$  with respect to  $x$  and  $\lambda$  implies the additional property that the solution  $p(\theta; \lambda)$  is differentiable with respect to  $\lambda$  near  $\lambda_0$ . To see this, write

$$p(\theta; \lambda) := p(0; \lambda) - \frac{1}{\omega(\lambda)} \int_0^\theta \frac{\partial f}{\partial x}(x^\gamma(s; \lambda), 0, \lambda)^\top p(s; \lambda) ds, \quad (\text{B.14})$$

Taking partial derivatives with respect to  $\lambda$  yields

$$\begin{aligned} S^p(\theta; \lambda) &:= S^p(0; \lambda) \\ &- \frac{1}{\omega(\lambda)} \int_0^\theta \left[ \left( \sum_{k=1}^n \frac{\partial^2 f}{\partial x_k \partial x}(x^\gamma(s; \lambda), 0, \lambda) S_k^{x^\gamma}(s; \lambda) \right. \right. \\ &\quad \left. \left. + \frac{\partial^2 f}{\partial \lambda \partial x}(x^\gamma(s; \lambda), 0, \lambda) \right)^\top p(s; \lambda) \right] ds \\ &- \frac{1}{\omega(\lambda)} \int_0^\theta \left[ \frac{\partial f}{\partial x}(x^\gamma(s; \lambda), 0, \lambda)^\top S^p(s; \lambda) \right] ds \\ &+ \frac{1}{\omega(\lambda)^2} \left[ \int_0^\theta \frac{\partial f}{\partial x}(x^\gamma(s; \lambda), 0, \lambda)^\top p(s; \lambda) ds \right] S^\omega(\lambda) \end{aligned} \quad (\text{B.15})$$

where  $S^p(\theta; \lambda) := \frac{\partial p}{\partial \lambda}(\theta; \lambda)$ . Differentiating with respect to  $\theta$ , it can be seen that  $S^p(\theta; \lambda)$  satisfies the differential equation

$$\frac{dS^p}{d\theta}(\theta; \lambda) = -\frac{1}{\omega(\lambda)} A(\theta; \lambda)^\top S^{x^\gamma}(\theta; \lambda) - \frac{1}{\omega(\lambda)} E^p(\theta; \lambda)^\top p(\theta; \lambda) \quad (\text{B.16})$$

where

$$\begin{aligned} E_{ij}^p(\theta; \lambda) &:= \sum_{k=1}^n \frac{\partial^2 f_i}{\partial x_j \partial x_k}(x^\gamma(\theta; \lambda), 0, \lambda) S_k^{x^\gamma}(\theta; \lambda) \\ &+ \frac{\partial^2 f_i}{\partial x_j \partial \lambda}(x^\gamma(\theta; \lambda), 0, \lambda) - \frac{1}{\omega(\lambda)} \frac{\partial f_i}{\partial x_j}(x^\gamma(\theta; \lambda), 0, \lambda) S^\omega(\lambda). \end{aligned} \quad (\text{B.17})$$

For  $\lambda$  sufficiently close to  $\lambda_0$ , the matrices  $A(\theta; \lambda)$  and  $E^p(\theta; \lambda)$ , and the vector  $p(\theta; \lambda)$  are defined on  $[0, 2\pi]$ . Hence,  $S^p(\theta; \lambda)$  is defined on the same interval. In addition, taking partial derivative of (B.13b) and (B.13c) with respect to  $\lambda$  yields

$$S^p(2\pi; \lambda) - S^p(0; \lambda) = 0 \quad (\text{B.18})$$

$$\langle S^p(\theta; \lambda), v(\theta; \lambda) \rangle + \langle p(\theta; \lambda), S^v(\theta; \lambda) \rangle = S^\omega(\lambda) \quad (\text{B.19})$$

where

$$S^v(\theta; \lambda) := \frac{\partial f}{\partial x}(x^\gamma(\theta; \lambda), 0, \lambda) S^{x^\gamma}(\theta; \lambda) + \frac{\partial f}{\partial \lambda}(x^\gamma(\theta; \lambda), 0, \lambda). \quad (\text{B.20})$$

Then the sensitivity function  $S^p(\theta; \lambda)$  is the unique solutions of the boundary value problem

$$\frac{dS^p}{d\theta}(\theta; \lambda) + \frac{1}{\omega(\lambda)} A(\theta; \lambda)^\top S^p(\theta; \lambda) = -\frac{1}{\omega(\lambda)} E^p(\theta; \lambda)^\top p(\theta; \lambda), \quad (\text{B.21a})$$

$$S^p(2\pi; \lambda) - S^p(0; \lambda) = 0, \quad (\text{B.21b})$$

$$\langle S^p(\theta; \lambda), v(\theta; \lambda) \rangle + \langle p(\theta; \lambda), S^v(\theta; \lambda) \rangle = S^\omega(\lambda). \quad (\text{B.21c})$$

# Bibliography

- [1] L. F. Abbott. Lapicque's introduction of the integrate-and-fire model neuron (1907). *Brain Res. Bull.*, 50(5–6):303–304, Nov. 1999.
- [2] A. Abouzeid and G. B. Ermentrout. Type-II phase resetting curve is optimal for stochastic synchrony. *Phys. Rev. E*, 80(1):011911, July 2009.
- [3] P.-A. Absil, R. Mahony, and R. Sepulchre. *Optimization Algorithms on Matrix Manifolds*. Princeton University Press, Princeton, NJ, 2008.
- [4] R. Agarwal and S. V. Sarma. The effects of DBS patterns on basal ganglia activity and thalamic relay: a computational study. *J. Comput. Neurosci.*, 33(1):151–167, Aug. 2012.
- [5] R. Agarwal and S. V. Sarma. Performance limitations of relay neurons. *PLoS Comput. Biol.*, 8(8):e1002626, Aug. 2012.
- [6] A. A. Andronov, A. A. Vitt, and S. È. Khaïkin. *Theory of Oscillators*. Pergamon Press, Oxford, United Kingdom, 1966.
- [7] D. Angeli. A Lyapunov approach to incremental stability properties. *IEEE Trans. Autom. Control*, 47(3):410–421, Mar. 2002.
- [8] D. Angeli and E. D. Sontag. Monotone control systems. *IEEE Trans. Autom. Control*, 48(10):1684–1698, Oct. 2003.
- [9] D. Angeli and E. D. Sontag. Oscillations in i/o monotone systems under negative feedback. *IEEE Trans. Autom. Control*, 53(Special Issue):166–176, Jan. 2008.
- [10] M. Arcak. Passivity as a design tool for group coordination. *IEEE Trans. Autom. Control*, 52(8):1380–1390, Aug. 2007.
- [11] U. M. Ascher, R. M. M. Mattheij, and R. D. Russell. *Numerical Solution of Boundary Value Problems for Ordinary Differential Equations*. Prentice Hall, Englewood Cliffs, NJ, Feb. 1988.

- [12] V. K. Astashev, M. Z. Kolovsky, and V. I. Babitsky. *Dynamics and Control of Machines*. Foundations of Engineering Mechanics. Springer, Berlin Heidelberg, Germany, 2000.
- [13] N. Bagheri, J. Stelling, and F. J. Doyle III. Circadian phase entrainment via nonlinear model predictive control. *Int. J. Robust Nonlinear Control*, 17(17):1555–1571, Nov. 2007.
- [14] N. Bagheri, J. Stelling, and F. J. Doyle III. Quantitative performance metrics for robustness in circadian rhythms. *Bioinformatics*, 23(3):358–364, Feb. 2007.
- [15] N. Bagheri, J. Stelling, and F. J. Doyle III. Circadian phase resetting via single and multiple control targets. *PLoS Comput. Biol.*, 4(7):e1000104, July 2008.
- [16] V. N. Belykh, G. V. Osipov, N. Kuckländer, B. Blasius, and J. Kurths. Automatic control of phase synchronization in coupled complex oscillators. *Physica D*, 200(1–2):81–104, Jan. 2005.
- [17] I. I. Blekhman. *Synchronization in Science and Technology*. American Society of Mechanical Engineers, New York, NY, Sept. 1988.
- [18] E. T. Brown, J. Moehlis, and P. Holmes. On the phase reduction and response dynamics of neural oscillator populations. *Neural Comput.*, 16(4):673–715, Apr. 2004.
- [19] G. L. Brown and J. C. Eccles. The action of a single vagal volley on the rhythm of the heart beat. *J. Physiol.*, 82(2):211–241, 1934.
- [20] H. L. Bryant and J. P. Segundo. Spike initiation by transmembrane current: a white-noise analysis. *J. Physiol.*, 260(2):279–314, 1976.
- [21] M. K. Bunger, L. D. Wilsbacher, S. M. Moran, C. Clendenin, L. A. Radcliffe, J. B. Hogenesch, M. C. Simon, J. S. Takahashi, and C. A. Bradfield. Mop3 is an essential component of the master circadian pacemaker in mammals. *Cell*, 103(7):1009–1017, Dec. 2000.
- [22] E. G. Buré and E. Rosenwasser. The study of the sensitivity of oscillatory systems. *Automat. Remote Contr.*, 7:1045–1052, 1974.
- [23] A. Campbell. The theoretical basis of synchronization by shifts in environmental conditions. In E. Zeuthen, editor, *Synchrony in Cell Division and Growth*, pages 469–484. Wiley, New York, NY, 1964.
- [24] B. Chance, B. Hess, and A. Betz. DPNH oscillations in a cell-free extract of *S. carlsbergensis*. *Biochem. Biophys. Res. Commun.*, 16(2):182–187, 1964.

- [25] B. Chance, E. K. Pye, A. K. Ghosh, and B. Hess, editors. *Biological and Biochemical Oscillators*. Academic Press, London, United Kingdom, 1973.
- [26] P. Danzl, J. Hespanha, and J. Moehlis. Event-based minimum-time control of oscillatory neuron models: phase randomization, maximal spike rate increase, and desynchronization. *Biol. Cybern.*, 101(5–6):387–399, Dec. 2009.
- [27] P. Danzl and J. Moehlis. Spike timing control of oscillatory neuron models using impulsive and quasi-impulsive charge-balanced inputs. In *Proc. 2008 Am. Control Conf.*, pages 171–176, Seattle, WA, 2008.
- [28] P. Danzl, A. Nabi, and J. Moehlis. Charge-balanced spike timing control for phase models of spiking neurons. *Discrete Contin. Dyn. Syst.*, 28(4):1413–1435, 2010.
- [29] K. De Cock and B. De Moor. Subspace angles and distances between ARMA models. In *Proc. 14th Int. Symp. Mathematical Theory of Networks and Systems*, Perpignan, France, June 2000.
- [30] P. J. DeCoursey. Daily light sensitivity rhythm in a rodent. *Science*, 131(3392):33–35, Jan. 1960.
- [31] A. Demir, A. Mehrotra, and J. Roychowdhury. Phase noise in oscillators: a unifying theory and numerical methods for characterization. *IEEE Trans. Circuits Syst. I*, 47(5):655–674, May 2000.
- [32] R. P. Dickinson and R. J. Gelinas. Sensitivity analysis of ordinary differential equation systems—a direct method. *J. Comput. Phys.*, 21(2):123–143, 1976.
- [33] F. Dörfler and F. Bullo. Exploring synchronization in complex oscillator networks. In *Proc. 51st IEEE Conf. Decision and Control*, pages 7157–7170, Maui, HI, Oct. 2012.
- [34] F. Dorfler and F. Bullo. Synchronization in complex oscillator networks: A survey. Apr. 2013. Submitted to *Automatica* (preprint <http://motion.me.ucsb.edu/pdf/2013b-db.pdf>).
- [35] L. N. M. Duysens and J. Amesz. Fluorescence spectrophotometry of reduced phosphopyridine nucleotide in intact cells in the near-ultraviolet and visible region. *Biochim. Biophys. Acta*, 24:19–26, 1957.
- [36] J. C. Eccles and H. E. Hoff. The rhythm of the heart beat. *Proc. R. Soc. Lond. B*, 115(794):307–368, 1934.

- [37] D. V. Efimov. *Robust and adaptive control of nonlinear oscillators*. Nauka, 2005.
- [38] D. V. Efimov, P. Sacré, and R. Sepulchre. Controlling the phase of an oscillator: a phase response curve approach. In *Proc. 48th IEEE Conf. Decision and Control and 28th Chinese Control Conf.*, pages 7692–7697, Shanghai, China, Dec. 2009.
- [39] A. K. El-Sakkary. The gap metric: robustness of stabilization of feedback systems. *IEEE Trans. Autom. Control*, 30(3):240–247, Mar. 1985.
- [40] I. R. Epstein and J. A. Pojman. *An Introduction to Nonlinear Chemical Dynamics: Oscillations, Waves, Patterns, and Chaos*. Oxford University Press, New York, NY, Oct. 1998.
- [41] G. B. Ermentrout. Type I membranes, phase resetting curves, and synchrony. *Neural Comput.*, 8(5):979–1001, July 1996.
- [42] G. B. Ermentrout, L. Glass, and B. E. Oldeman. The shape of phase-resetting curves in oscillators with a saddle node on an invariant circle bifurcation. *Neural Comput.*, Sept. 2012.
- [43] G. B. Ermentrout and N. Kopell. Frequency plateaus in a chain of weakly coupled oscillators. I. *SIAM. J. Math. Anal.*, 15(2):215–237, 1984.
- [44] M. Farkas. *Periodic Motions*, volume 104 of *Applied Mathematical Sciences*. Springer-Verlag, New York, NY, 1994.
- [45] N. Fenichel. Persistence and smoothness of invariant manifolds for flows. *Indiana Univ. Math. J.*, 21(3):193–226, 1972.
- [46] N. Fenichel. Geometric singular perturbation theory for ordinary differential equations. *J. Differential Equations*, 31(1):53–98, Jan. 1979.
- [47] R. Fitzhugh. Thresholds and plateaus in the hodgkin-huxley nerve equations. *J. Gen. Physiol.*, 43(5):867–896, May 1960.
- [48] R. FitzHugh. Impulses and physiological states in theoretical models of nerve membrane. *Biophys. J.*, 1(6):445–466, July 1961.
- [49] D. B. Forger and C. S. Peskin. A detailed predictive model of the mammalian circadian clock. *Proc. Natl. Acad. Sci. USA*, 100(25):14806–14811, Dec. 2003.
- [50] A. L. Fradkov and A. Y. Pogromsky. *Introduction to Control of Oscillations and Chaos*, volume 35 of *World Scientific Series on Nonlinear Science Series A*. World Scientific, Singapore, Oct. 1998.

- [51] A. Franci, G. Drion, and R. Sepulchre. Modeling neuronal bursting: singularity theory meets neurophysiology. *arXiv*, May 2013.
- [52] A. Franci, G. Drion, and R. Sepulchre. An organizing center in a planar model of neuronal excitability. *SIAM J. Applied Dynamical Systems*, 11(4):1698–1722, Jan. 2013.
- [53] P. M. Frank. *Introduction to System Sensitivity Theory*. Academic Press, San Diego, CA, Sept. 1978.
- [54] R. F. Galán, G. B. Ermentrout, and N. N. Urban. Reliability and stochastic synchronization in type I vs. type II neural oscillators. *Neurocomputing*, 70:2102–2106, 2007.
- [55] R. F. Galán, G. B. Ermentrout, and N. N. Urban. Stochastic dynamics of uncoupled neural oscillators: Fokker-planck studies with the finite element method. *Phys. Rev. E*, 76(5 Pt 2):056110, Nov. 2007.
- [56] R. F. Galán, N. Fourcaud-Trocmé, G. B. Ermentrout, and N. N. Urban. Correlation-induced synchronization of oscillations in olfactory bulb neurons. *J. Neurosci.*, 26(14):3646–3655, 2006.
- [57] T. T. Georgiou. Distances and Riemannian metrics for spectral density functions. *IEEE Trans. Signal Process.*, 55(8):3995–4003, Aug. 2007.
- [58] T. T. Georgiou and M. C. Smith. Optimal robustness in the gap metric. *IEEE Trans. Autom. Control*, 35(6):673–686, June 1990.
- [59] A. Ghosh and B. Chance. Oscillations of glycolytic intermediates in yeast cells. *Biochem. Biophys. Res. Commun.*, 16(2):174–181, 1964.
- [60] L. Glass and M. C. Mackey. *From Clocks to Chaos: the Rhythms of Life*. Princeton University Press, Princeton, NJ, 1988.
- [61] L. Glass and R. Perez. Fine structure of phase locking. *Phys. Rev. Lett.*, 48(26):1772–1775, June 1982.
- [62] A. Goh and R. Vidal. Unsupervised Riemannian clustering of probability density functions. In *Machine Learning and Knowledge Discovery in Databases*, pages 377–392. Springer-Verlag, Berlin Heidelberg, Germany, 2008.
- [63] A. Goldbeter. A minimal cascade model for the mitotic oscillator involving cyclin and cdc2 kinase. *Proc. Natl. Acad. Sci. USA*, 88(20):9107–9111, Oct. 1991.
- [64] A. Goldbeter. A model for circadian oscillations in the *Drosophila* period protein (PER). *Proc. R. Soc. Lond. B*, 261(1362):319–324, Sept. 1995.

- [65] A. Goldbeter. *Biochemical Oscillations and Cellular Rhythms: the Molecular Bases of Periodic and Chaotic Behaviour*. Cambridge University Press, Cambridge, United Kingdom, 1996.
- [66] D. Gonze, J. Halloy, and A. Goldbeter. Robustness of circadian rhythms with respect to molecular noise. *Proc. Natl. Acad. Sci. USA*, 99(2):673–678, Jan. 2002.
- [67] D. Gonze, J.-C. Leloup, and A. Goldbeter. Theoretical models for circadian rhythms in *Neurospora* and *Drosophila*. *C.R. Acad. Sci. Paris, Sciences de la vie*, 323(1):57–67, Jan. 2000.
- [68] B. C. Goodwin. Oscillatory behavior in enzymatic control processes. *Adv. Enzyme Regul.*, 3:425–438, 1965.
- [69] B. C. Goodwin. An entrainment model for timed enzyme syntheses in bacteria. *Nature*, 209(5022):479–481, Jan. 1966.
- [70] W. Govaerts and B. Sautois. Computation of the phase response curve: a direct numerical approach. *Neural Comput.*, 18(4):817–847, Apr. 2006.
- [71] J. Guckenheimer. Isochrons and phaseless sets. *J. Math. Biol.*, 1(3):259–273, 1975.
- [72] J. Guckenheimer and P. Holmes. *Nonlinear Oscillations, Dynamical Systems, and Bifurcations of Vector Fields*, volume 42 of *Applied Mathematical Sciences*. Springer-Verlag, New York, NY, 2nd edition, 1983.
- [73] J. Guckenheimer and B. Meloon. Computing periodic orbits and their bifurcations with automatic differentiation. *SIAM J. Sci. Comput.*, 22(3):951–985, 2000.
- [74] M. Guevara and L. Glass. Phase locking, period doubling bifurcations and chaos in a mathematical model of a periodically driven oscillator: A theory for the entrainment of biological oscillators and the generation of cardiac dysrhythmias. *J. Math. Biol.*, 14(1):1–23, 1982.
- [75] A. Guillemon and G. Huguet. A computational and geometric approach to phase resetting curves and surfaces. *SIAM J. Applied Dynamical Systems*, 8(3):1005–1042, 2009.
- [76] R. Gunawan and F. J. Doyle III. Isochron-based phase response analysis of circadian rhythms. *Biophys. J.*, 91(6):2131–2141, Sept. 2006.
- [77] R. Gunawan and F. J. Doyle III. Phase sensitivity analysis of circadian rhythm entrainment. *J. Biol. Rhythms*, 22(2):180–194, Apr. 2007.

- [78] M. Hafner, P. Sacré, L. Symul, R. Sepulchre, and H. Koepl. Multiple feedback loops in circadian cycles: robustness and entrainment as selection criteria. In *Proc. 7th Int. Workshop Computational Systems Biology*, pages 51–54, Luxembourg, June 2010.
- [79] A. Hajimiri and T. H. Lee. *The Design of Low Noise Oscillators*. Kluwer Academic Publishers, New York, NY, 1999.
- [80] A. Hamadeh, G.-B. Stan, R. Sepulchre, and J. Gonçalves. Global state synchronization in networks of cyclic feedback systems. *IEEE Trans. Autom. Control*, 57(2):478–483, Feb. 2012.
- [81] D. Hansel, G. Mato, and C. Meunier. Synchrony in excitatory neural networks. *Neural Comput.*, 7(2):307–337, Mar. 1995.
- [82] L. H. Hartwell, J. Culotti, J. R. Pringle, and B. J. Reid. Genetic control of the cell division cycle in yeast: A model to account for the order of cell cycle events is deduced from the phenotypes of yeast mutants. *Science*, 183(4120):46–51, 1974.
- [83] S. Hata, K. Arai, R. F. Galán, and H. Nakao. Optimal phase response curves for stochastic synchronization of limit-cycle oscillators by common poisson noise. *Phys. Rev. E*, 84:016229, Jul 2011.
- [84] A. L. Hodgkin and A. F. Huxley. A quantitative description of membrane current and its application to conduction and excitation in nerve. *J. Physiol.*, 117(4):500–544, Aug. 1952.
- [85] F. C. Hoppensteadt and E. M. Izhikevich. *Weakly Connected Neural Networks*, volume 126 of *Applied Mathematical Sciences*. Springer-Verlag, New York, NY, 1997.
- [86] C. Huygens. *Horologium Oscillatorium*. Apud F. Muguet, Paris, France, 1673.
- [87] B. P. Ingalls. Autonomously oscillating biochemical systems: parametric sensitivity of extrema and period. *Syst. Biol.*, 1(1):62–70, June 2004.
- [88] E. M. Izhikevich. Phase equations for relaxation oscillators. *SIAM J. Appl. Math.*, 60(5):1789–1804, 2000.
- [89] E. M. Izhikevich. *Dynamical Systems in Neuroscience: the Geometry of Excitability and Bursting*. The MIT Press, Cambridge, MA, 2007.
- [90] C. H. Johnson. An atlas of phase responses curves for circadian and circatidal rhythms. Department of Biology, Vanderbilt University, 1990.

- [91] C. K. R. T. Jones. Geometric singular perturbation theory. In *Dynamical Systems*, pages 44–118. Springer, Berlin Heidelberg, Germany, 1995.
- [92] H. K. Khalil. *Nonlinear Systems*. Prentice Hall, Upper Saddle River, NJ, 3rd edition, 2002.
- [93] B. W. Knight. Dynamics of encoding in a population of neurons. *J. Gen. Physiol.*, 59(6):734–766, June 1972.
- [94] A. S. Kovaleva. Frequency and phase control of the resonance oscillations of a non-linear system under conditions of uncertainty. *J. Appl. Math. Mech.*, 68(5):699–706, 2004.
- [95] M. A. Kramer, H. Rabitz, and J. M. Calo. Sensitivity analysis of oscillatory systems. *Appl. Math. Modelling*, 8(5):328–340, Oct. 1984.
- [96] T. Kreuz, D. Chicharro, C. Houghton, R. G. Andrzejak, and F. Mormann. Monitoring spike train synchrony. *J. Neurophysiol.*, 109(5):1457–1472, 2013.
- [97] M. Krupa and P. Szmolyan. Extending geometric singular perturbation theory to nonhyperbolic points—fold and canard points in two dimensions. *SIAM. J. Math. Anal.*, 33(2):286–314, 2001.
- [98] M. Krupa and P. Szmolyan. Extending slow manifolds near transcritical and pitchfork singularities. *Nonlinearity*, 14(6):1473–1491, 2001.
- [99] M. Krupa and P. Szmolyan. Relaxation oscillation and canard explosion. *J. Differential Equations*, 174(2):312–368, 2001.
- [100] Y. Kuramoto. Self-entrainment of a population of coupled non-linear oscillators. In *International Symposium on Mathematical Problems in Theoretical Physics*, pages 420–422. Springer-Verlag, Berlin Heidelberg, Germany, 1975.
- [101] Y. Kuramoto. *Chemical Oscillations, Waves, and Turbulence*, volume 19 of *Springer Series in Synergetics*. Springer-Verlag, Berlin Heidelberg, Germany, 1st edition, 1984.
- [102] Y. Kuramoto. Phase- and center-manifold reductions for large populations of coupled oscillators with application to non-locally coupled systems. *Int. J. Bifurcat. Chaos*, 7(4):789–805, Apr. 1997.
- [103] Y. A. Kuznetsov. *Elements of Applied Bifurcation Theory*, volume 112 of *Applied Mathematical Sciences*. Springer-Verlag, New York, NY, 1st edition, June 1998.

- [104] R. Larter, H. Rabitz, and M. A. Kramer. Sensitivity analysis of limit cycles with application to the brusselator. *The Journal of Chemical Physics*, 80(9):4120, 1984.
- [105] M. Lauret, F. Felici, G. Witvoet, T. P. Goodman, G. Vandersteen, O. Sauter, M. R. de Baar, and the TCV team. Demonstration of sawtooth period locking with power modulation in tcv plasmas. *Nuclear Fusion*, pages 1–5, Mar. 2012.
- [106] J.-C. Leloup and A. Goldbeter. A model for circadian rhythms in *Drosophila* incorporating the formation of a complex between the PER and TIM proteins. *J. Biol. Rhythms*, 13(1):70–87, Feb. 1998.
- [107] J.-C. Leloup and A. Goldbeter. Modeling the molecular regulatory mechanism of circadian rhythms in *Drosophila*. *BioEssays*, 22(1):84–93, Jan. 2000.
- [108] J.-C. Leloup and A. Goldbeter. Toward a detailed computational model for the mammalian circadian clock. *Proc. Natl. Acad. Sci. USA*, 100(12):7051–7056, June 2003.
- [109] J.-C. Leloup and A. Goldbeter. Modeling the mammalian circadian clock: sensitivity analysis and multiplicity of oscillatory mechanisms. *J. Theoret. Biol.*, 230(4):541–562, Oct. 2004.
- [110] J.-C. Leloup, D. Gonze, and A. Goldbeter. Limit cycle models for circadian rhythms based on transcriptional regulation in *Drosophila* and *Neurospora*. *J. Biol. Rhythms*, 14(6):433–448, Dec. 1999.
- [111] K. K. Lin, E. Shea-Brown, and L.-S. Young. Reliability of coupled oscillators. *J. Nonlinear Sci.*, 19(5):497–545, 2009.
- [112] W. Lohmiller and J.-J. E. Slotine. On contraction analysis for non-linear systems. *Automatica*, 34(6):683–696, June 1998.
- [113] A. J. Lotka. Undamped oscillations derived from the law of mass action. *J. Am. Chem. Soc.*, 42(8):1595–1599, 1920.
- [114] A. J. Lotka. *Elements of Physical Biology*. Williams and Wilkins, Baltimore, MD, 1925.
- [115] K. Lust. Improved numerical Floquet multipliers. *Int. J. Bifurcat. Chaos*, 11(9):2389–2410, 2001.
- [116] Z. F. Mainen and T. J. Sejnowski. Reliability of spike timing in neocortical neurons. *Science*, 268(5216):1503–1506, 1995.

- [117] I. G. Malkin. *The Methods of Lyapunov and Poincare in the Theory of Nonlinear Oscillations*. Gostexizdat, Moscow, Russia, 1949.
- [118] I. G. Malkin. *Some Problems in the Theory of Nonlinear Oscillations*. Gostexizdat, Moscow, Russia, 1956.
- [119] S. Marella and G. B. Ermentrout. Class-II neurons display a higher degree of stochastic synchronization than class-I neurons. *Phys. Rev. E*, 77(4 Pt 1):041918, Apr. 2008.
- [120] R. J. Martin. A metric for arma processes. *IEEE Trans. Signal Process.*, 48(4):1164–1170, Apr. 2000.
- [121] A. Mauroy and I. Mezić. On the use of Fourier averages to compute the global isochrons of (quasi)periodic dynamics. *Chaos*, 22(3):033112, 2012.
- [122] A. Mauroy, I. Mezić, and J. Moehlis. Isostables, isochrons, and koopman spectrum for the action–angle representation of stable fixed point dynamics. *Physica D: Nonlinear Phenomena*, (0):–, 2013.
- [123] A. Mauroy, P. Sacré, and R. Sepulchre. Kick synchronization versus diffusive synchronization. In *Proc. 51st IEEE Conf. Decision and Control*, pages 7171–7183, Maui, HI, Dec. 2013.
- [124] A. Mauroy and R. Sepulchre. Contraction of monotone phase-coupled oscillators. *Systems & Control Letters*, 61(11):1097–1102, Nov. 2012.
- [125] G. R. Mines. On circulating excitations in heart muscles and their possible relation to tachycardia and fibrillation. *Trans. R. S. C.*, 4:43–53, 1914.
- [126] R. E. Mirollo and S. H. Strogatz. Synchronization of pulse-coupled biological oscillators. *SIAM J. Appl. Math.*, 50(6):1645–1662, 1990.
- [127] C. Morris and H. Lecar. Voltage oscillations in the barnacle giant muscle fiber. *Biophys. J.*, 35(1):193–213, July 1981.
- [128] A. Nabi, M. Mirzadeh, F. Gibou, and J. Moehlis. Minimum energy desynchronizing control for coupled neurons. *J. Comput. Neurosci.*, 34(2):259–271, 2013.
- [129] A. Nabi and J. Moehlis. Time optimal control of spiking neurons. *J. Math. Biol.*, 64(6):981–1004, May 2012.
- [130] J. Nagumo, S. Arimoto, and S. Yoshizawa. An active pulse transmission line simulating nerve axon. *Proc. IRE*, 50(10):2061–2070, Oct. 1962.

- [131] A. H. Nayfeh and D. T. Mook. *Nonlinear Oscillations*. John Wiley & Sons, Inc., New York, NY, 1979.
- [132] J. C. Neu. Coupled chemical oscillators. *SIAM J. Appl. Math.*, 37(2):307–315, 1979.
- [133] H. Nijmeijer and A. Rodríguez-Ángeles. *Synchronization of Mechanical Systems*. World Scientific, River Edge, NJ, 2003.
- [134] B. Novák and J. J. Tyson. Design principles of biochemical oscillators. *Nature Rev. Mol. Cell Biol.*, 9(12):981–991, Dec. 2008.
- [135] H. M. Osinga and J. Moehlis. Continuation-based computation of global isochrons. *SIAM J. Applied Dynamical Systems*, 9(4):1201–1228, 2010.
- [136] A. V. Pavlov. *The output regulation problem: a convergent dynamics approach*. PhD thesis, Technische Universiteit Eindhoven, The Netherlands, 2004.
- [137] A. V. Pavlov, N. van de Wouw, and H. Nijmeijer. Convergent systems: analysis and synthesis. In *Control and Observer Design for Nonlinear Finite and Infinite Dimensional Systems*, pages 131–146. Springer-Verlag, Berlin Heidelberg, Germany, 2005.
- [138] B. Pfeuty, Q. Thommen, and M. Lefranc. Robust entrainment of circadian oscillators requires specific phase response curves. *Biophys. J.*, 100(11):2557–2565, June 2011.
- [139] A. Pikovsky, M. Rosenblum, and J. Kurths. *Synchronization: A Universal Concept in Nonlinear Sciences*, volume 12 of *Cambridge Nonlinear Science Series*. Cambridge University Press, Cambridge, United Kingdom, 2001.
- [140] C. S. Pittendrigh. Circadian systems: entrainment. In *Biological Rhythms*, pages 95–124. Plenum Press, New York, NY, 1981.
- [141] H. Rabitz, M. A. Kramer, and D. Dacol. Sensitivity analysis in chemical kinetics. *Annu. Rev. Phys. Chem.*, 34(1):419–461, Oct. 1983.
- [142] H. Remmert. *Der Schüpfrythmus der Insekten*. Franz Steiner, Wiesbaden, Germany, 1962.
- [143] J. Rinzel and G. B. Ermentrout. Analysis of neural excitability and oscillations. In *Methods in Neuronal Modeling: From Ions to Networks*, pages 251–291. The MIT Press, Cambridge, MA, 1998.
- [144] E. Rosenwasser and R. Yusupov. *Sensitivity of Automatic Control Systems*. CRC Press, Boca Raton, FL, 1999.

- [145] P. Ruoff, M. Vinsjevnik, C. Monnerjahn, and L. Rensing. The Goodwin oscillator: on the importance of degradation reactions in the circadian clock. *J. Biol. Rhythms*, 14(6):469–479, Dec. 1999.
- [146] G. Russo, M. di Bernardo, and E. D. Sontag. Global entrainment of transcriptional systems to periodic inputs. *PLoS Comput. Biol.*, 6(4):e1000739, Apr. 2010.
- [147] G. Russo, M. di Bernardo, and E. D. Sontag. Stability of networked systems: a multi-scale approach using contraction. In *Proc. 49th IEEE Conf. Decision and Control*, pages 6559–6564, Atlanta, GA, Dec. 2010.
- [148] P. Sacré, A. Franci, and R. Sepulchre. On the phase response curve for relaxation and bursting oscillators. In preparation.
- [149] P. Sacré and R. Sepulchre. Sensitivity analysis of circadian entrainment in the space of phase response curves. In V. Kulkarni, G.-B. Stan, and K. Raman, editors, *Systems and Synthetic Biology: A Systematic Approach*. Springer. To appear (preprint <http://arxiv.org/abs/1211.7317>).
- [150] P. Sacré and R. Sepulchre. Sensitivity analysis of oscillator models in the space of phase response curves: oscillators as open systems. Submitted to *IEEE Control Syst. Mag.* (preprint <http://arxiv.org/abs/1206.4144>).
- [151] P. Sacré and R. Sepulchre. Matching an oscillator model to a phase response curve. In *Proc. 50th IEEE Conf. Decision and Control and 2011 European Control Conf.*, pages 3909–3914, Orlando, FL, Dec. 2011.
- [152] A. Saltelli, S. Tarantola, and F. Campolongo. Sensitivity analysis as an ingredient of modeling. *Stat. Sci.*, 15(4):377–395, Nov. 2000.
- [153] A. Saltelli, S. Tarantola, F. Campolongo, and M. Ratto. *Sensitivity Analysis in Practice: a Guide to Assessing Scientific Models*. John Wiley & Sons, Ltd, Chichester, United Kingdom, Apr. 2004.
- [154] L. Scardovi, M. Arcak, and E. D. Sontag. Synchronization of interconnected systems with applications to biochemical networks: an input–output approach. *IEEE Trans. Autom. Control*, 55(6):1367–1379, June 2010.
- [155] N. W. Schultheiss, A. A. Prinz, and R. J. Butera, editors. *Phase Response Curves in Neuroscience: Theory, Experiment, and Analysis*, volume 6 of *Springer Series in Computational Neuroscience*. Springer, New York, NY, 2012.

- [156] R. Sepulchre. Oscillators as systems and synchrony as a design principle. In L. Menini, L. Zaccarian, and C. T. Abdallah, editors, *Current Trends in Nonlinear Systems and Control: In Honor of Petar Kokotović and Turi Nicosia*, pages 123–141. Birkhäuser, Boston, MA, 2006.
- [157] R. Seydel. *Practical Bifurcation and Stability Analysis*, volume 5 of *Interdisciplinary Applied Mathematics*. Springer, New York, NY, 3rd edition, 2010.
- [158] W. E. Sherwood and J. Guckenheimer. Dissecting the phase response of a model bursting neuron. *SIAM J. Applied Dynamical Systems*, 9(3):659–703, 2010.
- [159] J.-J. E. Slotine and W. Wang. A study of synchronization and group cooperation using partial contraction theory. In *Cooperative Control*, pages 207–228. Springer-Verlag, Berlin Heidelberg, Germany, 2005.
- [160] D. Somers and N. Kopell. Rapid synchronization through fast threshold modulation. *Biol. Cybern.*, 68(5):393–407, Mar. 1993.
- [161] E. D. Sontag. *Mathematical Control Theory: Deterministic Finite Dimensional Systems*, volume 6 of *Texts in Applied Mathematics*. Springer-Verlag, New York, NY, 2nd edition, July 1998.
- [162] E. D. Sontag. Contractive systems with inputs. In *Perspectives in Mathematical System Theory, Control, and Signal Processing*, pages 217–228. Springer, Berlin Heidelberg, Germany, 2010.
- [163] E. D. Sontag and M. Arcak. Passivity-based stability of interconnection structures. In *Recent Advances in Learning and Control*, pages 195–204. Springer-Verlag, London, England, 2008.
- [164] C. Sparrow. *The Lorenz Equations: Bifurcations, Chaos, and Strange Attractors*, volume 41 of *Applied Mathematical Sciences*. Springer-Verlag, New York, NY, Dec. 1982.
- [165] G.-B. Stan. *Global analysis and synthesis of oscillations: a dissipativity approach*. PhD thesis, University of Liège, Belgium, 2005.
- [166] G.-B. Stan and R. Sepulchre. Global analysis of limit cycles in networks of oscillators. In *Proc. 6th IFAC Symp. Nonlinear Control Systems*, pages 1433–1438, Stuttgart, Germany, Sept. 2005.
- [167] G.-B. Stan and R. Sepulchre. Analysis of interconnected oscillators by dissipativity theory. *IEEE Trans. Autom. Control*, 52(2):256–270, Feb. 2007.

- [168] J. Stelling, E. D. Gilles, and F. J. Doyle III. Robustness properties of circadian clock architectures. *Proc. Natl. Acad. Sci. USA*, 101(36):13210–13215, Sept. 2004.
- [169] S. H. Strogatz. *Nonlinear Dynamics and Chaos: with Applications in Physics, Biology, Chemistry, and Engineering*. Perseus Books, Cambridge, MA, 1994.
- [170] S. H. Strogatz. *Sync: the Emerging Science of Spontaneous Order*. Hyperion, New York, NY, 2003.
- [171] S. H. Strogatz and I. Stewart. Coupled oscillators and biological synchronization. *SciAm*, 269(6):102–109, Dec. 1993.
- [172] P. A. Tass. *Phase Resetting in Medicine and Biology: Stochastic Modelling and Data Analysis*. Springer Series in Synergetics. Springer-Verlag, Berlin Heidelberg, Germany, 1999.
- [173] S. R. Taylor, R. Gunawan, L. R. Petzold, and F. J. Doyle III. Sensitivity measures for oscillating systems: application to mammalian circadian gene network. *IEEE Trans. Autom. Control*, 53:177–188, Jan. 2008.
- [174] R. Tomović. *Sensitivity analysis of dynamic systems*. McGraw-Hill Book Company, Oxford, United Kingdom, 1963.
- [175] R. Tomović and M. Vukobratović. *General sensitivity theory*, volume 35 of *Modern analytic and computational methods in science and mathematics*. American Elsevier, New York, NY, 1972.
- [176] K. Tsumoto, H. Kitajima, T. Yoshinaga, K. Aihara, and H. Kawakami. Bifurcations in Morris-Lecar neuron model. *Neurocomputing*, 69(4–6):293–316, 2006.
- [177] J. J. Tyson. Modeling the cell division cycle: cdc2 and cyclin interactions. *Proc. Natl. Acad. Sci. USA*, 88(16):7328–7332, Aug. 1991.
- [178] B. van der Pol. A theory of the amplitude of free and forced triode vibrations. *Radio Rev.*, 1:701–710, 1920.
- [179] S. Varigonda. Robustness analysis of a relay oscillator. In L. Basañez, editor, *Proc. 15th IFAC World Congress*, Barcelona, Spain, July 2002. IFAC, Elsevier.
- [180] S. Varigonda and T. T. Georgiou. Dynamics of relay relaxation oscillators. *IEEE Trans. Autom. Control*, 46(1):65–77, Jan. 2001.

- [181] A. Varma, M. Morbidelli, and H. Wu. *Parametric Sensitivity in Chemical Systems*. Cambridge Series in Chemical Engineering. Cambridge University Press, Cambridge, United Kingdom, 1999.
- [182] G. Vinnicombe. Frequency domain uncertainty and the graph topology. *IEEE Trans. Autom. Control*, 38(9):1371–1383, Sept. 1993.
- [183] G. Vinnicombe. *Uncertainty and Feedback:  $\mathcal{H}_\infty$  Loop-Shaping and the  $\nu$ -Gap Metric*. Imperial College Press, London, United Kingdom, 2000.
- [184] V. Volterra. Variazioni e fluttuazioni del numero d'individui in specie animali conviventi. *Mem. Accad. Lincei.*, 2:31–113, 1926. Translation by R. N. Chapman in [185].
- [185] V. Volterra. Variations and fluctuations of a number of individuals in animal species living together. In *Animal Ecology*, pages 409–448. McGraw Hill, New York, NY, 1931.
- [186] C. von Gall, E. Noton, C. Lee, and D. R. Weaver. Light does not degrade the constitutively expressed small protein in the mouse suprachiasmatic nucleus. *Eur. J. Neurosci.*, 18(1):125–133, July 2003.
- [187] I. Vytyaz, D. C. Lee, P. K. Hanumolu, U.-K. Moon, and K. Mayaram. Sensitivity analysis for oscillators. *IEEE Trans. Comput.-Aided Design Integr. Circuits Syst.*, 27(9):1521–1534, Sept. 2008.
- [188] I. Vytyaz, D. C. Lee, P. K. Hanumolu, U.-K. Moon, and K. Mayaram. Automated design and optimization of low-noise oscillators. *IEEE Trans. Comput.-Aided Design Integr. Circuits Syst.*, 28(5):609–622, May 2009.
- [189] W. Wang and J.-J. E. Slotine. On partial contraction analysis for coupled nonlinear oscillators. *Biol. Cybern.*, 92(1):38–53, Dec. 2004.
- [190] N. Wiener. Application to the study of brain waves, random time, and coupled oscillators. In *Nonlinear Problems in Random Theory*, chapter 8, pages 67–77. The MIT Press, Cambridge, MA, 1958.
- [191] A. K. Wilkins, P. I. Barton, and B. Tidor. The Per2 negative feedback loop sets the period in the mammalian circadian clock mechanism. *PLoS Comput. Biol.*, 3(12):e242, Dec. 2007.
- [192] A. K. Wilkins, B. Tidor, J. White, and P. I. Barton. Sensitivity analysis for oscillating dynamical systems. *SIAM J. Sci. Comput.*, 31(4):2706–2732, 2009.
- [193] A. T. Winfree. Biological rhythms and the behavior of populations of coupled oscillators. *J. Theoret. Biol.*, 16(1):15–42, July 1967.

- [194] A. T. Winfree. Patterns of phase compromise in biological cycles. *J. Math. Biol.*, 1(1):73–95, 1974.
- [195] A. T. Winfree. *The Geometry of Biological Time*, volume 8 of *Biomathematics*. Springer-Verlag, New York, NY, 1st edition, 1980.
- [196] D. E. Zak, J. Stelling, and F. J. Doyle III. Sensitivity analysis of oscillatory (bio)chemical systems. *Comput. Chem. Eng.*, 29(3):663–673, 2005.
- [197] G. Zames and A. K. El-Sakkary. Unstable systems and feedback: the gap metric. In *Proc. 16th Allerton Conf.*, pages 380–385, Oct. 1980.